



**HAL**  
open science

# Pickering Foams : Particle Design and Catalysis

Andong Feng

► **To cite this version:**

Andong Feng. Pickering Foams : Particle Design and Catalysis. Catalysis. Université de Lyon, 2021. English. NNT : 2021LYSEN088 . tel-03934697

**HAL Id: tel-03934697**

**<https://theses.hal.science/tel-03934697>**

Submitted on 11 Jan 2023

**HAL** is a multi-disciplinary open access archive for the deposit and dissemination of scientific research documents, whether they are published or not. The documents may come from teaching and research institutions in France or abroad, or from public or private research centers.

L'archive ouverte pluridisciplinaire **HAL**, est destinée au dépôt et à la diffusion de documents scientifiques de niveau recherche, publiés ou non, émanant des établissements d'enseignement et de recherche français ou étrangers, des laboratoires publics ou privés.



Numéro National de Thèse : 2021LYSEN088

**THESE DE DOCTORAT DE L'UNIVERSITE DE LYON**  
opérée par  
**l'Ecole Normale Supérieure de Lyon**

**Ecole Doctorale ED 206**  
**Ecole Doctorale de Chimie de Lyon**

**Discipline : Chimie**

Soutenue publiquement le 14/12/2021, par :  
**Andong FENG**

---

**Pickering Foams: Particle Design and  
Catalysis**

**Mousses de Pickering: Conception de Particules et  
Catalyse**

---

Devant le jury composé de :

NARDELLO-RATAJ Véronique, Professeure, Ecole Centrale de Lille  
PELLET-ROSTAING Stéphane, Directeur de Recherche, ICSM CEA  
GIROIR-FENDLER Anne, Professeure, UCBL1  
ALBELA Belen, Maitre de Conférences, ENS de Lyon  
LENG Jacques, Charge de Recherche CNRS, LOF

Rapporteuse  
Rapporteur  
Examinatrice  
Examinatrice  
Examineur

PERA-TITUS Marc, Professeur, FRSC, CNRS / Université de Cardiff

Directeur de thèse

*I know that I know nothing. The unexamined life is not worth living.*  
*Socrates*

## ACKNOWLEDGEMENTS

This dissertation would not be accomplished without the support and assistance that I received from many people. It has been a great honor to be a PhD student of École Normale Supérieure de Lyon (ENS de Lyon). In the first year of my PhD, I worked at Laboratory of the Future (LOF), University of Bordeaux. After that, I continued my research at the Eco-Efficient Products & Processes Laboratory (E2P2L), Shanghai. I am very grateful for the opportunity to be a joint PhD candidate between LOF and E2P2L.

Firstly, I would like to express my sincere thanks to my supervisor Prof. Marc PERA-TITUS for his guidance and encouragement. In this period of deep study and research, he offered me lots of suggestions and help. He taught me how to work efficiently and gave me authority to develop my ideas. It was lucky and happy to work with him. I would also like to acknowledge my co-supervisors Dr. Dmytro Dedovets, Dr. Yunjiao Gu and Dr. Jacques Leng. I was always inspired by their ideas in physical chemistry and catalysis. During my stay in Bordeaux, Dr. Dedovets and Dr. Leng helped me not only in the scientific works, but also in my daily life, and provided guidance for improving my French level.

My deep appreciation goes to all the team members at E2P2L and LOF: Dr. Stéphane Streiff, Dr. Pierre Guillot, Dr. Bing Hong, Dr. Zhen Yan, Dr. Fan Jiang, Dr. Wenjuan Zhou, Dr. Jianxia Zheng, Dr. Raphael Wischert, Dr. Bright Kusema, Dr. Gongming Peng, Dr. Li Gao and Mr. Shi Zhang. They gave me plenty of useful suggestions and advice in all aspects. Special thanks go to my colleagues Dr. Jin Sha, Dr. Jie Gao and Dr. Renate Schwiedernoch for their kind help in material characterization and discussion of this manuscript.

I greatly appreciate the support received through the collaborative work with Prof. Xia Han from East China University of Science and Technology, and Dr. Claudio Oldani from Solvay Specialty Polymer. The solid-NMR characterization studies in this manuscript were conducted with the help of Prof. Xia Han. Dr. Claudio Oldani gave us kind advice on Aquivion samples.

I am heartily thankful to the all members of the jury, with emphasis on Prof. Veronique Nardello-Rataj and Dr. Stéphane Pellet-Rostaing for their participation as jury members and critical reading of my manuscript.

Last but not the least, my family is all my support to achieve the degree and this dissertation. They encourage me to pursue the dream and the life I wanted. I am so proud of them and they are the most precious treasure in my life.

Andong Feng  
November 2021

## GLOSSARY

$\Phi$	Liquid fraction
$P$	Laplace pressure inside the bubbles
$R_1, R_2$	Principal radii of the curvatur
$r$	Particle radius
$E_{gw}$	Free energy of particle at gas-water interface
$E_w$	Free energy of particle in water
$\gamma_{gl}$	Gas-liquid surface tension
$\gamma_{gw}$	Gas-water interfacial tension
$\gamma_{pg}$	Particle-gas surface tension
$\gamma_{pw}$	Particle-water surface tensions
$\gamma_{sg}$	Solid-gas surface tension
$\gamma_{sl}$	Solid-liquid surface tension
$\gamma_{lg}$	Liquid-gas surface tension
$\gamma_c$	Critical surface tension
$\gamma_{sa}$	Solid-air surface tension
$\gamma_{la}$	Liquid-air surface tension
$\tau$	Line tension
$S$	Total surface area of the particle
$L_{pgw}$	Length of the three-phase contact line
$\theta$	Three-phase contact angle
$F$	Adsorption barrier
$\Pi(h)$	Disjoining pressure of the liquid film
$h$	Distance between the particle and interface
$x$	Diffusion distance
$D$	Brownian motion
$k_B$	Boltzmann constant
$\eta$	Viscosity of the fluid
$T$	Temperature

## ABSTRACT

The versatility of colloidal particles endows Pickering foams with unique features, which can potentially be used for engineering gas-liquid-solid (G-L-S) catalytic microreactors for multiphase reactions. These systems show high potential for reformulating conventional G-L-S multiphase reactors, suffering from low gas solubility in liquids, to render them more eco-efficient. G-L-S microreactors based on Pickering foams can promote the G-L-S contact and enhance the catalytic activity, showing promising credentials for oxidation and hydrogenation reactions with broad industrial impact. This PhD thesis aims to boost our understanding of particle behavior at gas-liquid interfaces, and construct novel foaming systems for efficient multiphase reactions.

It is known that fluorinated materials with low surface energy are effective in stabilizing aqueous and non-aqueous foams. Based on these findings, we investigated the foaming behavior of Aquivion<sup>®</sup> PFSA, a perfluorinated superacid resin commercialized by Solvay, in different types of organic solvents and water. The foaming performance was found to be strongly promoted by hydrogen binding between Aquivion<sup>®</sup> PFSA and the solvent molecules. By comparing Aquivion<sup>®</sup> PFSA with various foaming agents in benzyl alcohol, the former outperformed previously reported polytetrafluoroethylene and fluorinated particles both in terms of foamability and foam stability.

Owing to its unique structure, Aquivion<sup>®</sup> PFSA can behave concomitantly as foaming agent and acid catalyst. By taking advantage of these properties, we constructed a foaming system for one-pot cascade deacetalization and hydrogenation reaction by combining Aquivion<sup>®</sup> PFSA with a homemade catalyst Pd/SiO<sub>2</sub> catalyst. The catalytic performance of the foam system was superior to that of the conventional non-foam multiphase system. Such a significant improvement was attributed to a pronounced increase of the gas-water interface area.

Foams stabilized solely by solid particles are of great interest due to their long-term stability, lower stabilizer content and potentials to replace surfactants. To achieve good foamability, the wettability of particles needs to be finely tuned to adjust the liquid-particle and gas-particle surface tensions. To this aim, we designed the surface-active particles by mimicking the structure of the solvent and gas. A variety of bridged organosilica particles was prepared by sol-gel synthesis using bisilylated organic precursors. The foaming properties of resulting particles were studied after handshaking, high-speed homogenization in Ultra-Turrax, and also using a homemade microfluidic device. The influence of particle wettability and solvent properties on foam formation were systematically investigated. Among the particles, biphenyl-bridged

organosilicas afforded the preparation of stable foams.

In order to obtain bifunctional particles that can serve as foaming agent and catalyst, a library of organosilica particles was prepared by co-condensation of aromatic silanes with alkylsilanes or fluorinated silanes. The surface properties of the organosilicas could be readily tuned by adjusting the organic groups incorporated into the framework. The key parameters (*i.e.* chain length of alkylsilanes, stabilizer concentration) controlling the foam formation were studied in detail. It was shown that stable oil foams could be obtained with fluorinated organosilica particles in benzyl alcohol. Eventually, we extended the utility of these fluorinated particles by incorporating a noble metal (Pd) with promising preliminary results.

**KEYWORDS:** Pickering foam, surface property, interfacial catalysis, fluorinated material, organosilica particle

## RESUME

Les particules colloïdales de silice sont des objets versatiles permettant la genèse de mousses dites de Pickering. Ces mousses peuvent être utilisées pour concevoir des nouveaux microréacteurs catalytiques gaz-liquide-solide (G-L-S). Ces systèmes sont prometteurs afin de rendre les réacteurs G-L-S industriels, dont la performance est fortement limitée par la faible solubilité des gaz dans les liquides, plus éco-efficaces. Les microréacteurs G-L-S fondés sur des mousses de Pickering, avec une amélioration accrue du contact G-L-S, permettent d'envisager une activité catalytique améliorée pour mener des réactions d'oxydation et d'hydrogénation, à fort intérêt industriel. Les travaux réalisés dans le cadre de cette thèse ont pour but de mieux comprendre le comportement des particules adsorbées à l'interface gaz-liquide et ainsi de développer des nouveaux systèmes catalytiques à base de mousses de Pickering pour mener efficacement des réactions G-L-S.

En règle générale, les matériaux fluorés, présentant une faible énergie de surface, permettent de stabiliser des mousses à base d'eau et des solvants non aqueux. Partant de ce principe, dans un premier temps, nous avons étudié la propension de l'Aquivion® PFSA, une résine fluorée commercialisée par Solvay, à stabiliser des mousses à base d'eau et de plusieurs solvants organiques. La genèse et la stabilité des mousses dépendent en grande mesure de la formation de liaisons d'hydrogène entre l'Aquivion® PFSA et les molécules du solvant. En outre, l'Aquivion® PFSA montre une performance améliorée par rapport à une série d'agents moussants dans l'alcool benzylique, parmi lesquels le polytetrafluoroéthylène and des particules fluorées.

A cause de son architecture moléculaire unique, l'Aquivion® PFSA présente un double comportement moussant et catalytique (acide). Prenant compte de ces propriétés, nous avons développé un système catalytique en cascade à base d'une mousse aqueuse pour réaliser une réaction de deacétylisation combinée avec une hydrogénation sélective, en présence d'Aquivion® PFSA et d'un catalyseur Pd/SiO<sub>2</sub>. La présence de mousse offre une amélioration nette de l'activité catalytique par rapport à un système G-L-S conventionnel sans mousse. Ce résultat peut s'expliquer par l'augmentation nette de la surface gaz-eau générée en présence de mousse.

Les mousses de Pickering peuvent être stabilisées avec une faible teneur de solide actif en absence de tensioactif. La mouillabilité des particules doit être maîtrisée afin d'ajuster les tensions de surface liquide-particule et gaz-particule. Dans ce but, nous avons préparé une famille de particules avec une surface reproduisant l'architecture moléculaire du solvant et du



gaz. Les particules, préparées par la méthode sol-gel utilisant des précurseurs bissylilés, comprennent des groupements organiques « pontés ». Celles-ci ont été ensuite utilisées pour préparer des mousses par agitation manuelle et homogénéisation en Ultra-turrax, et utilisant aussi un dispositif microfluidique « maison ». En particulier, nous avons étudié l'effet de la mouillabilité et des propriétés des solvants sur la formation et la stabilité des mousses. Ces travaux ont mené à la préparation de mousses organiques stables basées sur l'alcool benzylique utilisant des particules préparées avec des précurseurs du type diphényle.

Afin de préparer des particules fonctionnelles servant à la fois en tant qu'agent moussant et catalyseur, nous avons préparé une série de silices moyennant la co-condensation de précurseurs silane aromatiques et alkyl or fluorés. Les propriétés de surface des silices ont été ajustées en fonction de la teneur en groupement aromatique et alkyl / fluoré. Ensuite, nous avons évalué l'effet de la longueur de chaîne des groupements alkyl et la concentration des particules sur la formation des mousses organiques. Nous avons réussi la préparation de mousses stables d'alcool benzylique utilisant des particules avec des précurseurs fluorés. Nous avons exploré par la suite l'incorporation de nanoparticules de palladium sur ces nouveaux matériaux avec des résultats préliminaires encourageants.

**MOTS CLES** : Mousse de Pickering, activité de surface, catalyse interfaciale, matériau fluoré, silice

## GENERAL INTRODUCTION

Gas-liquid-solid catalytic reactions play an important role in biochemical processes, industrial fabrication, energy utilization and laboratory synthesis. Due to the extremely low gas solubility in liquids, these reactions often suffer from poor activity. To address this limitation, numerous strategies involving flow chemistry and packed column and microbubble generators have been developed to promote the G-L-S contact. However, these approaches require complicated designs or intensive energy input (*e.g.* high temperature/pressure) to drive the reaction. In these regards, novel technologies enhancing the G-L contact are required.

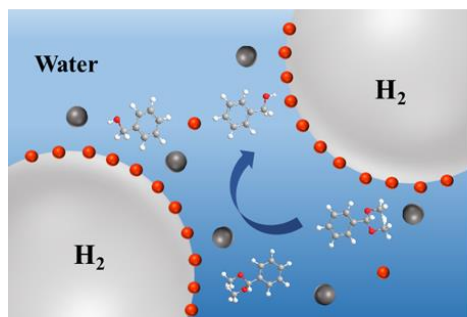
Pickering foams are attractive platforms for engineering G-L-S catalytic microreactors with enhanced G-L-S contact, allowing potential application at milder reaction conditions. Using this concept, we constructed Pickering foam systems based on water and non-aqueous solvents with an emphasis on catalytic applications. In particular, we rationally designed and prepared surface-active materials for stabilizing foams based on diversity of solvents.

This manuscript has been divided into five chapters. Chapter 1 provides an overview of the state of the art on the preparation and applications of foams. We highlight the fundamental principles of foam formation and destabilization. We list the available surface-active materials for stabilizing Pickering foams and outline the underlying thermodynamic and kinetic principles for their stabilization. Chapter 2 describes the materials and experimental protocols used along the study.

The results and discussion are covered by chapters 3-5 (see graphical abstract). Chapter 3 compiles the surface-active properties of Aquivion<sup>®</sup> PFSA for stabilizing aqueous and non-aqueous foams. Based on the unique properties of Aquivion<sup>®</sup> PFSA, we developed a foaming system for a one-pot cascade deacetalization and hydrogenation reaction. In chapter 4, we synthesized a series of bridged organosilica particles from bisilylated organic precursors, which are structurally similar to aromatic solvents. The foaming behavior of the resulting particles were studied systematically by handshaking, high-speed homogenization in Ultra-Turrax, and microfluidics. In chapter 5, a variety of organosilica particles was prepared by co-condensation of different organosilane precursors. The main parameters governing the foaming properties were investigated in detail. Moreover, an attempt was made to design bifunctional particles that can behave concomitantly as foamer and catalyst. Finally, a brief summary of conclusions and suggestions for future work are provided.

# GRAPHICAL ABSTRACT

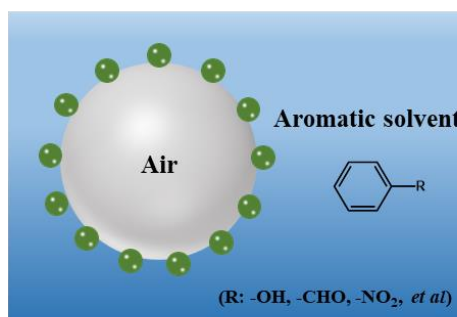
## Chapter 3



### 1 Aquivion® PFSA

Organic foams  
Aqueous foams

## Chapter 4, 5



### Organosilica particles prepared from:

- 2 Bridged organosilane  $(R'O)_3Si-Si(OR')$  3 Organoalkoxysilane  $(R'O)_3Si-$

# TABLE OF CONTENTS

<b>ACKNOWLEDGEMENTS</b> .....	<b>II</b>
<b>GLOSSARY</b> .....	<b>III</b>
<b>ABSTRACT</b> .....	<b>IV</b>
<b>RESUME</b> .....	<b>VI</b>
<b>GENERAL INTRODUCTION</b> .....	<b>VIII</b>
<b>GRAPHICAL ABSTRACT</b> .....	<b>IX</b>
<b>CHAPTER 1 State of the Art</b> .....	<b>1</b>
1.1 Gas-liquid dispersions .....	2
1.1.1 Definition and application of foams .....	2
1.1.2 Stabilization mechanisms of foams .....	3
1.2 Aqueous foams .....	6
1.2.1 Surfactant-stabilized foams .....	6
1.2.2 Particle-stabilized foams .....	8
1.2.2.1 Thermodynamics of foam systems .....	8
1.2.2.2 Dynamics of foam systems.....	11
1.3 Non-aqueous (organic) foams .....	13
1.3.1 Specialty surfactants.....	14
1.3.2 Solid particles .....	14
1.3.3 Crystalline particles.....	16
1.4 Catalysis at the gas-liquid interface.....	17
1.5 Aquivion® PFSA.....	18
1.6 Organosilica hybrid materials.....	20
1.6.1 Design of organosilica materials .....	20
1.6.2 Emulsions and foams stabilized by silica-based materials .....	21
1.7 Objectives.....	23
1.8 References .....	24
<b>CHAPTER 2 Materials &amp; Methods</b> .....	<b>36</b>
2.1 Introduction .....	37
2.2 Chemicals .....	37
2.3 Preparation of Pd/SiO <sub>2</sub> catalyst .....	39
2.4 General procedure for one-pot cascade reaction .....	39
2.5 Preparation of bridged organosilica particles from bisilylated precursors.....	40
2.6 Preparation of alkyl-modified organosilicas from phenyltriethoxysilane .....	41
2.7 Preparation of fluorinated silica particles.....	41
2.8 Characterization techniques .....	42

2.8.1	Transmission electronic microscopy .....	42
2.8.2	Thermogravimetric analysis .....	42
2.8.3	Fourier-transform infrared spectra.....	42
2.8.4	Nuclear magnetic resonance.....	42
2.8.5	X-ray photoelectron spectroscopy.....	42
2.8.6	Inductively coupled plasma-optical emission spectrometry.....	42
2.8.7	Dynamic light scattering .....	42
2.8.8	Zeta potential.....	43
2.8.9	Gel permeation chromatography .....	43
2.8.10	Contact angle.....	44
2.8.11	Surface tension .....	44
2.8.12	Optical microscopy.....	44
2.9	Preparation of foams using different methods.....	45
2.9.1	Hand shaking.....	45
2.9.2	High speed homogenizer .....	45
2.9.3	Microfluidics .....	45
2.10	References .....	47
<b>CHAPTER 3 Foams Stabilized by Aquivion® PFSA.....</b>		<b>50</b>
3.1	Introduction .....	51
3.2	Characterization of Aquivion® D98-20BS-P .....	52
3.3	Foaming studies of Aquivion® D98-20BS-P .....	55
3.3.1	Effect of solvent type.....	57
3.3.2	Effect of temperature and Aquivion® D98-20BS-P concentration .....	60
3.4	Catalytic studies of Aquivion® D98-20BS-P.....	62
3.4.1	Characterization of the Pd/SiO <sub>2</sub> catalyst .....	63
3.4.2	Effect of foam and acidity on benzaldehyde hydrogenation .....	64
3.4.3	Cascade reaction: effect of stirring rate and concentration .....	66
3.5	Conclusion.....	69
3.6	References .....	70
<b>CHAPTER 4 Organic Foams Stabilized by Biphenyl-bridged Particles .....</b>		<b>76</b>
4.1	Introduction .....	77
4.2	Characterization of bridged organosilica particles .....	78
4.3	Foaming studies of bridged organosilica particles .....	80
4.4	Effect of the solvent nature on foamability .....	87
4.5	Comparison of foams stabilized by different particles and surfactants.....	91
4.6	Foaming studies of bridged organosilica particles after Pd loading.....	92
4.7	Conclusion.....	94

4.8	References .....	95
<b>CHAPTER 5</b>	<b>Organic Foams Stabilized by Fluorinated Organosilica Particles .....</b>	<b>100</b>
5.1	Introduction .....	101
5.2	Organic foams stabilized by alkyl-modified organosilicas .....	102
5.2.1	Characterization of alkyl-modified organosilicas.....	102
5.2.2	Foaming studies of alkyl-modified organosilicas.....	103
5.3	Organic foams stabilized by fluorinated organosilica particles.....	104
5.3.1	Characterization of fluorinated organosilica particles .....	104
5.3.2	Foaming studies of fluorinated organosilica particles .....	106
5.3.3	Foaming studies of fluorinated organosilica particles after Pd loading.....	108
5.4	Conclusions .....	110
5.5	References .....	111
	<b>Conclusion and Perspectives .....</b>	<b>114</b>
	<b>Annex.....</b>	<b>117</b>
	<b>Publications.....</b>	<b>118</b>

# **CHAPTER 1**

---

## **State of the Art**

---

## 1.1 Gas-liquid dispersions

### 1.1.1 Definition and application of foams

A colloidal dispersion is a complex system, comprising a dispersed phase of small particles, droplets or bubbles, and a continuous medium surrounding them [1]. Either or both phases may be in gas, liquid, solid, or supercritical phase states. Accordingly, colloidal systems can be divided into foams, emulsions, suspensions, gels and aerosols. This work mainly focuses on the fundamentals and applications of foams. Like other colloidal systems, the foams are characterized by a highly developed interface.

Foams are conceptually similar to emulsions, but their behavior differ in practice [2]. A foam is commonly defined as a dispersion of gas bubbles in a liquid, while an emulsion is a colloidal dispersion in which a liquid is dispersed in an immiscible liquid phase [1, 3]. The main difference between foams and emulsions relies on the size of the dispersed phase: foams are often constituted by large gas bubbles (diameters higher than 10  $\mu\text{m}$  and may be larger than 1000  $\mu\text{m}$ ), whereas the typical size of emulsion droplets is about 10-100  $\mu\text{m}$  [4, 5]. Besides, the bubbles are compressible and can often be easily deformed into polyhedral structures [6], which is more difficult to occur in emulsions.

Foams can be broadly classified as *dry foam* and *wet foam* according to the liquid fraction  $\Phi$  [7]. For  $\Phi < 0.05$ , the bubbles are polyhedral and have very thin films, and this state can be called dry foam. As  $\Phi$  increases, the bubbles become round and approach to spherical geometry. At high liquid fraction ( $\Phi > 0.36$ ), the system enters “bubbly liquid” state, where the bubbles are spherical and isolated without contact with neighbors. Nevertheless, the definition of those states is vague and the dry-wet transition of foams depends on each particular gas-liquid system.

Foams are common and desirable in a number of applications such as food manufacturing processes, cosmetics, health care products, detergents, fire extinguishing, oil recovery and processing, synthesis of porous materials, foam flotation and other engineering processes (**Figure 1.1**) [8-14]. Foams are encountered in a variety of commercial products widely used in our everyday lives. Food foams such as ice cream, whipped cream, protein-sugar foams, and fresh cheese are becoming increasingly popular among consumers due to their visual appeal and peculiar sensory properties [15, 16]. Natural surfactants and proteins, such as casein or egg white are classic foaming agents in foods. Foam assisted enhanced oil recovery (EOR) has gained increasing attention by oil & gas companies and academia [17, 18]. For instance, carbon dioxide foaming affords outstanding improvement in the EOR process at both the microscopic and macroscopic levels [19].





**Figure 1.1** Illustration of the versatile applications of foams.

Foams can also occur during processing of health care products and fire prevention [20, 21]. In early 2020, the World Health Organization declared the pandemic diffusion of COVID-19. One of the effective ways implemented to prevent the spread of this virus is frequent hand sanitization by the traditional handwashing or using alcohol-based hand sanitizers [22, 23]. Foams are much easier to handle and spread on the skin than traditional gels.

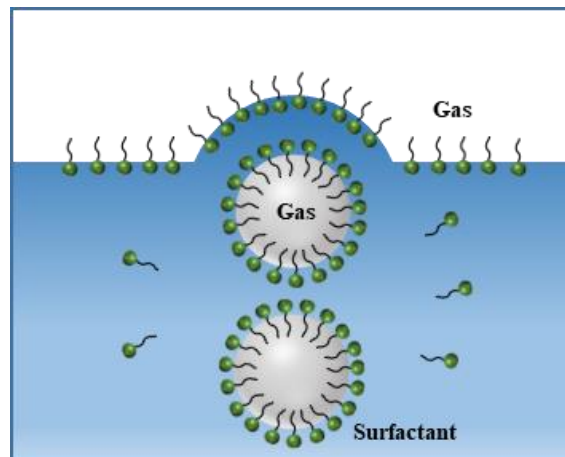
Solid polymeric foams such as polystyrene and polyurethane have emerged as promising materials for a variety of applications, such as the construction industry, sport and leisure (lightweight seating furniture), agriculture and packaging [24, 25]. These materials derive from the use of blowing agents in the foam manufacturing process. There are two types of blowing agents: chemical blowing agents (such as thermal decompositions of azodicarbonamide) and physical blowing agents (inert gases like  $N_2$  and  $CO_2$ ) [26]. Solid foams can also be made of metals, nowadays used in the automotive, railway or aerospace industry [27].

### 1.1.2 Stabilization mechanisms of foams

Numerous studies have investigated the stabilization mechanism of foams. Foam formation is affected by the gas-liquid interfacial properties, since foaming promotes the generation of a large surface area, increasing the surface energy of the gas-liquid system. As a result, the formation of foams is not a spontaneous process, and the energy input is indispensable for their

generation [28]. Foams made from pure liquids are generally very unstable due to the buoyancy forces and thermodynamic instability of the systems [29, 30]. Foam instability mainly arises from the high energy associated to the generation of the gas-liquid interface, and constitutes a driving force for decreasing the total interfacial area by coalescence and/or disproportionation of bubbles [31]. Introduction of surface active molecules or particles into the liquid can substantially enhance foam stability by adsorption at the gas-liquid interface, thus stabilizing liquid films [32, 33].

Based on their morphology, bubbles can be broadly divided into two general types: (1) well-separated spherical bubbles, and (2) interlinked polyhedral bubbles (foams) [34]. The main stages of foam formation can be established by observing the behavior of a certain number of bubbles. In a surfactant-containing system, the adsorption of the surfactant molecules starts at the gas-liquid interface when bubbles are created. The bubbles rise toward the surface of the liquid due to buoyancy forces, and thus form a hemispherical liquid film consisting of two surfactant adsorption layers and a liquid core between them (**Figure 1.2**) [35]. With the increase of bubbles at the interface, they begin to draw closer, leading to the formation of a monolayer of bubbles. At this stage, capillary attraction between bubbles promote their interaction [36], leading to a second layer of bubbles, and so on until a three-dimensional foam is obtained.



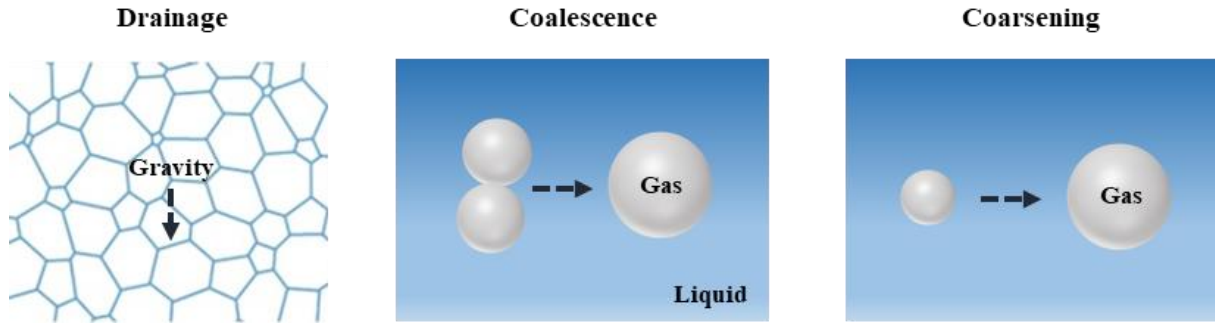
**Figure 1.2** Formation of a foam film when bubbles reach the liquid surface.

Foams are thermodynamically unstable, and foam destabilization mainly occurs by three major mechanisms: drainage, coalescence, and coarsening (**Figure 1.3**) [37-40]. First, the liquid and gas in the foam tend to separate because of gravity and large density differences [41]. This effect (drainage) plays a dominant role in the foam destabilization process. This lowers the liquid fraction and lead to drier foams. Second, coalescence occurs by thinning and rupture of films between two bubbles, which results in the merging of neighboring bubbles and foam

collapse. The third destabilization mechanism is coarsening, which is induced by differences in the Laplace pressure (Eq 1), i.e. the smaller the bubble the higher the pressure [37].

$$\Delta P = P_1 - P_2 = \gamma \left( \frac{1}{R_1} + \frac{1}{R_2} \right) \quad (1)$$

where  $\gamma$  is the surface tension of liquid and  $R_1, R_2$  are the principal radii of the curvature [42].



**Figure 1.3** Scheme of the three main foam destabilization mechanisms: liquid drainage, coalescence of two bubbles, and bubble coarsening.

Foams also evolve by gas diffusion within the liquid films from smaller bubbles to bigger bubbles. For well separated droplets, this process is known as Ostwald ripening, and results in coarsening for cellular materials, like foams [41]. The average bubble diameter grows with time because of coalescence and coarsening.

The combined effects of these mechanisms determine the foam lifetime (foam stability). Small bubbles can be initially generated (diameter  $< 30 \mu\text{m}$ ), but progressively coalesce or coarsen to become micro-foams ( $< 250 \mu\text{m}$ ), mini-foams ( $250\text{-}500 \mu\text{m}$ ) and eventually macro-foams ( $> 500 \mu\text{m}$ ) [43, 44]. It is difficult to count the number of bubbles, and the most important parameters characterizing the foams are *foamability* and *foam stability*. On the one hand, the foamability of the solution or dispersion is a measure of its capacity to produce foams [28], and it can be assessed using the initial foam volume (or foam height) obtained under certain conditions. On the other hand, foam stability refers to the lifetime of foams in which the volume decreases with the time from its formation [45], and is sometimes determined by the half-life time or time when the foam reaches half of its initial volume [46].

While commonly used to characterize foams, these two parameters (foamability and foam stability) are not fully satisfactory because they do not only depend on the chemical composition of the foaming systems, but also on the foam preparation method [28]. Depending on the energy input, foaming techniques can be categorized into physical, chemical and biological foaming [47]. Physical techniques include mechanical action (bubbling, shaking, gas sparging, whipping, etc.) or phase transition (boiling, cavitation, effervescence, etc.). Chemical methods

create bubbles by a gas-releasing chemical or electrochemical reaction, while the most common biological approach relies on gas-generating species such as yeast.

So far, a general theory to explain the mechanisms of formation and stability for all types of foaming systems does not exist, because the magnitude and mutual importance of the different types of effects can vary significantly, depending on the stage of foam life and the conditions of its existence [48].

## **1.2 Aqueous foams**

An aqueous foam is a dispersion of gas bubbles in water that can be stabilized by surface-active agents such as surfactants, proteins, polymers or solid particles. Aqueous foams are the most common types of liquid foams, and have broad beneficial applications such as in food, detergency, cosmetics, firefighting (as barriers to oxygen), oil recovery, and deliquification of natural gas [9, 49]. In recent years, remarkable progress has been achieved in the study of aqueous foams with special focus on foam stabilizers [50].

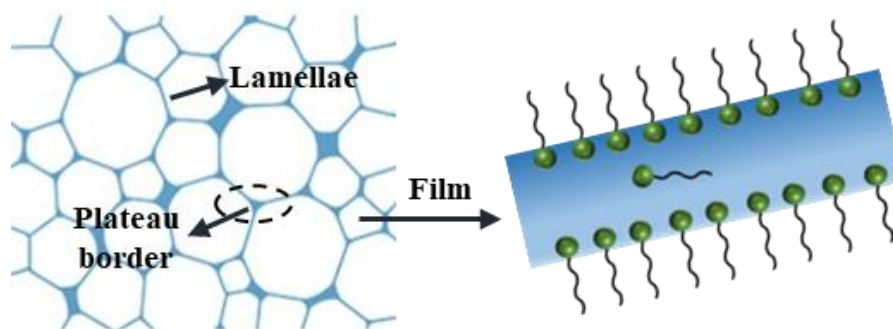
Below we provide a literature overview on surfactant- and particle-stabilized aqueous foams. While most of the studies focus on aqueous foams given their broad use, the concepts and mechanisms should be regarded as general and extensive to non-aqueous foams (see **section 1.3** for non-aqueous foams).

### **1.2.1 Surfactant-stabilized foams**

Surfactants are the most common foaming agents, and are generally classified into four types based on their head groups: anionic surfactants (positively charged), cationic surfactants (negatively charged), nonionic surfactants (uncharged) and zwitterionic surfactants (containing both positive charge and negative charge) [51]. Food foams are usually stabilized by proteins (macromolecules), which are not discussed here. Proteins can behave as surfactants and adsorb at air-water interfaces due to their amphiphilic nature [52]. Surfactants have two parts: a head (hydrophilic part) that has affinity for water, and a tail (hydrophobic part) that is exposed towards the gas. Owing to their amphiphilic structure, the surfactants can assemble at the gas-liquid interface and reduce the surface tension of water. To stabilize foams efficiently, surfactant molecules need to diffuse rapidly to the gas-liquid interface.

Aqueous foams can be studied at both the macro- and microscale. At the macroscale, an aqueous foam is regarded as a continuous fluid, while in microscale, the foam's elements includes films, Plateau borders, and nodes [53]. A single isolated bubble consists of a thin membrane of fluid stabilized by two amphiphilic adsorption layers (lamella) [54], separating

the neighbouring bubbles. In a cluster of bubbles, three lamellae meet at junctions known as Plateau borders, and the angle between them is  $120^\circ$  (**Figure 1.4**) [55]. Besides, there are always four Plateau borders meeting in a node at the tetrahedral angle of approximately  $109.5^\circ$ . The foam dynamics depends on the complex interaction between the fluid flow inside the lamellae and Plateau borders (microscale), and the gas motion inside the bubbles (macroscale).



**Figure 1.4** Structure of aqueous foams and liquid film between bubbles covered by surfactant monolayers.

The gas-liquid surface tension is affected by the chemical composition of surfactant concentration and temperature, which are often termed as soluto- and thermocapillary effects, respectively [53]. With a dense adsorption monolayer of surfactants, the interfacial film can stabilize foams by lowering the surface tension and increasing the surface viscosity [13]. Indeed, a high surface viscosity can act as a resistance to film thinning and rupturing. The surface surfactant concentration gradient results in a surface tension gradient [56]. It is usually difficult to determine the amount of surfactant adsorbed at the interface, since an excess of molecules is dissolved in bulk water. As a rule, the surface tension decreases with the surface surfactant concentration until a critical concentration beyond which the surface tension remains constant [53].

There is a minimum concentration of surface-active molecules required for foam production. In the case of surfactants, this concentration is associated with the surface coverage of the bubbles. The critical micelle concentration (CMC) is one of the most important parameters. At this concentration, surfactant molecules start to aggregate and form micelles. Foams may occur at a bulk concentration of the order of one tenth of the CMC, and is associated with the formation of Newton black films (if the lateral pressure is larger than the electrostatic barrier, a very small film thickness is reached after drainage, and the water layer thickness is of order 1 nm) [50]. The surfactant concentration required affects the amount of surfactant adsorbed at the surface of the bubbles, and therefore depends on the methods used to generate the foam. The

amount of surfactant is larger for high-energy input than for low-energy one, which is most likely associated with the fact that high-energy input produces small bubbles and hence high surface areas, requiring a larger amount of surfactant.

It is usually believed that the surfactant concentration must be higher than its respective CMC to boost foaming [34]. Indeed, the stability of micelles may significantly affect the generation of bubbles when using a micellar solution. However, very stable micelles cannot break up immediately to provide enough monomers to adsorb onto the newly created interfaces of the bubbles, thus they are not favored for bubble generation. As a result, the more stable the micelles are, the lower the ability to generate bubbles. However, stable micelles (aggregates) could greatly contribute to foam stability [57].

## 1.2.2 Particle-stabilized foams

The behavior of foams stabilized by surface-active particles has attracted much attention in recent years. Particle-stabilized foams are often called Pickering foams by analogy to Pickering emulsions consisting of oil and water, which will be used in the remainder of this manuscript. Unlike surfactants or polymers, solid particles with intermediate wettability possess much higher adsorption energy at the air-water interface, giving rise to foams with long-term stability [58, 59]. Foams stabilized by particles alone or together with appropriate surfactants can survive for long periods or even under extremely harsh conditions, and the aforementioned destabilization mechanisms can be halted to a large extent (**section 1.1.2**) [60].

The formation of Pickering foams is both governed by thermodynamics and kinetics of particle adsorption at the gas-liquid interface. While the considerations below refer to aqueous foams, these should be regarded as general and extensive to non-aqueous and oil systems.

### 1.2.2.1 Thermodynamics of foam systems

Upon mixing a gas and water, the formation of dispersed gas bubbles within water increases the interfacial area, and thus the free energy of the system. This effect is counterbalanced by the interfacial adsorption of a single particle well dispersed in water to reduce the energy  $\Delta E$ .  $\Delta E$  can be expressed by comparing the energy of a particle dispersed in water ( $E_w$ ), and at the interface ( $E_{gw}$ ). For a non-Janus spherical particle, both energies read as follows [61]:

$$E_w = \gamma_{gw}S + \gamma_{pw}(S_g + S_w) \quad (2)$$

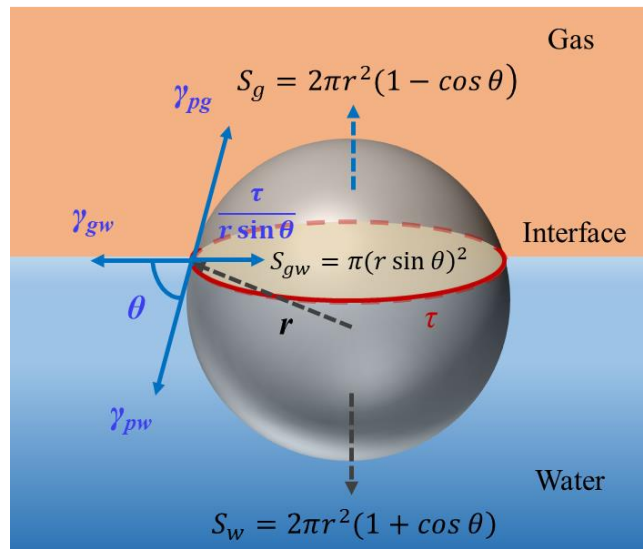
$$E_{gw} = \gamma_{gw}(S - S_{gw}) + \gamma_{pg}S_g + \gamma_{pw}S_w + \tau L_{pgw} \quad (3)$$

$$\Delta E = E_{gw} - E_w \quad (4)$$

where  $\gamma_{gw}$  is the gas-water surface tension,  $\gamma_{pg}$  and  $\gamma_{pw}$  are the particle-gas and particle-water

surface tensions, respectively;  $S$  is the total surface area of the particle; and surfaces  $S_g$ ,  $S_w$  and  $S_{gw}$ , and length of the three-phase contact line  $L_{pgw}$ , are defined in **Figure 1.5**. Geometrically, we have  $S=S_g+S_w$ .

In Eq 2, we have included the contribution of the line tension  $\tau$ , which is ascribed to the excess free energy of the three-phase contact line around the spherical particle [62, 63]. The line tension, which has unit length of force, can be regarded as a 1D analogue, for a curved line, of the surface tension. The contribution of the line tension is particularly relevant for systems with low interfacial tensions, as those commonly found for oil-oil emulsions and in oil-gas foams.



**Figure 1.5** Definition of the three-phase contact angle  $\theta$ , the line tension  $\tau$  contribution, and particle radius  $r$ . Water is considered as reference, and the contact line is labeled in red.

The different surface tensions can be related by the generalized Young equation, which can be obtained by minimizing the energy difference of a particle adsorbed at the interface with respect to the three-phase contact angle  $\theta$ . For foaming systems,  $\theta$  is measured through the liquid phase [64].

$$\gamma_{gw} \cos \theta = (\gamma_{pg} - \gamma_{pw}) + \frac{\tau \cos \theta}{r \sin \theta} \quad (5)$$

By combining Eq 4 and Eq 5, the following equation can be used relating  $\Delta E$  and  $\theta$ :

$$\Delta E = -\pi r^2 \gamma_{gw} \left[ (1 \pm \cos \theta)^2 \frac{2\tau(1 \pm \cos \theta) \cos \theta}{r \gamma_{gw} \sin \theta} - \frac{2\tau \sin \theta}{r \gamma_{gw}} \right] \quad (6)$$

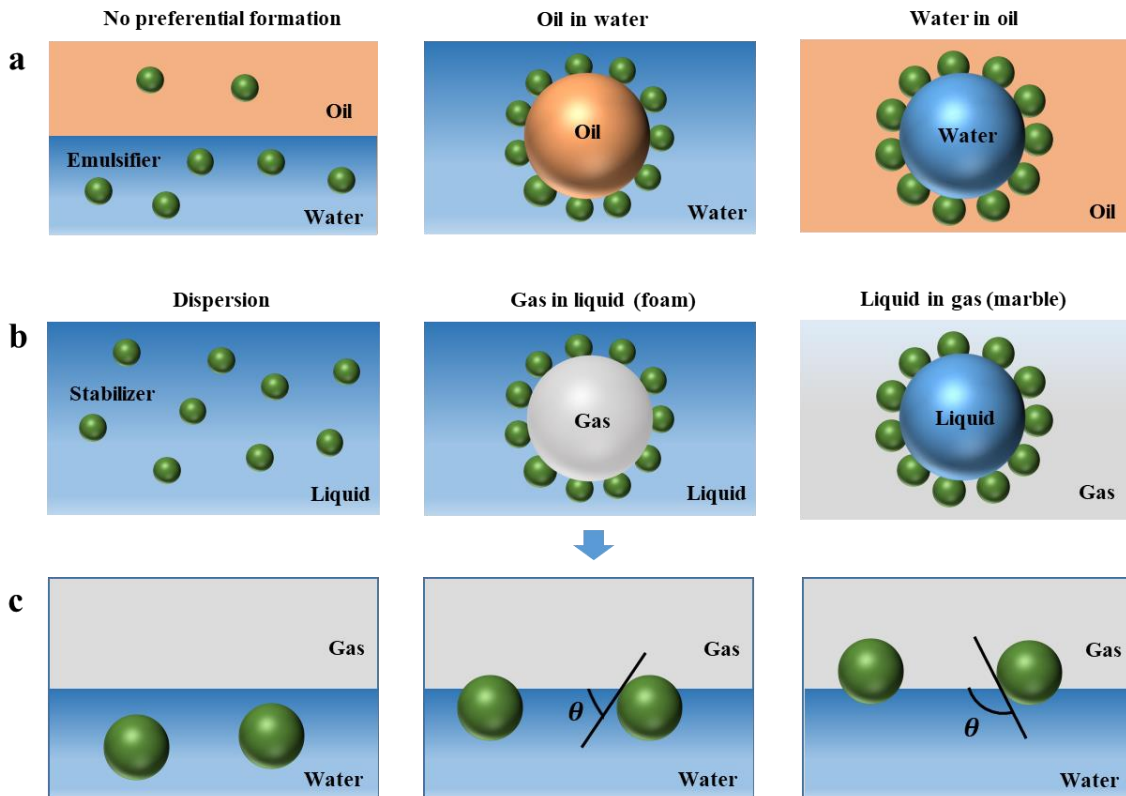
where the sign within the brackets corresponds to particle centers above (+) or below (-) the interface.

If  $\tau \ll r\gamma_{gw}$ , Eq 6 can be simplified to the well-known expression:

$$\Delta E = -\pi r^2 \gamma_{gw} (1 \pm \cos \theta)^2 \quad (7)$$

Unlike surfactant, solid particles can adsorb irreversibly at the interface, and they require greater energy to detach from the interface [40]. According to Eq (7), the optimum contact angle for foam stabilization is about  $90^\circ$ , as at this value the desorption energy of particle reaches the maximum.

The three-phase contact angle  $\theta$  is a primary descriptor for predicting the type of emulsions generated (*e.g.*, oil-in-water, or water-in-oil) or gas-water dispersions (*e.g.*, bubbles or marbles) [3, 40, 65]. **Figure 1.6** shows the arrangement of particles with different contact angle at the interface. The behavior of solid particles can remarkably differ depending on the particle hydrophobicity. Partially hydrophobic particles can spread at the gas-water interface, while hydrophilic particles tend to settle inside the liquid film and display small contact angles. Therefore, the particles must be partially hydrophobic to enable them to adsorb at the gas-water surface and increase foam lifetime.



**Figure 1.6** Classification of emulsions (a) and foams (b), and position of colloidal particles in gas and liquid mixtures as a function of contact angle  $\theta$  (c).

According to the theoretical results based on a simplified model of a single layer of particles,



particles can stabilize foams only in the contact angle interval between 20 and 90° [66]. Earlier reports have demonstrated that particles with contact angles in this range ensure the highest foam stability [30, 67, 68], while hydrophobic particles ( $\theta > 90^\circ$ ) often behave as defoamers.

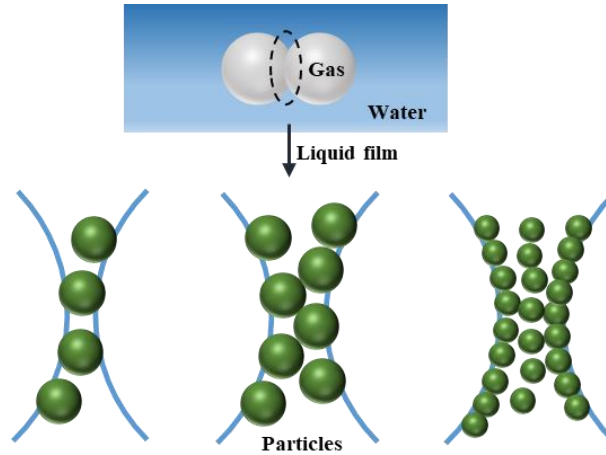
Chemical modification of the particle surface is a typical method for adjusting the particle contact angle. For example, Yang *et al.* developed a protocol to prepare surface-active silicas by modification with a mixture of hydrophobic octyl organosilane and hydrophilic triamine organosilane [69, 70]. Pickering foams could be easily stabilized by tuning the wettability of the particles. Another example of partially hydrophobic silica particles coated with short-chain silane (dichlorodimethylsilane) was demonstrated by Binks *et al.* [64, 68, 71]. The surface content of silanol groups in the particles varied from 100 to 14%, and the maximum foam height was found for a SiOH content of 32%. No foam was formed for hydrophilic (>70% SiOH) or very hydrophobic particles (14% SiOH, the powder remained on the water surface).

Another approach to enhance the surface activity of particles is to mix them with suitable surfactants [38]. The adsorption of oppositely charged surfactants onto particle surfaces can increase the lifetime of particle-stabilized foams by affecting the particle hydrophobicity, which may offer a novel technique for generating stable foams [60]. Examples of such surfactant-coated particles include silicas and cationic surfactants (n-amylamine, alkyltrimethylammonium bromides and N'-dodecyl-N,N-dimethylacetamidinium bicarbonate) [38, 72, 73], laponite and cationic or nonionic surfactants [74, 75], calcium carbonate and anionic surfactants (sodium dodecyl sulfate) [60, 76], and alumina with short chain carboxylic acids [31]. The latter study points out that the co-assembly of hydrophobic silica particles and hydrophilic polymer could provide a convenient and time saving alternative to particle surface modification for foam stabilization [77].

There are different possible stabilization mechanisms of particle-stabilized foams. Some authors claim that particles stabilize foams by attaching themselves to gas-liquid interfaces and serving as elastic separators during the primary impact of two bubbles (**Figure 1.7**) [30, 78]. Solid particles at sufficiently high concentrations can form a layered structure inside the thinning film, thus stabilizing it.

### 1.2.2.2 Dynamics of foam systems

The dynamics of particle adsorption at the gas-liquid interface is affected by an adsorption barrier  $F$ , that depends on the charge of already adsorbed particles. The magnitude of the adsorption barrier correlates with the disjoining pressure of the liquid film  $\Pi(h)$ , which is a function of the distance  $h$ , between the particle and the interface.



**Figure 1.7** Possible mechanisms for liquid film stabilization. From left to right: a monolayer of particles, bilayer of close-packed particles, and network of particle aggregates inside the film.

$$F \approx 2\pi r \int_h^\infty \Pi(h) dh \quad (8)$$

The presence of a barrier for particle adsorption relies on the fact that charged particles approaching a neutral interface between two media with different dielectric constants experiences repulsive image-charge forces [79]. Since the adsorption barrier is proportional to the object size, it is much more important for particles than for surfactants [80]. The presence of a barrier may require certain energy to overpass repulsive forces and bring the particles to the gas-water interface. Additionally, weak repulsive interactions lead to particle aggregation and the formation of particle gels, both of which are reported to be favorable for Pickering stabilization [81, 82].

Despite its positive impact on the adsorption energy, the average particle size increases the time needed to stabilize bubbles. The adsorption time also depends on the foaming process. The diffusion coefficient for a spherical particle subjected to Brownian motion  $D$ , can be expressed by the Stokes-Einstein equation [83]:

$$D = \frac{k_B T}{6\pi\eta r} \quad (9)$$

where  $k_B$  is the Boltzmann constant,  $T$  is the temperature, and  $\eta$  is the viscosity of the fluid in which the particles are dispersed.

From Eq 9, a first estimate of the time required for the particles to diffuse a distance  $x$ , from one bulk phase to the interface can be obtained using the following expression:

$$t \approx \frac{x^2}{D} \quad (10)$$

If the energy required to form the dispersions is high, the surface coverage is only partial.

As a rule, the thickness of particle-stabilized interfaces is much larger than that of interfaces stabilized by surfactants. As a result, particle-stabilized dispersions can exhibit large interfacial contact areas and short diffusion paths, allowing fast mass/heat transfer [4]. This property is of significance for engineering the interfacial microreactors.

### 1.3 Non-aqueous (organic) foams

Contrary to aqueous foams, few studies have been devoted to the understanding of non-aqueous foams despite their occurrence in many industrial fields [84]. Due to the formation of hydrogen bonds, water has a higher surface tension ( $72.8 \text{ mN}\cdot\text{m}^{-1}$  at  $20 \text{ }^\circ\text{C}$ ) than most other liquids [85]. The low surface tension of organic solvents (typically ranging from 14 to  $50 \text{ mN}\cdot\text{m}^{-1}$ ) limits the adsorption of common surface-active agents at the gas-liquid interface [86], thus stabilizers with low surface energy (*e.g.*, fluorinated materials) are required to generate non-aqueous foams. As we mentioned in **section 1.2**, there is abundant literature on stabilization mechanisms of aqueous foams, and the general concepts used to describe aqueous foams can be useful to understand non-aqueous foams. There are three types of foam stabilizers, namely, specialty surfactants, solid particles and crystalline particles (**Table 1.1**) [87].

**Table 1.1** Summary of works on oil foams obtained from different stabilizers.

Category	Stabilizer	Non-aqueous systems	Ref.
Specialty surfactants	Fluoroalkyl ester	Dodecane	[88]
	PDMS based-surfactants	Polyurethane	[89]
	Asphaltenes and resins	Crude oil	[90, 91]
	Dispersant	Lubricating oil	[92]
Solid particles	PTFE, OTFE	Peanut oil, sunflower oil, rapeseed oil, eugenol, tricresyl phosphate, ahexyl cinnamaldehyde, benzyl acetate, bromonaphthalene, etc.	[93-95]
	Fluorinated particles (silica, sericite, clays and zinc oxide)	Oils with surface tensions higher than $26 \text{ mN}\cdot\text{m}^{-1}$ ( <i>e.g.</i> , sunflower oil, toluene, benzene, benzyl acetate and hexadecane)	[96-98]
	Silicas coated with dichlorodimethylsilane	Ethylene glycol, glycerine	[99]
	POM modified with alkyl chains	Benzyl alcohol, phenylethyl alcohol	[100]
Surfactant crystals	Fatty alcohols, fatty acids, monoglycerides, etc.	Vegetable oils ( <i>e.g.</i> , olive oil, sunflower oil, squalane and liquid paraffin)	[101-105]

### 1.3.1 Specialty surfactants

Studies using specialty surfactants for stabilizing organic foams are scarce, and it is difficult to obtain general trends for foam stabilization. Although the gas-oil interfacial tension is much smaller than that for the gas-water interface, some surface-active surfactants can adsorb at the gas-oil interface and modify its surface rheology [84]. These molecules usually have high molecular weights and complex structures.

Polydimethylsiloxane (PDMS) based surfactants have proved to be useful in stabilizing organic foams in polyurethane manufacture [89]. Due to the presence of hydrophilic Si-O groups, PDMS-based surfactants can orient and pack at the gas-interface. The function of these surfactants is cell size control and stability of organic foams near the mold [106].

Asphaltenes and resins in the crude oil are responsible for the formation of certain petroleum foams [84, 90, 107]. They are operationally defined as two solubility classes containing various types of polar components with aromatic rings, and are normally considered as a nuisance mainly as a result of their problematic precipitation and adsorption at the oil-water interface [108]. Sun and Zhang suggested that surface-active asphaltenes can stabilize the gas-oil interface by reducing surface tension [109]. Moreover, the high oil viscosity can decrease the rate of oil film thinning, thereby resulting in an increase in foam lifetime.

Fluorinated surfactants can reduce the surface tension of liquids to very low values ( $< 20 \text{ mN}\cdot\text{m}^{-1}$ ) due to their fluorocarbon moieties [110]. Bergeron *et al.* studied the foaming behavior of two novel fluorocarbon surfactants (fluoroalkyl ester and fluorosilicone surfactant) in dodecane [88]. These surfactants can significantly lower the surface tension of dodecane at relatively low concentration (0.4 wt%). The stability of the foam film has been attributed to the repulsive disjoining pressure between the surfactant-coated interfaces. However, such surfactants are not efficient for oils with very low surface tension, as their adsorption at the interface is weak.

### 1.3.2 Solid particles

Solid particles with intermediate wettability can adsorb at gas-liquid interfaces leading to the stabilization of aqueous and non-aqueous foams [4]. Particle adsorption at the interface is thermodynamically favourable if the sum of the solid-gas tension  $\gamma_{sg}$  and the solid-liquid tension  $\gamma_{sl}$  is less than the original liquid-gas tension  $\gamma_{lg}$  ( $\gamma_{sg} + \gamma_{sl} < \gamma_{lg}$ ) [93]. This depends on the wettability of the particles, which could be quantified by the contact angle  $\theta$  measured through the liquid phase (**Figure 1.6c**) [87]. The contact angle  $\theta$  is given by the Young's equation (Eq 5). In the case of gas-oil system, if  $\theta$  is  $0^\circ$  (wetted by liquid) or  $180^\circ$  (wetted by gas), no foams

are generated. For  $0^\circ < \theta < 90^\circ$ , particles are more oleophilic than oleophobic, and stable non-aqueous foams can be formed after aeration. If  $\theta > 90^\circ$ , the particles are extremely oleophobic resulting in oil-in-gas systems (*i.e.* marbles). It can be seen that the particle wettability or contact angle can be altered in two ways: (a) by tuning the surface energy of the particles, and (2) by changing the surface tension of the oil [111].

The common approach for tuning the particle wettability involves the modification of the particle surface chemistry in a similar manner as for aqueous foams. Dyab *et al.* prepared stable non-aqueous foams in glycerin and ethylene glycol using dichlorodimethylsilane-modified silica particles as stabilizers [99]. However, the surface tension of these liquids is relatively high ( $\gamma > 47 \text{ mN}\cdot\text{m}^{-1}$ ), limiting their scope of application. Particles coated with hydrocarbon-containing groups can be wetted by many oils, while those coated with fluoro groups can be oleophobic to certain oils [94]. This is partly due to the lower surface energy of fluorocarbons compared to hydrocarbons. Previous studies have shown that stable non-aqueous foams can be achieved using fluorinated particles. By tuning the fluorination degree of the particles and varying the surface tension of oils, air-in-oil foams or oil-in-air liquid marbles could be easily obtained [96, 97]. For oils with surface tension higher than  $32 \text{ mN}\cdot\text{m}^{-1}$ , oil foams stabilized by particles with intermediate fluorine content (59% SiOH) were obtained, where the contact angle lies between *ca.*  $80^\circ$  and  $140^\circ$  [97]. In terms of foamability, the particle concentration is an important parameter. The foam volume increases progressively with the particle concentration since a larger air-oil surface area can be covered and stabilized.

Recently, organic-inorganic hybrids (POMs) have been developed to stabilize foams in different alcohols (*e.g.*, benzyl alcohol and 1-phenylethanol) [100]. The lacunary Keggin  $\text{Na}_7[\text{PW}_{11}\text{O}_{39}]$  was modified with alkyl trimethyl siloxane under acidic conditions. 3C-silyl-POM could adsorb at the gas-oil interface and stabilize foams in benzyl alcohol, while 8C-silyl-POM and 12C-silyl-POM generated larger aggregates in solution, and thus discouraged foamability.

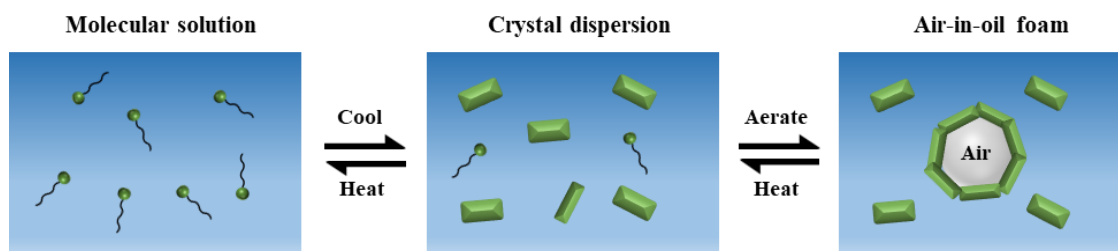
Commercial polytetrafluoroethylene (PTFE) and oligomeric tetrafluoroethylene (OTFE) have been used to stabilize non-aqueous foams [93]. Fox and Zisman established a direct relation between the contact angle  $\theta$  and the surface tension of liquids  $\gamma_{lg}$  for wetting PTFE [112]. A critical surface tension  $\gamma_c$  was defined so that liquids with  $\gamma_{lg} \leq \gamma_c$  wet the solid completely, whereas liquids with  $\gamma_{lg} > \gamma_c$  do not. For PTFE,  $\gamma_c$  is  $18 \text{ mN}\cdot\text{m}^{-1}$  at  $20^\circ\text{C}$  [87]. Using this concept, Binks *et al.* studied the foaming properties of PTFE and OTFE particles in various liquids ranging from non-polar hydrocarbons and polar oils. In the case of PTFE particles, for oils with relatively moderate surface tension ( $30\text{-}45 \text{ mN}\cdot\text{m}^{-1}$ ) partially wetting the particles,

stable foams could be prepared, where particles form a close-packed layer enveloping air bubbles [93]. However, an oil dispersion of particles was obtained for apolar oils such as dodecane and pentane. For polar liquids with higher surface tension like glycerol and water, the interface curvature was inverted and a powder-like material was formed. A direct relation was found between the foamability and the contact angle of oils with PTFE. Indeed, particle-stabilized non-aqueous foams formed for contact angle between approx. 40 and 90°, with a maximum foamability at *ca.* 55°.

### 1.3.3 Crystalline particles

Studies on edible oil foams stabilized by surfactant crystals are emerging [111]. Introducing air into an oil matrix can reduce saturated fat intake, provide a more desirable mouth feel and reduce delivery costs [103]. Examples of surfactants that can form crystals and stabilize vegetable oil foams include fatty alcohols, fatty acids, monoglycerides, diglycerides, triglycerides, and diglycerol esters [101-104]. Such surfactant crystals have been shown to stabilize foams by forming a robust coating on the surface of air bubbles to arrest diffusion [101].

The basic idea behind surfactant crystals in stabilizing is to choose an appropriate surfactant (normally with long hydrocarbon chains) that dissolves in oil at relatively high temperature (around 60 °C). In general, these surfactants are not surface-active and the molecular solution does not foam. On cooling this one-phase solution below the solubility limit, the formation of surfactant crystals begin to occur (**Figure 1.8**). Further cooling leads to the formation of oleogels where the crystals interact through van der Waals forces locking up the vegetable oil in a viscous gel. Aeration of these oleogels results in the formation of oil foams. The stability of oil foams originates from both surface and bulk contributions. Surfactant crystals adsorb on newly created bubble surfaces protecting them to some extent from disproportionation and coalescence. In addition, excess crystals in oil form a 3D network that serves to suspend the bubbles in oil and reduces gravity-driven drainage. Conveniently, surfactant crystals in foams melt upon heating, which could cause foam breakdown in a controlled manner.



**Figure 1.8** Scheme of one-phase molecular solution of surfactants (left), crystal dispersion upon cooling (center), and foam stabilized by crystals after aeration (right).

## 1.4 Catalysis at the gas-liquid interface

Gas-liquid-solid (G-L-S) reactions are extensively used in chemical, petrochemical and environmental catalytic processes. Conventional G-L-S reactors such as packed beds and slurry reactors typically suffer from low solubility of gases in liquids (**Table 1.2**) and resilient mass-heat transfer limitations due to their low specific interface areas [113]. There are several models to describe mass transfer between phases, including the so-called “two-film theory” (**Figure 1.9a**) [114]. Mass transfer of solute from one phase to another involves transport from the bulk of one phase to the phase boundary or interface, then transfer from the interface into the bulk of the second phase [115]. Most of the resistance to mass transfer resides in liquid films instead of the bulk liquid. In practice, co-solvents, surfactants, phase-transfer reagents, and high gas pressures are required to enhance the catalytic activity [116, 117]. Besides, microfluidic devices and microbubble generators can promote the G-L interfacial contact [118-121]. However, these methods require complex equipment and still do not guarantee an efficient contact at the surface. For a major improvement on current systems in terms of cost efficiency and energy savings, G-L-S reactors operating at the nanoscale are required.

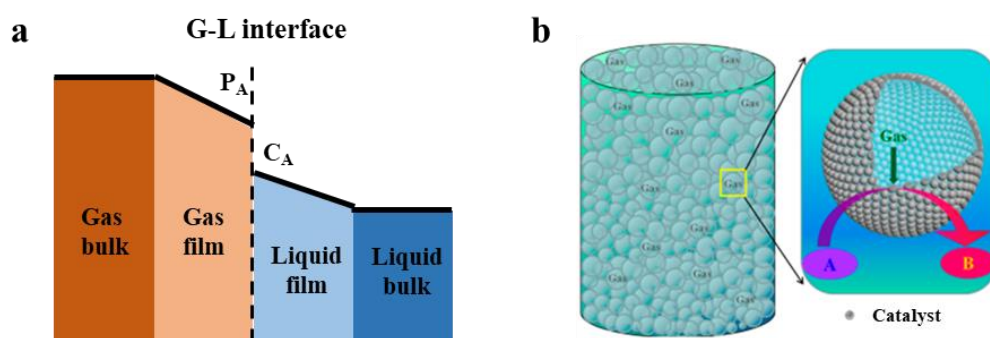
The amount of gas-liquid surface area per unit volume of material that is attainable in a foam is greater than that in comparable two-phase systems [122]. This property makes gas-liquid foams particularly attractive for interphase mass transfer operations. Therefore, these systems can be used for engineering G-L-S catalytic microreactors with an enhanced triphasic contact at the nanoscale. They constitute original platforms for reengineering multiphase reactors towards a higher degree of sustainability [4].

**Table 1.2** Solubility of gases in water at 20 °C and 1 bar pressure [123-125].

Entry	Gas	Solubility (mg·kg <sup>-1</sup> )
1	Oxygen	44.33
2	Hydrogen	1.62
3	Nitrogen	19.22
4	Carbon dioxide	1721
5	Argon	63

Two examples of G-L-S microreactors based on particle-stabilized aqueous foams have been recently reported. Yuan *et al.* synthesized surface-active particles based on monodisperse Au nanoparticles embedded in polyoxometalate anion [PV<sub>2</sub>Mo<sub>10</sub>O<sub>40</sub>]<sup>5-</sup> assembled with rigid tripodal ligand by electrostatic interactions [126]. The multi-functional catalyst could self-assemble at the O<sub>2</sub>/water interface, and the resulting system showed high activity in the

oxidation of aliphatic/aromatic alcohols into aldehydes and ketones. Likewise, silica particles modified with octyl and triamine groups were prepared by Yang and co-workers to stabilize gas bubbles in water (**Figure 1.9b**) [70]. By incorporating Pd or Au nanoparticles, the particles became active for aqueous hydrogenation and oxidation reactions in  $H_2$  and  $O_2$  foams, respectively, at high particle concentration (7.5-12.5 wt%). The catalytic foams exhibited an enhanced activity compared to non-foam multiphase reactors, which was attributed to a pronounced increase of the surface area. The particles could be recovered and recycled after reaction by adjusting the pH to 3-4 with an HCl solution.

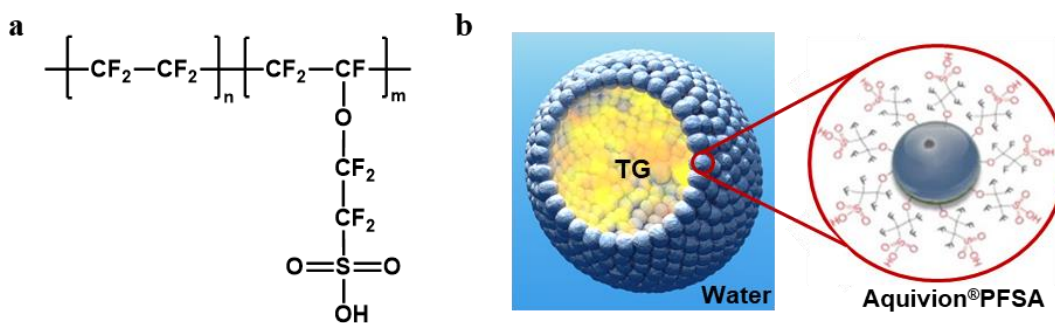


**Figure 1.9** Conventional G-L-S multiphase reaction where the catalytic activity can be strongly inhibited by G-L diffusional resistance (a); innovative multiphase microreactors consisting of particle-stabilized foams.

### 1.5 Aquivion<sup>®</sup> PFSA

Perfluorosulfonic superacid (PFSA) resins with short side-chain show great interest due to their outstanding chemical stability, strong acid strength, high proton conductivity and suitable mechanical strength [127-129]. In particular, Aquivion<sup>®</sup> PFSA represents a new family of perfluorosulfonic superacid resins with an acid strength comparable to that of sulphuric acid (Hammett acidity  $\sim -12$ ) [130]. A number of reports highlight the exceptional catalytic performance of Aquivion<sup>®</sup> PFSA in a variety of acid-catalyzed reactions [131-133]. Aquivion<sup>®</sup> PFSA is a copolymer based on tetrafluoroethylene and a vinyl ether with sulphonic acid functionalities produced by Solvay Specialty Polymers [131]. The general structure of Aquivion<sup>®</sup> PFSA is shown below (**Figure 1.10a**), where typically  $n$  has a value of about eight, with  $m$  about two [134, 135].





**Figure 1.10** Structure of Aquivion® PFSA (a) and Pickering emulsions stabilized by Aquivion® PFSA (b).

Owing to its surface-active properties, Aquivion® PFSA is capable of stabilizing emulsions in the presence of two immiscible liquids, and has been demonstrated as a robust and highly active catalyst in biphasic reactions. For instance, Shi *et al.* reported a series of interfacial acid catalysts based on Aquivion® PFSA (PW98, PW66 and D79), which promotes the hydrolysis of triglyceride (TG) to lauric acid (LA) by stabilizing TG-in-water emulsions (**Figure 1.10b**) [136]. At low catalyst loading (1.0 wt%), Aquivion® PW98 favoured the formation of emulsions at a much higher dispersion degree and smaller droplet size, which in turn alleviated external mass transfer resistance towards the acid centers. As a result, the highest GTL conversion and LA yield was obtained over PW98 with values of 46% and 34%, respectively.

The surface properties of Aquivion® PFSA can be tuned by immobilizing with carbon-based materials, generating Aquivion®-carbon composites. Surface-active composites were prepared by one-pot hydrothermal carbonization of Aquivion® PW98 with guar gum or cellulose. The as-synthesized composites showed the additional advantage of a potential cost reduction, as well as an improvement of their recyclability compared to the parent® PFSA [137]. Aquivion®-carbon composites have also been used for the biphasic acetalization reaction of dodecyl aldehyde with ethylene glycol (EG) towards the cyclic acetal [138]. Homogeneous *p*-toluenesulfonic acid and pristine PW98 showed a lower productivity than Aquivion®-carbon composites (10 mmol H<sup>+</sup>). The enhanced catalytic activity of the composites was ascribed to the higher capacity for stabilizing emulsions. The catalytic performance of the Aquivion-carbon composites was further assessed in the transesterification of glyceryl trioleate (GTO) with methanol [137]. Compared with the parent PW98, Aquivion®-carbon composites (5:1) displayed higher activity and reusability for GTO transesterification with methanol at 100 °C, which could be correlated with the formation of a larger emulsion volume and a smaller average droplet diameter (11.2 μm).

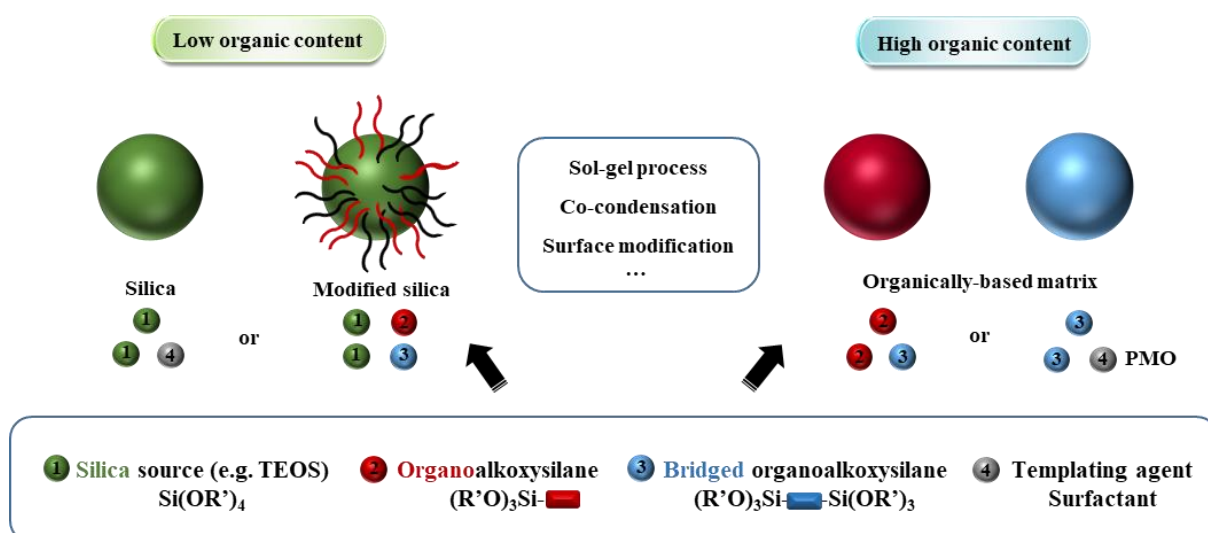
## 1.6 Organosilica hybrid materials

Over the past decades, organosilica hybrid materials containing inorganic and organic components have attracted great attention [139, 140]. The construction of hybrid silica materials combine the advantages of a robust inorganic framework (*e.g.*, high thermal and mechanical stability) with the intrinsic properties of organic fragments (*e.g.*, flexibility and hydrophobicity) [141]. Since the discovery of mesostructured silicas in the early 1990s, a broad family of silica-based materials has been successfully established and utilized for a variety of applications such as adsorption, drug and gene delivery, electronics and sensing, and catalysis [142-145].

### 1.6.1 Design of organosilica materials

The properties of silica-based materials are highly related to their structure and morphology in addition to the composition [146]. The sol-gel methodology can be used to design silica-based materials with controlled shape and surface properties [140, 147]. It opens the possibility of incorporating organic components and synthesizing organic-inorganic hybrids. In general, functionalization of silica materials can be performed in three ways: (1) by subsequent modification of a pure silica matrix (grafting), (2) by simultaneous reaction of organosilane precursors (co-condensation), and (3) using bisilylated organic precursors that lead to periodic mesoporous organosilicas (PMOs) [139, 140, 148].

Monodispersed silica particles can be synthesized by the Stöber method (sol-gel process), and the particle diameter can be controlled in the range from tens of nanometers to several micrometers [149]. Silica particles have a large number of hydroxyl groups that facilitates the introduction of functionalities. Surface modification of silica particles with organic moieties (post-functionalized strategy) can be carried out primarily by reaction of organoalkoxysilanes bearing simple functionalities, such as amino, mercapto and iso(thio)cyanato (**Figure 1.11**). An alternative method to synthesize organically functionalized silica materials is the co-condensation method. Mixed organosilicas can be obtained by direct co-condensation of silica precursors ( $\text{SiO}_4$  environments: tetraalkoxysilanes) with organoalkoxysilanes ( $\text{R-SiO}_3$  environments, R represents organic groups). The incorporated organofunctional groups are usually more homogeneously distributed than in materials prepared by the grafting. However, the main drawback of this one-pot synthesis relates to the limited achievable density of the functional groups [150], and the fact that a high content of organic units can lead to a disordered product.



**Figure 1.11** Structures and synthetic pathways of various organosilica composites.

Pure organosilica materials with a high organic content such as silsesquioxanes ( $R\text{-SiO}_{1.5}$ ) and bridged silsesquioxanes ( $O_{1.5}\text{Si-R-SiO}_{1.5}$ ) can also be obtained by the sol-gel process using organoalkoxysilanes or bisilylated organosilica precursors [151, 152]. In the presence of structure directing agents (*e.g.*, surfactants or amphiphilic block copolymers), the condensation of bridged organosilane precursors may lead to a new class of mesostructured organic-inorganic hybrid materials (PMOs). Unlike mesoporous silica particles, PMO frameworks are based on organic functional groups covalently linking siloxane domains [153]. To date, a large number of bridged organoalkoxysilane (*e.g.*, alkyl, aromatic and heteroelement fragments) have been used to synthesize PMOs with single or even multiple organic groups [143, 144, 154].

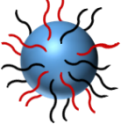
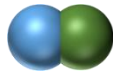

### 1.6.2 Emulsions and foams stabilized by silica-based materials

Colloidal silica particles have been widely employed as stabilizers in Pickering emulsions and foams because of their high stability, easy surface modification, and controllable size and structure [4, 155]. As mentioned above, silica particles with intermediate wettability allow the stabilization of emulsions and foams. For instance, emulsions of different types, stabilities and droplet diameters can be prepared with silica particles of different surface properties [156].

Surface modification of silica particles is one of the most useful methods to achieve the desired wettability (**Table 1.3**). Zhou *et al.* functionalized silica particles with alkyl chains and sulfonic acid groups to provide the particles with both surface activity and catalytic properties [157]. The emulsification properties of such particles was evaluated for the acetalization of long-chain fatty aldehydes and ethylene glycol. Similarly, Yang and co-workers prepared pH-responsive silica microspheres for the formation of Pickering emulsions using combined

organosilanes [158, 159].

**Table 1.3** Summary of the literature on emulsion and foam stabilized by silica-based materials.

Morphology	Representative example	System type	Ref.
Surface modification	Silica with octyl and triamine groups	Aqueous foam	[69, 70]
	Silica coated with dichlorodimethylsilane	Aqueous foam	[64, 68, 71]
	Silica modified with dichlorodimethylsilane	Oil foam	[99]
	Silica grafted with fluorinated silane	Oil foam	[97]
	Silica with methyl groups	Emulsion	[160-164]
	 Silica with dimethyloctadecylammonium group	Emulsion	[165, 166]
	Silica with octyl and triamine groups	Emulsion	[158, 159]
Janus-type structure	Silica with alkyl and sulfonic acid groups	Emulsion	[157, 167-169]
	Sulfonated polystyrene-grafted silicas	Emulsion	[170]
	Titanosilicates grafted with alkylsilanes	Emulsion	[171]
	Polymer-grafted Au-SiO <sub>2</sub> Janus particles	Bubbles in water	[172]
	Dumbbell-shaped carbon-organosilica particle	Emulsion	[173]
	Snowman-like SiO <sub>2</sub> @PDVB/PS particles	Emulsion	[174]
	 Janus silica particles with a hydrophilic domain and a hydrophobic domain	Emulsion	[175, 176]
	Ionic liquid-functionalized silica particles	Emulsion	[177]
	Aldehyde-functionalized particle CHO-JNPs	Emulsion	[178]
	Janus mesosilica nanosheet	Emulsion	[179]
Core-shell structure	Janus N-doped carbon@silica hollow sphere	Emulsion	[180]
	Fe <sub>3</sub> O <sub>4</sub> @mC&mSiO <sub>2</sub> Janus composites	Emulsion	[181]
	Carbon-organosilica particles with phosphotungstic component	Emulsion	[182]
	Silica core incorporated with hydrophilic and hydrophobic moieties in the shell	Emulsion	[183]
	 Silica sphere consisting of a hydrophobic core and a hydrophilic shell	Emulsion	[184]
	Mesoporous organosilica nanosphere	Emulsion	[185]
	TS-1 core with silica/carbon shell	Emulsion	[186, 187]

Janus particles are named after the two-faced Roman god of beginning and ending, doors, and gates [188]. These particles possess two (or more) distinct chemical and physical properties on its surface. Janus particles show surface activity like surfactants due to their asymmetric

shape, composition and chemical functionalities [189]. It was theoretically predicted that Janus particles exhibit higher interfacial activity than particles with homogeneous surfaces [190]. This was confirmed by Xue *et al.*, who investigated silica particles with one-half surface composed of triamine and the other half of octyl groups [176]. The desorption energy of Pickering emulsions using Janus particles was 3-fold higher than that of emulsions formed by non-Janus particles. To date, Janus particles of different shapes, including sphere, snowman and dumbbell, have been reported and shown superior emulsifying capacity [189]. In contrast, few studies have been reported on foams and bubbles stabilized by Janus particles [172].

Core-shell architectures allow preferential location of molecular functionalities either in the inner core or on the outer shell [191]. Often, the presence of particle stabilizers featuring a hydrophobic core-hydrophilic shell structure is sufficient to bring the desired properties for a specific application. For instance, the hydrophilic shell ensures good dispersibility of functionalized particles in water, while the hydrophobic core can trap organic molecules from water. This special feature has proved advantageous for adsorption of hydrophobic compounds in water [184].

## 1.7 Objectives

Contrary to aqueous foams, few studies have been reported to date on organic foams due to a rather low surface tension of non-aqueous liquids. It is still a target to develop a simple and cheap strategy that can achieve optimal foaming properties in organic solvents. In addition, although different length scales of foam structure (*e.g.*, gas-liquid interface and liquid film) have been studied to elucidate the stabilization and destabilization mechanisms of foams, as well as the key parameters controlling foam formation (*e.g.*, particle wettability, nature of oil phase, concentration), open questions remain still unanswered. The main aim of this study is to design the surface-active materials and further the understanding of foam generation and stability in non-aqueous systems.

The low solubility of gases in liquids largely affects the catalytic performance of solid-liquid-gas multiphase reactions. To address this limitation, a microbubble strategy has been developed to increase the gas-liquid interface area in detriment of vigorous stirring and high pressure. Nevertheless, only a limited number of studies have investigated the catalytic properties of foams, focusing on gas-water-solid multiphase systems. Therefore, it is highly desirable to construct novel aqueous and non-aqueous foam systems and further extend their applications in catalysis.

To meet these aims, this thesis has been conducted following three main objectives: (1)

rationalization of the interaction between fluorinated materials and solvent molecules at the gas-liquid interface; (2) engineering of foaming systems for multiphase catalytic reactions by combining catalytic foaming materials and non-foaming palladium catalyst; and (3) conception and development of new non-fluorinated surface-active particles with defined wettability.

## 1.8 References

1. Laurier L, S., *Emulsions, Foams, and Suspensions Fundamentals and applications*. 2005, Wiley VCH.
2. Walstra, P., *Overview of emulsion and foam stability*. Food emulsions and foams, 1987: p. 242-257.
3. Hunter, T.N., et al., *The role of particles in stabilising foams and emulsions*. Advances in colloid and interface science, 2008. **137**(2): p. 57-81.
4. Dedovets, D., et al., *Multiphase Microreactors Based on Liquid–Liquid and Gas–Liquid Dispersions Stabilized by Colloidal Catalytic Particles*. Angewandte Chemie International Edition, 2022. **61**(4): p. e202107537.
5. Langevin, D., *Coalescence in foams and emulsions: Similarities and differences*. Current Opinion in Colloid & Interface Science, 2019. **44**: p. 23-31.
6. Pugh, R., *Experimental techniques for studying the structure of foams and froths*. Advances in colloid and interface science, 2005. **114**: p. 239-251.
7. Furuta, Y., N. Oikawa, and R. Kurita, *Close relationship between a dry-wet transition and a bubble rearrangement in two-dimensional foam*. Scientific reports, 2016. **6**: p. 37506.
8. Binks, B.P. and T.S. Horozov, *Colloidal particles at liquid interfaces*. 2006: Cambridge University Press.
9. Pugh, R.J., *Bubble and foam chemistry*. 2016: Cambridge University Press.
10. Cantat, I., et al., *Foams: structure and dynamics*. 2013: OUP Oxford.
11. Suja, V.C., et al., *Single bubble and drop techniques for characterizing foams and emulsions*. Advances in Colloid and Interface Science, 2020: p. 102295.
12. Yang, Y.-C., et al., *An intensified ozonation system in a tank reactor with foam block stirrer: Synthetic textile wastewater treatment and mass transfer modeling*. Separation and Purification Technology, 2021. **257**: p. 117909.
13. Schramm, L.L. and F. Wassmuth, *Foams: basic principles*. 1994.
14. Micheau, C., et al., *Evaluation of ion separation coefficients by foam flotation using a carboxylate surfactant*. Colloids and Surfaces A: Physicochemical and Engineering Aspects, 2015. **470**: p. 52-59.
15. Müller-Fischer, N. and E.J. Windhab, *Influence of process parameters on microstructure of food foam whipped in a rotor–stator device within a wide static pressure range*. Colloids and Surfaces A: Physicochemical and Engineering Aspects, 2005. **263**(1-3): p. 353-362.

16. Amagliani, L., et al., *On the foaming properties of plant proteins: Current status and future opportunities*. Trends in Food Science & Technology, 2021.
17. Majeed, T., et al., *A Review on Foam Stabilizers for Enhanced Oil Recovery*. Energy & Fuels, 2021. **35**(7): p. 5594-5612.
18. Kumar, S. and A. Mandal, *A comprehensive review on chemically enhanced water alternating gas/CO<sub>2</sub> (CEWAG) injection for enhanced oil recovery*. Journal of Petroleum Science and Engineering, 2017. **157**: p. 696-715.
19. Talebian, S.H., et al., *Foam assisted CO<sub>2</sub>-EOR: A review of concept, challenges, and future prospects*. Journal of Petroleum Science and Engineering, 2014. **120**: p. 202-215.
20. Vinogradov, A.V., et al., *Silica foams for fire prevention and firefighting*. ACS applied materials & interfaces, 2016. **8**(1): p. 294-301.
21. Larson, E.L., B. Cohen, and K.A. Baxter, *Analysis of alcohol-based hand sanitizer delivery systems: efficacy of foam, gel, and wipes against influenza A (H1N1) virus on hands*. American journal of infection control, 2012. **40**(9): p. 806-809.
22. Fameau, A.-L., et al., *Foamitizer: High ethanol content foams using fatty acid crystalline particles*. Journal of Colloid and Interface Science, 2021. **600**: p. 882-886.
23. Golin, A.P., D. Choi, and A. Ghahary, *Hand sanitizers: A review of ingredients, mechanisms of action, modes of delivery, and efficacy against coronaviruses*. American journal of infection control, 2020. **48**(9): p. 1062-1067.
24. Zakaria, Z., Z. Ariff, and C. Sipaut, *Effects of parameter changes on the structure and properties of low-density polyethylene foam*. Journal of Vinyl and Additive Technology, 2009. **15**(2): p. 120-128.
25. Lee, S.-T., C.B. Park, and N.S. Ramesh, *Polymeric foams: science and technology*. 2006: CRC press.
26. Khemani, K.C., *Polymeric foams: an overview*. 1997.
27. Banhart, J., *Manufacture, characterisation and application of cellular metals and metal foams*. Progress in materials science, 2001. **46**(6): p. 559-632.
28. Wang, J., A.V. Nguyen, and S. Farrokhpay, *A critical review of the growth, drainage and collapse of foams*. Advances in colloid and interface science, 2016. **228**: p. 55-70.
29. Studart, A.R., et al., *Materials from foams and emulsions stabilized by colloidal particles*. Journal of Materials Chemistry, 2007. **17**(31): p. 3283-3289.
30. Kaptay, G., *Interfacial criteria for stabilization of liquid foams by solid particles*. Colloids and Surfaces A: Physicochemical and Engineering Aspects, 2003. **230**(1-3): p. 67-80.
31. Gonzenbach, U.T., et al., *Ultrastable particle-stabilized foams*. Angewandte Chemie International Edition, 2006. **45**(21): p. 3526-3530.
32. Sadoc, J.-F. and N. Rivier, *Foams and emulsions*. Vol. 354. 2013: Springer Science & Business Media.

33. Weaire, D.L. and S. Hutzler, *The physics of foams*. 2001: Oxford University Press.
34. Xu, Q., et al., *Effects of surfactant and electrolyte concentrations on bubble formation and stabilization*. Journal of Colloid and Interface science, 2009. **332**(1): p. 208-214.
35. Exerowa, D. and P.M. Kruglyakov, *Foam and foam films: theory, experiment, application*. 1997: Elsevier.
36. Brugarolas, T., et al., *Generation of amphiphilic janus bubbles and their behavior at an air–water interface*. Advanced Functional Materials, 2011. **21**(20): p. 3924-3931.
37. Fameau, A.-L. and A. Salonen, *Effect of particles and aggregated structures on the foam stability and aging*. Comptes rendus physique, 2014. **15**(8-9): p. 748-760.
38. Arriaga, L.R., et al., *On the long-term stability of foams stabilised by mixtures of nano-particles and oppositely charged short chain surfactants*. Soft Matter, 2012. **8**(43): p. 11085-11097.
39. Germain, J.C. and J.M. Aguilera, *Structural Image Analysis of Food Foams and Aerated Food Products*, in *Bubbles in Food 2*. 2008, Elsevier. p. 109-116.
40. Zhou, J., P. Ranjith, and W. Wanniarachchi, *Different strategies of foam stabilization in the use of foam as a fracturing fluid*. Advances in colloid and interface science, 2020. **276**: p. 102104.
41. Saint-Jalmes, A., *Physical chemistry in foam drainage and coarsening*. Soft Matter, 2006. **2**(10): p. 836-849.
42. Schick, C., *A mathematical analysis of foam films*. 2004.
43. Cameron, E., et al., *Sclerosant foam structure and stability is strongly influenced by liquid air fraction*. European Journal of Vascular and Endovascular Surgery, 2013. **46**(4): p. 488-494.
44. Watkins, M.R. and R.J. Oliver, *Physiochemical properties and reproducibility of air-based sodium tetradecyl sulphate foam using the Tessari method*. Phlebology, 2017. **32**(6): p. 390-396.
45. Pugh, R., *Foaming, foam films, antifoaming and defoaming*. Advances in colloid and interface science, 1996. **64**: p. 67-142.
46. Derikvand, Z. and M. Riazi, *Experimental investigation of a novel foam formulation to improve foam quality*. Journal of Molecular Liquids, 2016. **224**: p. 1311-1318.
47. Drenckhan, W. and A. Saint-Jalmes, *The science of foaming*. Advances in Colloid and Interface Science, 2015. **222**: p. 228-259.
48. Malysa, K. and K. Lunkenheimer, *Foams under dynamic conditions*. Current Opinion in Colloid & Interface Science, 2008. **13**(3): p. 150-162.
49. Yang, J., V. Jovancicevic, and S. Ramachandran, *Foam for gas well deliquification*. Colloids and Surfaces A: Physicochemical and Engineering Aspects, 2007. **309**(1-3): p. 177-181.
50. Langevin, D., *Aqueous foams: a field of investigation at the frontier between chemistry and physics*. ChemPhysChem, 2008. **9**(4): p. 510-522.
51. Kume, G., M. Gallotti, and G. Nunes, *Review on anionic/cationic surfactant mixtures*. Journal of Surfactants and Detergents, 2008. **11**(1): p. 1-11.



52. Wouters, A.G., et al., *Foaming and air-water interfacial characteristics of solutions containing both gluten hydrolysate and egg white protein*. Food Hydrocolloids, 2018. **77**: p. 176-186.
53. Anazadehsayed, A., et al., *A review of aqueous foam in microscale*. Advances in colloid and interface science, 2018. **256**: p. 203-229.
54. Koelsch, P. and H. Motschmann, *Relating foam lamella stability and surface dilational rheology*. Langmuir, 2005. **21**(14): p. 6265-6269.
55. Saye, R.I. and J.A. Sethian, *Multiscale modelling of evolving foams*. Journal of Computational Physics, 2016. **315**: p. 273-301.
56. Fournier, J. and A. Cazabat, *Tears of wine*. EPL (Europhysics Letters), 1992. **20**(6): p. 517.
57. Pandey, S., R.P. Bagwe, and D.O. Shah, *Effect of counterions on surface and foaming properties of dodecyl sulfate*. Journal of colloid and interface science, 2003. **267**(1): p. 160-166.
58. Binks, B.P. and H. Shi, *Aqueous foams in the presence of surfactant crystals*. Langmuir, 2020. **36**(4): p. 991-1002.
59. Kim, S., H. Barraza, and O.D. Velev, *Intense and selective coloration of foams stabilized with functionalized particles*. Journal of Materials Chemistry, 2009. **19**(38): p. 7043-7049.
60. Binks, B.P., et al., *Dispersion behavior and aqueous foams in mixtures of a vesicle-forming surfactant and edible nanoparticles*. Langmuir, 2015. **31**(10): p. 2967-2978.
61. Law, B.M., et al., *Line tension and its influence on droplets and particles at surfaces*. Progress in surface science, 2017. **92**(1): p. 1-39.
62. Wang, A., W.B. Rogers, and V.N. Manoharan, *Effects of contact-line pinning on the adsorption of nonspherical colloids at liquid interfaces*. Physical review letters, 2017. **119**(10): p. 108004.
63. Bresme, F. and M. Oettel, *Nanoparticles at fluid interfaces*. Journal of Physics: Condensed Matter, 2007. **19**(41): p. 413101.
64. Binks, B.P. and T.S. Horozov, *Aqueous foams stabilized solely by silica nanoparticles*. Angewandte Chemie International Edition, 2005. **44**(24): p. 3722-3725.
65. Kralchevsky, P., et al., *On the thermodynamics of particle-stabilized emulsions: curvature effects and catastrophic phase inversion*. Langmuir, 2005. **21**(1): p. 50-63.
66. Banhart, J., M. Ashby, and N. Fleck, *International Conference on Cellular Metals and Metal Foaming Technology*. 2001.
67. Fujii, S. and Y. Nakamura, *Stimuli-responsive bubbles and foams stabilized with solid particles*. Langmuir, 2017. **33**(30): p. 7365-7379.
68. Stocco, A., et al., *Aqueous foams stabilized solely by particles*. Soft Matter, 2011. **7**(4): p. 1260-1267.
69. Rong, X., H. Yang, and N. Zhao, *Rationally turning the interface activity of mesoporous silicas for preparing Pickering foam and "dry water"*. Langmuir, 2017. **33**(36): p. 9025-9033.
70. Huang, J., et al., *pH-responsive gas-water-solid interface for multiphase catalysis*. Journal of the American Chemical Society, 2015. **137**(47): p. 15015-15025.

71. Safouane, M., D. Langevin, and B. Binks, *Effect of particle hydrophobicity on the properties of silica particle layers at the air– water interface*. Langmuir, 2007. **23**(23): p. 11546-11553.
72. Binks, B.P., M. Kirkland, and J.A. Rodrigues, *Origin of stabilisation of aqueous foams in nanoparticle–surfactant mixtures*. Soft Matter, 2008. **4**(12): p. 2373-2382.
73. Zhu, Y., et al., *Responsive aqueous foams stabilised by silica nanoparticles hydrophobised in situ with a switchable surfactant*. Soft Matter, 2014. **10**(48): p. 9739-9745.
74. Zhang, S., et al., *Aqueous foams stabilized with particles and nonionic surfactants*. Colloids and Surfaces A: Physicochemical and Engineering Aspects, 2008. **324**(1-3): p. 1-8.
75. Liu, Q., et al., *Foams stabilized by Laponite nanoparticles and alkylammonium bromides with different alkyl chain lengths*. Colloids and Surfaces A: Physicochemical and Engineering Aspects, 2010. **355**(1-3): p. 151-157.
76. Cui, Z.-G., et al., *Aqueous foams stabilized by in situ surface activation of CaCO<sub>3</sub> nanoparticles via adsorption of anionic surfactant*. Langmuir, 2010. **26**(15): p. 12567-12574.
77. Sheng, Y., et al., *Ultra-stable aqueous foams induced by interfacial co-assembly of highly hydrophobic particles and hydrophilic polymer*. Journal of Colloid and Interface Science, 2020. **579**: p. 628-636.
78. Horozov, T.S., *Foams and foam films stabilised by solid particles*. Current Opinion in Colloid & Interface Science, 2008. **13**(3): p. 134-140.
79. Mbamala, E. and H. Von Grünberg, *Effective interaction of a charged colloidal particle with an air-water interface*. Journal of Physics: Condensed Matter, 2002. **14**(19): p. 4881.
80. Yao, X., et al., *Control of particle adsorption for stability of Pickering emulsions in microfluidics*. Small, 2018. **14**(37): p. 1802902.
81. Liascukiene, I., et al., *Capture of colloidal particles by a moving microfluidic bubble*. Soft matter, 2018. **14**(6): p. 992-1000.
82. Kostakis, T., R. Ettelaie, and B.S. Murray, *Effect of high salt concentrations on the stabilization of bubbles by silica particles*. Langmuir, 2006. **22**(3): p. 1273-1280.
83. Zoueshtiagh, F., M. Baudoin, and D. Guerin, *Capillary tube wetting induced by particles: towards armoured bubbles tailoring*. Soft matter, 2014. **10**(47): p. 9403-9412.
84. Blázquez, C., et al., *Non-aqueous and crude oil foams*. Oil & Gas Science and Technology–Revue d'IFP Energies nouvelles, 2014. **69**(3): p. 467-479.
85. Brini, E., et al., *How water's properties are encoded in its molecular structure and energies*. Chemical reviews, 2017. **117**(19): p. 12385-12414.
86. Kauffman, G.W. and P.C. Jurs, *Prediction of surface tension, viscosity, and thermal conductivity for common organic solvents using quantitative structure– property relationships*. Journal of chemical information and computer sciences, 2001. **41**(2): p. 408-418.
87. Fameau, A.-L. and A. Saint-Jalmes, *Non-aqueous foams: Current understanding on the formation and stability mechanisms*. Advances in Colloid and Interface Science, 2017. **247**: p. 454-464.

88. Bergeron, V., J.E. Hanssen, and F. Shoghl, *Thin-film forces in hydrocarbon foam films and their application to gas-blocking foams in enhanced oil recovery*. Colloids and Surfaces A: Physicochemical and Engineering Aspects, 1997. **123**: p. 609-622.
89. Robb, I.D., *Specialist surfactants*. 1996: Springer Science & Business Media.
90. Bauget, F., D. Langevin, and R. Lenormand, *Dynamic surface properties of asphaltenes and resins at the oil–air interface*. Journal of Colloid and Interface Science, 2001. **239**(2): p. 501-508.
91. Zaki, N.N., M.K. Poindexter, and P.K. Kilpatrick, *Factors contributing to petroleum foaming. 2. Synthetic crude oil systems*. Energy & fuels, 2002. **16**(3): p. 711-717.
92. Binks, B., et al., *Non-aqueous foams in lubricating oil systems*. Colloids and Surfaces A: Physicochemical and Engineering Aspects, 2010. **360**(1-3): p. 198-204.
93. Binks, B.P., A. Rocher, and M. Kirkland, *Oil foams stabilised solely by particles*. Soft Matter, 2011. **7**(5): p. 1800-1808.
94. Binks, B.P. and A. Rocher, *Stabilisation of liquid–air surfaces by particles of low surface energy*. Physical Chemistry Chemical Physics, 2010. **12**(32): p. 9169-9171.
95. Murakami, R. and A. Bismarck, *Particle-Stabilized Materials: Dry Oils and (Polymerized) Non-Aqueous Foams*. Advanced Functional Materials, 2010. **20**(5): p. 732-737.
96. Binks, B.P., et al., *Particles at oil–air surfaces: powdered oil, liquid oil marbles, and oil foam*. ACS applied materials & interfaces, 2015. **7**(26): p. 14328-14337.
97. Binks, B.P. and A.T. Tyowua, *Influence of the degree of fluorination on the behaviour of silica particles at air–oil surfaces*. Soft Matter, 2013. **9**(3): p. 834-845.
98. Binks, B.P., T. Sekine, and A.T. Tyowua, *Dry oil powders and oil foams stabilised by fluorinated clay platelet particles*. Soft Matter, 2014. **10**(4): p. 578-589.
99. Dyab, A.K. and H.N. Al-Haque, *Particle-stabilised non-aqueous systems*. RSC Advances, 2013. **3**(32): p. 13101-13105.
100. Bai, X., et al., *Environmentally benign multiphase solid–liquid–gas catalysis*. Green Chemistry, 2020. **22**(3): p. 895-902.
101. Fameau, A.-L., et al., *Smart nonaqueous foams from lipid-based oleogel*. Langmuir, 2015. **31**(50): p. 13501-13510.
102. Binks, B.P., E.J. Garvey, and J. Vieira, *Whipped oil stabilised by surfactant crystals*. Chemical science, 2016. **7**(4): p. 2621-2632.
103. Liu, Y. and B.P. Binks, *A novel strategy to fabricate stable oil foams with sucrose ester surfactant*. Journal of Colloid and Interface Science, 2021. **594**: p. 204-216.
104. Shrestha, L.K., et al., *Stabilization of nonaqueous foam with lamellar liquid crystal particles in diglycerol monolaurate/olive oil system*. Journal of colloid and interface science, 2008. **328**(1): p. 172-179.
105. Shrestha, L.K., et al., *Foaming properties of monoglycerol fatty acid esters in nonpolar oil systems*. Langmuir, 2006. **22**(20): p. 8337-8345.

106. Hill, R.M., *Siloxane Surfactants*. 2019: Routledge.
107. Kamkar, M. and G. Natale, *A review on novel applications of asphaltenes: A valuable waste*. Fuel, 2021. **285**: p. 119272.
108. Qiao, P., et al., *Fractionation of asphaltenes in understanding their role in petroleum emulsion stability and fouling*. Energy & Fuels, 2017. **31**(4): p. 3330-3337.
109. Sun, X., et al., *Comprehensive experimental study of the interfacial stability of foamy oil and identification of the characteristic responsible for foamy oil formation*. Fuel, 2019. **238**: p. 514-525.
110. Buck, R.C., P.M. Murphy, and M. Pabon, *Chemistry, properties, and uses of commercial fluorinated surfactants*, in *Polyfluorinated chemicals and transformation products*. 2012, Springer. p. 1-24.
111. Binks, B.P. and B. Vishal, *Particle-stabilized oil foams*. Advances in Colloid and Interface Science, 2021: p. 102404.
112. Fox, H. and W. Zisman, *The spreading of liquids on low energy surfaces. I. polytetrafluoroethylene*. Journal of Colloid Science, 1950. **5**(6): p. 514-531.
113. Trambouze, P. and J.-P. Euzen, *Chemical reactors: from design to operation*. Vol. 16. 2004: Editions Technip.
114. Li, S., F. Xin, and L. Li, *Reaction engineering*. 2017: Butterworth-Heinemann.
115. Doran, P.M., *Bioprocess Engineering Principles*. Waltham, MA. 2013, USA: Elsevier Ltda.
116. Minakata, S. and M. Komatsu, *Organic reactions on silica in water*. Chemical Reviews, 2009. **109**(2): p. 711-724.
117. Di Dio, S., et al., *Simple and efficient water soluble thioligands for rhodium and iridium catalyzed biphasic hydrogenation*. Applied Catalysis A: General, 2011. **399**(1-2): p. 205-210.
118. Kobayashi, J., et al., *A microfluidic device for conducting gas-liquid-solid hydrogenation reactions*. Science, 2004. **304**(5675): p. 1305-1308.
119. Irfan, M., T.N. Glasnov, and C.O. Kappe, *Heterogeneous catalytic hydrogenation reactions in continuous-flow reactors*. ChemSusChem, 2011. **4**(3): p. 300-316.
120. Gutmann, B., D. Cantillo, and C.O. Kappe, *Continuous-flow technology—a tool for the safe manufacturing of active pharmaceutical ingredients*. Angewandte Chemie International Edition, 2015. **54**(23): p. 6688-6728.
121. Reif, M. and R. Dittmeyer, *Porous, catalytically active ceramic membranes for gas-liquid reactions: a comparison between catalytic diffuser and forced through flow concept*. Catalysis today, 2003. **82**(1-4): p. 3-14.
122. Stevenson, P., *Foam engineering: fundamentals and applications*. 2012: John Wiley & Sons.
123. Kolev, N.I., *Solubility of O<sub>2</sub>, N<sub>2</sub>, H<sub>2</sub> and CO<sub>2</sub> in water*, in *Multiphase Flow Dynamics 4*. 2011, Springer. p. 209-239.

124. Li, Y.H. and T.F. Tsui, *The solubility of CO<sub>2</sub> in water and sea water*. Journal of Geophysical research, 1971. **76**(18): p. 4203-4207.
125. Clever, H.L., *Argon*. Vol. 4. 2013: Elsevier.
126. Huang, Z., et al., *Sustainable catalytic oxidation of alcohols over the interface between air and water*. Green Chemistry, 2015. **17**(4): p. 2325-2329.
127. Miyatake, K., et al., *Aromatic ionomers with superacid groups*. Chemical communications, 2009(42): p. 6403-6405.
128. Dou, Y., et al., *5-Hydroxymethylfurfural production from dehydration of fructose catalyzed by Aquivion® silica solid acid*. Fuel, 2018. **214**: p. 45-54.
129. Giancola, S., et al., *Study of annealed Aquivion® ionomers with the INCA method*. Membranes, 2019. **9**(10): p. 134.
130. Fang, W., et al., *Silica-immobilized Aquivion PFSA superacid: application to heterogeneous direct etherification of glycerol with n-butanol*. Catalysis Science & Technology, 2015. **5**(8): p. 3980-3990.
131. Andreoli, S., et al., *Superacid Aquivion® PFSA as an efficient catalyst for the gas phase dehydration of ethanol to ethylene in mild conditions*. Applied Catalysis A: General, 2020. **597**: p. 117544.
132. Karam, A., et al., *High catalytic performance of aquivion PFSA, a reusable solid perfluorosulfonic acid polymer, in the biphasic glycosylation of glucose with fatty alcohols*. ACS Catalysis, 2017. **7**(4): p. 2990-2997.
133. Karam, A., et al., *Impact of shaping Aquivion PFSA on its catalytic performances*. Catalysis Science & Technology, 2019. **9**(5): p. 1231-1237.
134. Karam, A., et al., *Mechanocatalytic depolymerization of cellulose with perfluorinated sulfonic acid ionomers*. Frontiers in chemistry, 2018. **6**: p. 74.
135. Paris, E., et al., *Silica Nanoparticles Decorated with Polymeric Sulfonic Acids Trigger Selective Oxidation of Benzylic Methylenes to Aldehydic and Ketonic Carbonyls*. ACS Sustainable Chemistry & Engineering, 2019. **7**(6): p. 5886-5891.
136. Shi, H., et al., *Aquivion Perfluorosulfonic Superacid as an Efficient Pickering Interfacial Catalyst for the Hydrolysis of Triglycerides*. ChemSusChem, 2017. **10**(17): p. 3363-3367.
137. Zhang, S., et al., *Aquivion–Carbon Composites with Tunable Amphiphilicity for Pickering Interfacial Catalysis*. ACS applied materials & interfaces, 2018. **10**(31): p. 26795-26804.
138. Fang, W., et al., *Aquivion®–carbon composites via hydrothermal carbonization: amphiphilic catalysts for solvent-free biphasic acetalization*. Journal of Materials Chemistry A, 2016. **4**(12): p. 4380-4385.
139. Hoffmann, F., et al., *Silica-based mesoporous organic–inorganic hybrid materials*. Angewandte Chemie International Edition, 2006. **45**(20): p. 3216-3251.

140. Ferré, M., et al., *Recyclable organocatalysts based on hybrid silicas*. *Green chemistry*, 2016. **18**(4): p. 881-922.
141. Chen, Y. and J. Shi, *Chemistry of mesoporous organosilica in nanotechnology: molecularly organic–inorganic hybridization into frameworks*. *Advanced Materials*, 2016. **28**(17): p. 3235-3272.
142. Kresge, C.T. and W.J. Roth, *The discovery of mesoporous molecular sieves from the twenty year perspective*. *Chemical Society Reviews*, 2013. **42**(9): p. 3663-3670.
143. Croissant, J.G., et al., *Syntheses and applications of periodic mesoporous organosilica nanoparticles*. *Nanoscale*, 2015. **7**(48): p. 20318-20334.
144. Teng, Z., et al., *Mesoporous organosilica hollow nanoparticles: synthesis and applications*. *Advanced Materials*, 2019. **31**(38): p. 1707612.
145. Ha, C.-S. and S.S. Park, *Periodic Mesoporous Organosilicas*. 2019: Springer.
146. Li, X., Y. Yang, and Q. Yang, *Organo-functionalized silica hollow nanospheres: synthesis and catalytic application*. *Journal of Materials Chemistry A*, 2013. **1**(5): p. 1525-1535.
147. Ciriminna, R., et al., *The sol–gel route to advanced silica-based materials and recent applications*. *Chemical reviews*, 2013. **113**(8): p. 6592-6620.
148. Putz, A.-M., et al., *Functionalized silica materials synthesized via co-condensation and post-grafting methods*. *Fullerenes, Nanotubes and Carbon Nanostructures*, 2019. **27**(4): p. 323-332.
149. Stöber, W., A. Fink, and E. Bohn, *Controlled growth of monodisperse silica spheres in the micron size range*. *Journal of colloid and interface science*, 1968. **26**(1): p. 62-69.
150. Hoffmann, F. and M. Fröba, *Vitalising porous inorganic silica networks with organic functions—PMOs and related hybrid materials*. *Chemical Society Reviews*, 2011. **40**(2): p. 608-620.
151. Corriu, R.J., et al., *New mixed organic-inorganic polymers: hydrolysis and polycondensation of bis (trimethoxysilyl) organometallic precursors*. *Chemistry of materials*, 1992. **4**(6): p. 1217-1224.
152. Dral, A.P., C. Lievens, and J.E. ten Elshof, *Influence of monomer connectivity, network flexibility, and hydrophobicity on the hydrothermal stability of organosilicas*. *Langmuir*, 2017. **33**(22): p. 5527-5536.
153. Li, H., et al., *Functionalized silica nanoparticles: classification, synthetic approaches and recent advances in adsorption applications*. *Nanoscale*, 2021.
154. Van Der Voort, P., et al., *Periodic mesoporous organosilicas: from simple to complex bridges; a comprehensive overview of functions, morphologies and applications*. *Chemical Society Reviews*, 2013. **42**(9): p. 3913-3955.
155. Rodriguez, A.M.B. and B.P. Binks, *Catalysis in Pickering emulsions*. *Soft Matter*, 2020.
156. Binks, B.P. and S. Lumsdon, *Influence of particle wettability on the type and stability of surfactant-free emulsions*. *Langmuir*, 2000. **16**(23): p. 8622-8631.

157. Zhou, W.-J., et al., *Tunable catalysts for solvent-free biphasic systems: Pickering interfacial catalysts over amphiphilic silica nanoparticles*. Journal of the American Chemical Society, 2014. **136**(13): p. 4869-4872.
158. Yang, H., T. Zhou, and W. Zhang, *A Strategy for Separating and Recycling Solid Catalysts Based on the pH-Triggered Pickering-Emulsion Inversion*. Angewandte Chemie International Edition, 2013. **52**(29): p. 7455-7459.
159. Huang, J. and H. Yang, *A pH-switched Pickering emulsion catalytic system: high reaction efficiency and facile catalyst recycling*. Chemical Communications, 2015. **51**(34): p. 7333-7336.
160. Binks, B.P., et al., *Phase inversion of particle-stabilised perfume oil–water emulsions: experiment and theory*. Physical Chemistry Chemical Physics, 2010. **12**(38): p. 11954-11966.
161. Binks, B.P., J. Philip, and J.A. Rodrigues, *Inversion of silica-stabilized emulsions induced by particle concentration*. Langmuir, 2005. **21**(8): p. 3296-3302.
162. Wei, L., et al., *Pickering emulsion as an efficient platform for enzymatic reactions without stirring*. ACS Sustainable Chemistry & Engineering, 2016. **4**(12): p. 6838-6843.
163. Chen, H., et al., *Flow Pickering emulsion interfaces enhance catalysis efficiency and selectivity for cyclization of citronellal*. ChemSusChem, 2017. **10**(9): p. 1989-1995.
164. Bago Rodriguez, A.M., et al., *Effect of Particle Wettability and Particle Concentration on the Enzymatic Dehydration of n-Octanaloxime in Pickering Emulsions*. Angewandte Chemie International Edition, 2021. **60**(3): p. 1450-1457.
165. Zhao, Y., et al., *Hydroformylation of 1-octene in Pickering emulsion constructed by amphiphilic mesoporous silica nanoparticles*. Journal of Catalysis, 2016. **334**: p. 52-59.
166. Tao, L., et al., *Heterogeneous hydroformylation of long-chain alkenes in IL-in-oil Pickering emulsion*. Green Chemistry, 2018. **20**(1): p. 188-196.
167. Chen, S., et al., *A simple strategy towards the preparation of a highly active bifunctionalized catalyst for the deacetalization reaction*. Applied Catalysis A: General, 2016. **513**: p. 47-52.
168. Yang, B., et al., *Acidic/amphiphilic silica nanoparticles: new eco-friendly Pickering interfacial catalysis for biodiesel production*. Green Chemistry, 2017. **19**(19): p. 4552-4562.
169. Yang, B., et al., *Colloidal tectonics for tandem synergistic Pickering interfacial catalysis: oxidative cleavage of cyclohexene oxide into adipic acid*. Chemical science, 2019. **10**(2): p. 501-507.
170. Shi, H., et al., *Glycerol/Dodecanol Double Pickering Emulsions Stabilized by Polystyrene-Grafted Silica Nanoparticles for Interfacial Catalysis*. ChemCatChem, 2015. **7**(20): p. 3229-3233.
171. Yang, Y., et al., *Amphiphilic titanosilicates as Pickering interfacial catalysts for liquid-phase oxidation reactions*. The Journal of Physical Chemistry C, 2015. **119**(45): p. 25377-25384.
172. Fujii, S., et al., *Gas bubbles stabilized by Janus particles with varying hydrophilic–hydrophobic surface characteristics*. Langmuir, 2018. **34**(3): p. 933-942.

173. Yang, T., et al., *Dumbbell-Shaped Bi-component Mesoporous Janus Solid Nanoparticles for Biphase Interface Catalysis*. *Angewandte Chemie International Edition*, 2017. **56**(29): p. 8459-8463.
174. Liu, Y., et al., *Preparation of Janus-type catalysts and their catalytic performance at emulsion interface*. *Journal of colloid and interface science*, 2017. **490**: p. 357-364.
175. Greydanus, B., D.K. Schwartz, and J.W. Medlin, *Controlling catalyst-phase selectivity in complex mixtures with amphiphilic janus particles*. *ACS applied materials & interfaces*, 2019. **12**(2): p. 2338-2345.
176. Xue, W., H. Yang, and Z. Du, *Synthesis of pH-responsive inorganic Janus nanoparticles and experimental investigation of the stability of their Pickering emulsions*. *Langmuir*, 2017. **33**(39): p. 10283-10290.
177. Zhang, M., et al., *An ionic liquid-functionalized amphiphilic Janus material as a Pickering interfacial catalyst for asymmetric sulfoxidation in water*. *Chemical Communications*, 2019. **55**(5): p. 592-595.
178. Wang, J., et al., *Oriented enzyme immobilization at the oil/water interface enhances catalytic activity and recyclability in a pickering emulsion*. *Langmuir*, 2017. **33**(43): p. 12317-12325.
179. Yan, S., et al., *Janus mesoporous silica nanosheets with perpendicular mesochannels: affording highly accessible reaction interfaces for enhanced biphasic catalysis*. *Chemical Communications*, 2018. **54**(74): p. 10455-10458.
180. Dai, J., et al., *Janus N-doped carbon@ silica hollow spheres as multifunctional amphiphilic nanoreactors for base-free aerobic oxidation of alcohols in water*. *ACS applied materials & interfaces*, 2018. **10**(39): p. 33474-33483.
181. Zhao, T., et al., *Spatial isolation of carbon and silica in a single Janus mesoporous nanoparticle with tunable amphiphilicity*. *Journal of the American Chemical Society*, 2018. **140**(31): p. 10009-10015.
182. Dou, S.-Y. and R. Wang, *The C-Si Janus nanoparticles with supported phosphotungstic active component for Pickering emulsion desulfurization of fuel oil without stirring*. *Chemical Engineering Journal*, 2019. **369**: p. 64-76.
183. Xue, F., et al., *Tuning the interfacial activity of mesoporous silicas for biphasic interface catalysis reactions*. *ACS applied materials & interfaces*, 2017. **9**(9): p. 8403-8412.
184. Li, S., X. Jiao, and H. Yang, *Hydrophobic core/hydrophilic shell structured mesoporous silica nanospheres: enhanced adsorption of organic compounds from water*. *Langmuir*, 2013. **29**(4): p. 1228-1237.
185. Zou, H., et al., *An organosilane-directed growth-induced etching strategy for preparing hollow/yolk-shell mesoporous organosilica nanospheres with perpendicular mesochannels and amphiphilic frameworks*. *Journal of Materials Chemistry A*, 2014. **2**(31): p. 12403-12412.



186. Ding, Y., et al., *An amphiphilic composite material of titanasilicate@ mesosilica/carbon as a Pickering catalyst*. Chemical Communications, 2018. **54**(57): p. 7932-7935.
187. Yu, H., et al., *An amphiphilic organosilicon framework (AOF): a new solid Pickering catalyst carrier*. Inorganic Chemistry Frontiers, 2019. **6**(5): p. 1253-1260.
188. Walther, A. and A.H. Muller, *Janus particles: synthesis, self-assembly, physical properties, and applications*. Chemical reviews, 2013. **113**(7): p. 5194-5261.
189. Agrawal, G. and R. Agrawal, *Janus nanoparticles: Recent advances in their interfacial and biomedical applications*. ACS Applied Nano Materials, 2019. **2**(4): p. 1738-1757.
190. Aveyard, R., *Can Janus particles give thermodynamically stable Pickering emulsions?* Soft Matter, 2012. **8**(19): p. 5233-5240.
191. Yang, H., X. Jiao, and S. Li, *Hydrophobic core–hydrophilic shell-structured catalysts: a general strategy for improving the reaction rate in water*. Chemical Communications, 2012. **48**(91): p. 11217-11219.

## **CHAPTER 2**

---

### **Materials & Methods**

---

## 2.1 Introduction

This chapter lists the materials, characterization techniques and preparation methods of particles and foams used in the thesis.

## 2.2 Chemicals

All chemicals were used without further purification (**Table 2.1**).

**Table 2.1** Summary of the chemicals used in this thesis.

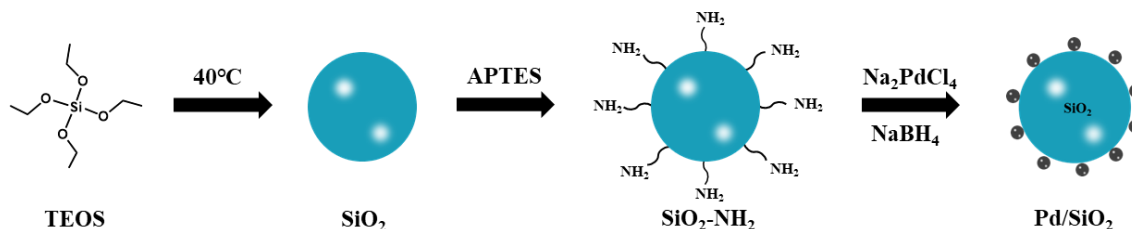
Chemical name	Abbreviation	Purity, %	Company
Ethanol	-	95	
Ethyl acetate	-	98	
Ammonium hydroxide	NH <sub>3</sub> ·H <sub>2</sub> O	25-28	
Sodium borohydride	NaBH <sub>4</sub>	98	
Sodium hydroxide	NaOH	96	
Ethylenediamine	EDA	99	
Dodecyltrimethylammnium bromide	DTAB	99	
Sodium dodecyl sulfate	SDS	99	Sinopharm Chemical Reagent Co., Ltd
Acetophenone	AP	99	
Anisole	-	99	
Phenyl acetate	PA	99	
Ethylbenzene	EB	98	
Toluene	-	99.5	
Tetrahydrofurfuryl alcohol	THFA	98	
Cyclopentanone	CP	97	
1-Octanol	-	99	
Sodium dodecylbenzenesulfonate	SDBS	-	
Polyoxyethylene (10) tridecyl ether	POTE	-	
Myristic acid	MA	99	Sigma-Aldrich
Polystyrene	PS	Mw = 35,000	
PSS-octaphenyl substituted	POSS	-	
Bis(trimethoxysilylethyl)benzene	BTMEB	95	
p-Methoxyphenyltriethoxysilane	MPTES	97	Gelest Inc.
4,4'-Bis(triethoxysilyl)-1,1'- biphenyl	BTEBP	-	Fluorochem Ltd.

**Table 2.1** (Continued)

Chemical name	Abbreviation	Purity, %	Company
Benzyl alcohol	BZA	99.5	
Benzaldehyde	BA	98	
Nitrobenzene	NB	99	
Aniline	-	99	
Iodobenzene	IB	97.5	
Pyridine	-	99	
Furfuryl alcohol	FA	98	
m-Xylene	-	99	
Ethylene glycol	EG	99.5	
1,5-Pentanediol	PD	98	
N,N-dimethylformamide	DMF	99.8	
Perfluorooctanoic acid	PFOA	98	
Trifluoromethanesulfonic acid	TFSA	99	
1,4-Bis(triethoxysilyl)benzene	BTEB	96	Beijing J&K Scientific Ltd
Tetraethyl orthosilicate	TEOS	98	
1H,1H,2H,2H- Perfluorodecyltriethoxysilane	-	97	
Triethoxyphenylsilane	TEPS	98	
Trimethoxy(propyl)silane	TMPS	98	
Trimethoxy(hexyl)silane	TMHS	97	
(3-Mercaptopropyl) trimethoxysilane	MPTMES	95	
Trimethoxy(3,3,3- trifluoropropyl)silane	TMFPS	97	
(3-Aminopropyl)triethoxysilane	APTES	98	
Sodium tetrachloropalladate(II)	Na <sub>2</sub> PdCl <sub>4</sub>	99.9	
Benzaldehyde dimethyl acetal	-	97.5	
Polytetrafluoroethylene	PTFE	Particle size: 5 μm	Aladdin Company
Acetone-d <sub>6</sub>	-	99.9 atom %D	Adamas-beta
Aquivion® D98-20BS dispersion in water	D98	Solid content: 19.3 wt%, acid loading: 1.0 mmol·g <sup>-1</sup> Equivalent weight: 980	Solvay Specialty Polymers
Aquivion® PW98 in powder form	PW98	g·eq <sup>-1</sup> , acid loading: 1.0 mmol·g <sup>-1</sup>	

### 2.3 Preparation of Pd/SiO<sub>2</sub> catalyst

The Pd/SiO<sub>2</sub> catalyst was synthesized in three steps (**Figure 2.1**): (1) preparation of silica particles by the Stöber method, (2) surface modification of silica particles with amino groups, and (3) immobilization of palladium nanoparticles on the silica particles. The detailed descriptions of synthetic methods are given in the following paragraphs.



**Figure 2.1** Preparation of Pd/SiO<sub>2</sub> catalyst.

Monodisperse silica particles were prepared by a modified Stöber method [1]. Briefly, 3 mL of TEOS was added to a mixture of 37 mL of ethanol, 5 mL of water and 1.6 mL of ammonia hydroxide solution (28 wt%) in a glass flask. After mixing at 40 °C for 2 h, the silica particles were collected by centrifuging and washed three times with ethanol and water.

To functionalize the surface of silica particles with amino groups, 0.6 g of silica particles was dispersed in 50 mL of ethanol by sonication in a water bath. Then, 0.3 mL of APTES was added under stirring. After stirring continuously for 24 h, the product was separated by centrifugation and washed with ethanol. After drying at 80 °C overnight, amino-functionalized silica particles (SiO<sub>2</sub>-NH<sub>2</sub>) were obtained.

Palladium was further supported over the amino-functionalized silica (Pd/SiO<sub>2</sub>) by conventional impregnation and subsequent NaBH<sub>4</sub> reduction [2-4]. First, 0.5 g of SiO<sub>2</sub>-NH<sub>2</sub> particles was dispersed in a mixture of 20 mL of ethanol and 15 mL of H<sub>2</sub>O by ultrasonication. Then a solution of Na<sub>2</sub>PdCl<sub>4</sub> (1 mL, 14 mg·mL<sup>-1</sup>) was added into this suspension and stirred at room temperature for 30 min. Afterwards, an aqueous NaBH<sub>4</sub> solution (4 mL, 100 mM) was slowly added into the mixed solution. After 2 h stirring, the solid was separated by centrifugation and washed with a mixture of water and ethanol. Finally, the resulting Pd/SiO<sub>2</sub> catalyst was obtained after drying at 80 °C overnight.

### 2.4 General procedure for one-pot cascade reaction

The cascade reaction of benzaldehyde dimethyl acetal to benzyl alcohol was carried out as follows: 10 mg of Pd/SiO<sub>2</sub> catalyst, 0.5 mmol of benzaldehyde dimethyl acetal, 2 mL of H<sub>2</sub>O and 210 mg of Aquivion<sup>®</sup> D98-20BS-P (~ 10 wt%) were added into a 10 mL glass vial. After

purging several times with H<sub>2</sub>, the pressure was raised to 1.5 bar, and the reaction was performed at room temperature at a stirring rate of 700 rpm (IKA Magnetic Stirrers C-MAG HS 7 control). After the reaction, an aqueous NaOH solution (1.25 M) was added until neutral pH, the mixture was extracted with ethyl acetate and analyzed by gas chromatography using an Agilent 7890 GC equipped with a HP-5 capillary column (30 m × 0.32 mm, 0.25 μm film thickness). Besides, the catalytic activity for the second hydrogenation step was investigated at the same reaction conditions using benzaldehyde as reactant.

## 2.5 Preparation of bridged organosilica particles from bissilylated precursors

The bridged organosilica particles were synthesized from bissilylated organic precursors following a modified Stöber method [1, 5]. In a typical synthesis, 1 mL of BTEBP was rapidly added into a mixture of ethanol (12 mL), deionized water (1.6 mL) and NH<sub>3</sub>·H<sub>2</sub>O (0.5 mL). The mixture was then vigorously stirred at 35 °C for 3 h, resulting in a precipitate. The as-prepared material was isolated by centrifugation and washed three times with ethanol. After drying at 80 °C overnight, biphenyl-bridged particles (denoted as br-BiPh) were obtained. The synthetic procedure for phenyl-bridged particles (br-Ph) and phenylethyl-bridged particles (br-PhEt) was similar to that for br-BiPh, except for the substitution of BTEBP with BTEB and BTMEB, respectively.

In order to load the palladium on the biphenyl-bridged particles, it is necessary to functionalize the surface of the particles with thiol or amino groups. Briefly, 41 μl of (3-mercaptopropyl)trimethoxysilane (MPTMES) and 1 mL of BTEBP were used as co-precursors to prepared the thiol-functionalized organosilicas (BiPh-SH) under the same condition. Afterwards, 0.2 g of BiPh-SH was dispersed in 20 mL of acetone, and a solution of Na<sub>2</sub>PdCl<sub>4</sub> (0.4 ml, 14 mg·ml<sup>-1</sup>) was added quickly. After stirring for 2 h, a reducing agent of 1 ml NaBH<sub>4</sub> solution (0.1 M) was added to the mixture dropwise. The mixture was then stirred continuously for 2 h. The solid product (Pd/BiPh) was isolated by centrifugation and dried at 80 °C overnight.

For comparison, fluorinated silica particles (SiO<sub>2</sub>-F<sub>17</sub>) were prepared by sol-gel process. Typically, 4 mL of TEOS, 80 mL of ethanol, 11.2 mL of deionized water and 3.2 mL NH<sub>3</sub>·H<sub>2</sub>O were mixed at 40 °C for 5 min. Then, a mixture of 1H,1H,2H,2H-perfluorodecyltriethoxysilane (1.97 mL) and (3-mercaptopropyl)trimethoxysilane (0.27 mL) was added under rapid stirring, and the solution was reacted for 30 min. The solid samples were collected by centrifugation and washed three times with ethanol. After drying at 80 °C overnight, the fluorinated silica particles were obtained.

## 2.6 Preparation of alkyl-modified organosilicas from phenyltriethoxysilane

Alkyl-modified organosilicas were prepared using triethoxyphenylsilane (TEPS), trimethoxy(propyl)silane (TMPS) and trimethoxy(hexyl)silane (THPS) as precursors. For the synthesis of PhC<sub>3</sub>, 12 mL of ethanol, 1.6 mL of deionized water, and 0.5 mL of NH<sub>3</sub>·H<sub>2</sub>O were mixed at room temperature. Then, 2 mL of TEPS and 1.5 mL of TMPS were rapidly added and the reaction was left under stirring for 20 h. The final product was obtained after washing with ethanol and drying overnight. For synthesis of PhC<sub>6</sub>, the volume of mixed precursors was 2 mL of TEPS and 1.9 mL of THPS. Finally, for the synthesis of unmodified organosilicas (Ph), 2 mL of TEPS was used.

## 2.7 Preparation of fluorinated silica particles

In a typical synthesis, 4 mL of TEOS, 80 mL of ethanol, 11.2 mL of deionized water and 3.2 mL of NH<sub>3</sub>·H<sub>2</sub>O were mixed at 40 °C for 5 min. Then, a mixture of 1H,1H,2H,2H-perfluorodecyltriethoxysilane (1.97 mL) and (3-mercaptopropyl)triethoxysilane (0.27 mL) was added under vigorous stirring, and the solution was reacted for 30 min. The solid samples were collected by centrifugation and washed three times with ethanol. After drying at 80 °C overnight, the fluorinated silica particles (SiO<sub>2</sub>-F<sub>17</sub>) were obtained.

The fluorinated organosilica particles were synthesized from the cohydrolysis of p-methoxyphenyltriethoxysilane (MPTES) with trimethoxy(3,3,3-trifluoropropyl)silane (TMFPS) in the basic medium. In a typical synthesis, 12 mL of ethanol, 1.6 mL of deionized water, and 0.5 mL of NH<sub>3</sub>·H<sub>2</sub>O were mixed at room temperature. Afterwards, a mixture of MPTES (0.5 mL) and TMFPS (0.18 mL) were rapidly added and the reaction was left under stirring for 24 h. The final product (denoted as MeOPhF<sub>3</sub>) was obtained after washing with ethanol and drying overnight. For comparison, non-fluorinated organosilica particles (MeOPhC<sub>3</sub>) were prepared using MPTES and TMPS as co-precursors under the same conditions.

To support immobilization of palladium particles, the bifunctional organosilica particles were prepared by direct co-condensation of (3-mercaptopropyl) trimethoxysilane (60 μl), MPTES (0.5 mL) and TMFPS (0.18 mL). The obtained solid product was denoted as PhF<sub>3</sub>-SH. Afterwards, the palladium supported on fluorinated organosilica particles (Pd/PhF<sub>3</sub>) were prepared by the conventional impregnation and subsequent NaBH<sub>4</sub> reduction method [2-4]. 0.2 g of PhF<sub>3</sub>-SH was dispersed in 20 mL of acetone by ultrasonication. Then a solution of Na<sub>2</sub>PdCl<sub>4</sub> (0.4 ml, 14 mg·ml<sup>-1</sup>) was added and stirred at room temperature for 2 h. Then, 0.1 M NaBH<sub>4</sub> solution (1 ml) was slowly added into the suspension. After stirring for 2 h, the solid samples were isolated by centrifugation and dried at 80 °C overnight.

## **2.8 Characterization techniques**

### **2.8.1 Transmission electronic microscopy**

The morphology of the as-prepared materials was investigated by transmission electron microscopy (TEM) using a JEOL JEM-2100 microscope operating at 200 kV. The samples were dispersed in acetone and then deposited on a carbon grid for observation.

### **2.8.2 Thermogravimetric analysis**

Thermogravimetric analysis (TGA) is an analytical technique used to determine the thermal stability of the materials [6, 7]. The test was carried out on a TA SDT Q600 Instrument by heating the samples from the room temperature to 900 °C at a rate of 10 °C·min<sup>-1</sup> in air.

### **2.8.3 Fourier-transform infrared spectra**

Fourier-transform infrared (FT-IR) spectra were recorded using a Thermo Scientific Nicolet iS50 equipped with an ATR accessory and operating in the range of 400-4000 cm<sup>-1</sup>.

### **2.8.4 Nuclear magnetic resonance**

<sup>13</sup>C and <sup>29</sup>Si CP-MAS solid-state NMR spectra were recorded on a Bruker AVANCE III 500 MHz spectrometer. <sup>13</sup>C and <sup>29</sup>Si liquid-state NMR spectra were recorded on a Bruker 600 MHz instrument using acetone d<sub>6</sub> as a solvent.

### **2.8.5 X-ray photoelectron spectroscopy**

X-ray photoelectron spectroscopy (XPS) is a commonly used technique for surface analysis, it can provide valuable quantitative and chemical state information from the surface to a depth of approximately 10 nm [8, 9].

XPS analyses were performed with a Thermo Scientific K-Alpha+ XPS instrument equipped with a micro-focused monochromatic Al K $\alpha$  X-ray source (1486.6 eV).

### **2.8.6 Inductively coupled plasma-optical emission spectrometry**

The Pd content of the catalysts was quantified using inductively coupled plasma-optical emission spectroscopy (ICP-OES 5800, Agilent Technologies). Before the measurements, the samples were dissolved using a HNO<sub>3</sub>/HF solution.

### **2.8.7 Dynamic light scattering**

Dynamic light scattering (DLS) is a noninvasive technique for characterizing the particle size distribution in suspension, taking only minutes for a measurement [10, 11]. It requires only a small volume of sample for analysis. The particles dispersed in liquid undergo a Brownian



motion due to random collisions with solvents. When a monochromatic light beam hits a solution containing spherical particles in Brownian motion, the wavelength of the incoming light is changed [12]. This change in wavelength is related to the size of the particles. It is possible to calculate the sphere size distribution by measuring the diffusion coefficient of the particle and using the autocorrelation function.

The DLS measurements of particle dispersions were carried out using a Malvern Zetasizer Nano ZS particle size analyzer at 25 °C.

### **2.8.8 Zeta potential**

The Zeta potential is commonly used to determine the surface charge of particles in a colloidal solution. From a theoretical viewpoint, the charged particle attracts a thin layer of opposite charge and firmly binds to it, forming a thin liquid layer named the Stern layer [13]. When the particle diffuses in solution, it will generate an outer diffuse layer (slipping plane) that consists of loosely associated ions. The electrostatic potential at this idealized slipping plane is termed the zeta potential, which depends on the composition and environment of the particles [14].

The surface charge of silica particles in aqueous suspensions was determined by zeta potential measurement on a Malvern Zetasizer Nano ZS apparatus. The measurement was repeated three times and the average from them was reported as final result.

### **2.8.9 Gel permeation chromatography**

Gel permeation chromatography (GPC) analysis is widely used to measure the molecular weight of polymers due to its relatively low cost and simplicity [15, 16]. It is based on the separation by molecular size rather than chemical properties of polymers or proteins [17]. A typical GPC instrument consists of a solvent pump, a sample injector, a thermostated column compartment, and a refractive index detector [18]. GPC employs the principle of size exclusion chromatography, which involves passage of a dilute polymer solution over a column of porous beads (stationary phase) [19]. An important step is dissolving the samples in a suitable solvent. Larger molecules (high-molecular-weight polymers) will be excluded from the stationary phase and elute first, whereas smaller molecules (lower-molecular-weight polymers) pass through the pores of the stationary phase. Therefore, solute polymers with a small size compared to the column pore size, will elute last from the column. Comparison of the elution time of the samples with those of monodisperse samples of known molecular weight allows determination of the entire molecular weight distribution.

The number- and weight-average molecular weights ( $M_n$  and  $M_w$ ) were acquired on a Malvern GPCmax equipped with Waters Styragel HT column eluted with N,N-dimethylacetamide (DMAc) containing 0.01 M LiBr at a flow rate of  $0.8 \text{ mL} \cdot \text{min}^{-1}$  calibrated by standard polystyrene samples.

### **2.8.10 Contact angle**

The contact angle is a measure of the wettability of a solid by a liquid. Consider a liquid drop resting on a flat and horizontal solid surface. The contact angle is defined as the angle formed by the intersection of the liquid-solid and the liquid-vapor interfaces (geometrically acquired by applying a tangent line from the contact point along the liquid-vapor interface in the droplet profile) [20].

The contact angles were measured at room temperature using the Attension Theta T200 optical tensiometer (Biolin Scientific) equipped with a video capture device. Typically, a drop of solvent was placed on the pellets made by compressing the samples in a 1.3 cm diameter steel die under a pressure of 5 Tons.

### **2.8.11 Surface tension**

The surface tension is a force that tends to minimize the surface area of liquids, causing individual liquid drops to round up and also causes the molecules of two immiscible liquids to sort out from one another when mixed [21]. Liquid surface tension results from intermolecular attractive forces that pull the individual liquid molecules toward one another. The molecules exposed at the surface do not have neighboring liquid molecules in all directions to provide a balanced net force. Instead, they are pulled inward by the neighboring molecules, creating an internal pressure. As a result, the liquid voluntarily contracts its surface area to maintain the lowest surface free energy [20].

The surface tension of the samples in benzyl alcohol were measured using a force tensiometer with a platinum Wilhelmy plate (Sigma 700, Biolin Scientific) at  $25 \text{ }^\circ\text{C}$ . The plate was flushed with ethanol before heating it red hot to ensure it was properly cleaned. The rate of immersion-emersion was  $20 \text{ mm} \cdot \text{min}^{-1}$  in benzyl alcohol, the wetting depth was 6 mm, and the stabilization and integration time is 4 s. The surface tension of the samples was measured three times to ensure proper repeatability.

### **2.8.12 Optical microscopy**

The foams obtained with Aquivion<sup>®</sup> PFSA and organosilicas were placed on glass microscope slides, and the images were captured under an Olympus IX-51 light transmission

microscope equipped with 10× ocular, 4× and 10× objectives. Olympus cellSens Standard software was used for size measurements, and ImageJ software was applied to quantify the size of bubbles.

## 2.9 Preparation of foams using different methods

### 2.9.1 Hand shaking

Typically, 20 mg of samples and 2 mL of solvent (1 wt%) were added into a 4 mL glass vial. After ultrasonication for 10 min, the vial was sealed and vigorously hand shaken for 30 s to produce the foam. This procedure allowed the reproducible preparation of foams.

### 2.9.2 High speed homogenizer

To achieve controlled and high energy input, we used a high-speed homogenizer (IKA Ultra-Turrax<sup>®</sup>T25 equipped with S25N-8G dispersing tool, **Figure 2.2**) to produce foams. In these tests, a certain amount of samples was dispersed in 2 mL of benzyl alcohol, and the dispersion was aerated at 16,000 rpm for 3 min.



**Figure 2.2** Appearance of Ultra-Turrax<sup>®</sup>T25 homogenizer.

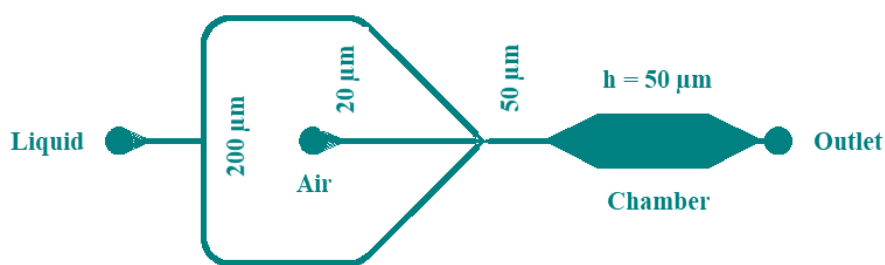
### 2.9.3 Microfluidics

Microfluidics can be used to produce highly-controlled dispersions of a gas in a liquid [22, 23]. Rapid generation of small and extremely monodisperse bubbles can be achieved using chips [24, 25]. Using purpose-designed microfluidic devices, the mixing of chemicals and gas and liquid flow rates can be readily adjusted to investigate the foaming properties.

Unlike materials such as silicon and glass, poly(dimethylsiloxane) (PDMS) offers intriguing advantages for chip manufacture. PDMS is non-toxic and readily available from commercial sources at acceptable prices, and it enables rapid prototyping of microfluidic devices in few

hours [26]. Another advantage of PDMS comes from its high elasticity (with a shear modulus of 0.25 MPa and a Young's modulus of roughly 0.5 MPa), which is useful for manufacturing and sealing microfluidic systems [27].

**Figure 2.3** shows the design of the microfluidic device (50  $\mu\text{m}$  in depth and 200  $\mu\text{m}$  wide for the channels), which was fabricated with PDMS using standard soft lithography methods in the clean room [28-33].



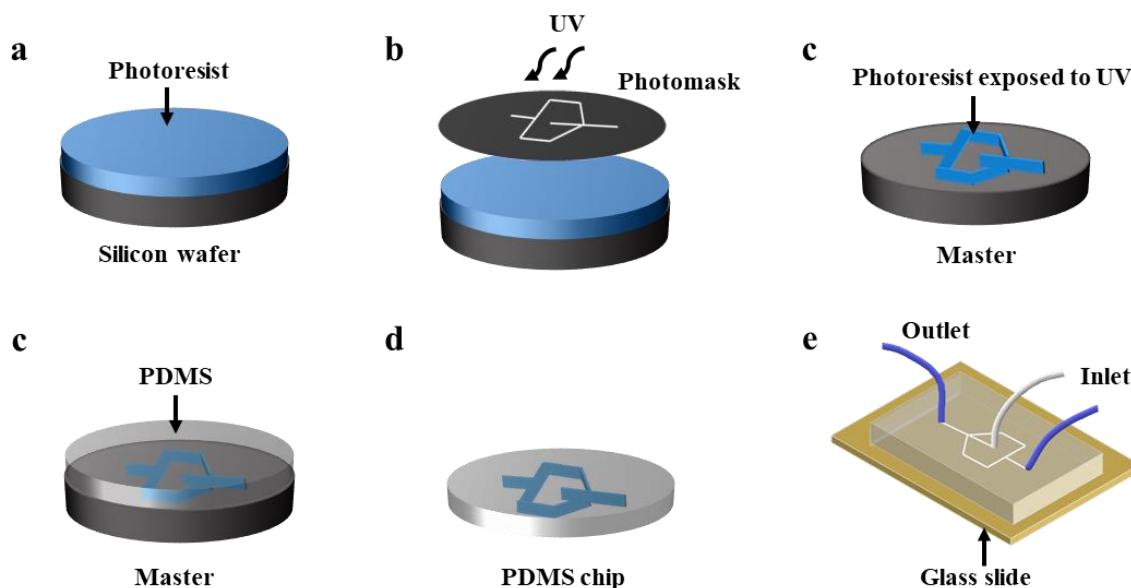
**Figure 2.3** The design of the microfluidic chip.

The fabrication process is represented in **Figure 2.4**. First, SU-8 master was prepared on a silicon wafer. Prior to processing, it is important to ensure wafers are clean. The negative photoresist (SU-8 3025, MicroChem Corp.) was spin-coated on the silicon wafer, and baked on a hotplate at 95 °C for 15 min to evaporate the solvent and densify the film. After cooling down to room temperature, the wafer was exposed to UV light through a photomask (MJB3 contact mask aligner, SUSS MicroTec). The post exposure bake (PEB) was subsequently carried out at 95 °C for 3 min to cross-link exposed regions [34, 35]. Finally, non-cross-linked polymer was washed out by SU-8 developer (PEGMEA, MicroChem Corp.), the wafer was rinsed with isopropyl alcohol and deionized water and dried with nitrogen gas. At the end, SU-8 master was silanized with HMDS (hexamethyldisilazane, Sigma Aldrich) at 95 °C for 1 h to prevent PDMS bonding to the master.

PDMS chip fabrication was carried out as following. A curing agent was mixed with PDMS base (Sylgard 184 silicone elastomer kit, Dow Corning Corp.) in a 1:10 ratio (w/w). The mixture was degassed under vacuum to remove air bubbles and poured onto the master. The mold was incubated for at least two h at 65 °C for PDMS cross-linking. The solid elastomer was carefully cut, peeled off and the inlet and outlet holes were punched for fluidic access. Finally, the PDMS slab patterned with desired channels and a glass slide were treated with oxygen plasma (Plasma Cleaner PDC-002-CE, Harrick Plasma at 600 mbar for 1 min) and bound together.

Microfluidic PDMS chips were used for bubble generation immediately after the oxygen plasma treatment. The foam stabilizers were first dispersed in benzyl alcohol by sonication, affording a uniform suspension. To operate the device, the dispersion was injected using

computer-controlled syringe pumps (2.5 mL, CETONI Nemesys), and the air flowrate was controlled by EL-FLOW® Prestige Mass Flow Meters/Controllers.



**Figure 2.4** Schematic illustration of the procedures for fabricating PDMS chips.

## 2.10 References

1. Stöber, W., A. Fink, and E. Bohn, *Controlled growth of monodisperse silica spheres in the micron size range*. Journal of colloid and interface science, 1968. **26**(1): p. 62-69.
2. Bulut, A., et al., *Pd-MnOx nanoparticles dispersed on amine-grafted silica: highly efficient nanocatalyst for hydrogen production from additive-free dehydrogenation of formic acid under mild conditions*. Applied Catalysis B: Environmental, 2015. **164**: p. 324-333.
3. Yuan, M., et al., *Ultra-fine Pd nanoparticles confined in a porous organic polymer: A leaching-and-aggregation-resistant catalyst for the efficient reduction of nitroarenes by NaBH<sub>4</sub>*. Journal of colloid and interface science, 2019. **538**: p. 720-730.
4. Celebi, M., et al., *Palladium nanoparticles supported on amine-functionalized SiO<sub>2</sub> for the catalytic hexavalent chromium reduction*. Applied Catalysis B: Environmental, 2016. **180**: p. 53-64.
5. Zou, H., et al., *An organosilane-directed growth-induced etching strategy for preparing hollow/yolk-shell mesoporous organosilica nanospheres with perpendicular mesochannels and amphiphilic frameworks*. Journal of Materials Chemistry A, 2014. **2**(31): p. 12403-12412.
6. Hunkel, M., H. Surm, and M. Steinbacher, *Handbook of Thermal Analysis and Calorimetry*. 2018, Elsevier: Amsterdam, The Netherlands.
7. Zafeiropoulos, N.E., *Interface engineering of natural fibre composites for maximum performance*. 2011: Elsevier.

8. Tougaard, S., *Accuracy of the non-destructive surface nanostructure quantification technique based on analysis of the XPS or AES peak shape*. Surface and Interface Analysis: An International Journal devoted to the development and application of techniques for the analysis of surfaces, interfaces and thin films, 1998. **26**(4): p. 249-269.
9. Tabačiarová, J., et al., *Study of polypyrrole aging by XPS, FTIR and conductivity measurements*. Polymer Degradation and Stability, 2015. **120**: p. 392-401.
10. Nickel, C., et al., *Dynamic light-scattering measurement comparability of nanomaterial suspensions*. Journal of nanoparticle research, 2014. **16**(2): p. 1-12.
11. Kaszuba, M., et al., *Measuring sub nanometre sizes using dynamic light scattering*. Journal of nanoparticle research, 2008. **10**(5): p. 823-829.
12. Chirayil, C.J., et al., *Instrumental techniques for the characterization of nanoparticles*, in *Thermal and Rheological Measurement Techniques for Nanomaterials Characterization*. 2017, Elsevier. p. 1-36.
13. Shnoudeh, A.J., et al., *Synthesis, characterization, and applications of metal nanoparticles*, in *Biomaterials and bionanotechnology*. 2019, Elsevier. p. 527-612.
14. Lowry, G.V., et al., *Guidance to improve the scientific value of zeta-potential measurements in nanoEHS*. Environmental Science: Nano, 2016. **3**(5): p. 953-965.
15. Montaudo, G., et al., *Molecular and structural characterization of polydisperse polymers and copolymers by combining MALDI-TOF mass spectrometry with GPC fractionation*. Macromolecules, 1995. **28**(24): p. 7983-7989.
16. Kissin, Y., *Molecular weight distributions of linear polymers: detailed analysis from GPC data*. Journal of Polymer Science Part A: Polymer Chemistry, 1995. **33**(2): p. 227-237.
17. Ugbolue, S.C., *Polyolefin fibres: Structure, properties and industrial applications*. 2017: Woodhead Publishing.
18. Dragostin, O. and L. Profire, *Molecular weight of polymers used in biomedical applications*, in *Characterization of Polymeric Biomaterials*. 2017, Elsevier. p. 101-121.
19. ALEXANDER, H., et al., *Classes of materials used in medicine*, in *Biomaterials Science*. 1996, Elsevier. p. 37-130.
20. Yuan, Y. and T.R. Lee, *Contact angle and wetting properties*, in *Surface science techniques*. 2013, Springer. p. 3-34.
21. Harris, A.K., *Is cell sorting caused by differences in the work of intercellular adhesion? A critique of the Steinberg hypothesis*. Journal of theoretical biology, 1976. **61**(2): p. 267-285.
22. Huerre, A., V. Miralles, and M.-C. Jullien, *Bubbles and foams in microfluidics*. Soft matter, 2014. **10**(36): p. 6888-6902.
23. Hashimoto, M., P. Garstecki, and G.M. Whitesides, *Synthesis of composite emulsions and complex foams with the use of microfluidic flow-focusing devices*. small, 2007. **3**(10): p. 1792-1802.

24. Arriaga, L.R., et al., *On the long-term stability of foams stabilised by mixtures of nano-particles and oppositely charged short chain surfactants*. *Soft Matter*, 2012. **8**(43): p. 11085-11097.
25. Mao, X., et al., *Milliseconds microfluidic chaotic bubble mixer*. *Microfluidics and Nanofluidics*, 2010. **8**(1): p. 139-144.
26. Ren, K., J. Zhou, and H. Wu, *Materials for microfluidic chip fabrication*. *Accounts of chemical research*, 2013. **46**(11): p. 2396-2406.
27. Clarson, S. and J. Semlyen, *In Siloxane Polymers; PTR Prentice Hall. Inc.:* Englewood Cliffs, New Jersey, 1993.
28. Qin, D., Y. Xia, and G.M. Whitesides, *Soft lithography for micro-and nanoscale patterning*. *Nature protocols*, 2010. **5**(3): p. 491.
29. Xia, Y. and G.M. Whitesides, *Soft Lithography*. *Angew. Chem. Int. Ed*, 1998. **37**: p. 550-575.
30. San-Miguel, A. and H. Lu, *Microfluidics as a tool for C. elegans research*. *WormBook: The Online Review of C. elegans Biology [Internet]*, 2018.
31. Prado, E., et al., *SERS spectra of oligonucleotides as fingerprints to detect label-free RNA in microfluidic devices*. *The Journal of Physical Chemistry C*, 2014. **118**(25): p. 13965-13971.
32. Beneyton, T., et al., *CotA laccase: high-throughput manipulation and analysis of recombinant enzyme libraries expressed in E. coli using droplet-based microfluidics*. *Analyst*, 2014. **139**(13): p. 3314-3323.
33. Ma, K., et al., *Wettability control and patterning of PDMS using UV–ozone and water immersion*. *Journal of colloid and interface science*, 2011. **363**(1): p. 371-378.
34. Tao, S.L., K. Papat, and T.A. Desai, *Off-wafer fabrication and surface modification of asymmetric 3D SU-8 microparticles*. *Nature protocols*, 2006. **1**(6): p. 3153-3158.
35. Chung, S. and S. Park, *Effects of temperature on mechanical properties of SU-8 photoresist material*. *Journal of Mechanical Science and Technology*, 2013. **27**(9): p. 2701-2707.

## **CHAPTER 3**

---

### **Foams Stabilized by Aquivion® PFSA**

---



### 3.1 Introduction

Gas-liquid-solid (G-L-S) catalytic reactions are widespread in the chemical industry for the synthesis of fine chemicals and depollution [1-3]. Typical examples of G-L-S reactions are the hydrodesulfurization of naphtha, the partial oxidation of liquid hydrocarbons with air or oxygen, and the wet air oxidation of pollutants for water remediation [4-6]. Conventional G-L-S catalytic reactors comprise packed beds (*e.g.*, trickle beds and bubble columns), stirred tank and bubble column slurry reactors and fluidized beds [7]. These technologies usually suffer from low gas solubility in liquids, and mass/heat transfer limitations due to their low G-L and L-S specific interface areas [8-10]. As a way out of this problem, continuous flow microreactors, catalytic membrane reactors and microbubble generator can promote the G-L interfacial area and enhance catalytic reactions [11-15], but require complex equipment. Therefore, it is highly desirable to develop a simple and cheap strategy to achieve better catalytic performance.

Liquid foams are multiphase systems consisting of dispersed gas bubbles in a continuous liquid phase [16-19]. Aqueous foams can be readily stabilized by a variety of surface-active particles, including partially hydrophobic silicas, polymers and surfactant crystals [20-24]. In contrast, fewer reports are available on non-aqueous foams due to the low surface tension of organic liquids [25]. Since the particles coated by hydrocarbon-containing groups can be wetted by many oils, the preparation of particle-stabilized oil foams is much more challenging than for aqueous foams [17, 26]. To generate some repellency against oil on particle surface, fluorinated particles (*e.g.*, polytetrafluoroethylene, oligomeric tetrafluoroethylene and particles bearing fluorocarbon chains) have been recently used to stabilize non-aqueous foams [27-30]. Owing to the low surface energy of fluoro groups, stable air-in-oil foams can be obtained in oils of intermediate tension. However, few efforts have been devoted to oil foams in polar solvents (*e.g.*, ethanol and benzyl alcohol) [31, 32].

Particle-stabilized foams can be used to engineer G-L-S catalytic microreactors with an enhanced triphasic contact at the nanoscale. Yuan and co-workers synthesized particles based on monodisperse Au nanoparticles embedded in polyoxometalate anion  $[PV_2Mo_{10}O_{40}]^{5-}$  assembled with rigid tripodal ligand by electrostatic interactions [33]. The multifunctional catalyst could self-assemble at the  $O_2$ /water interface, stabilizing the bubbles. This catalytic process shows high activity in the oxidation of aliphatic/aromatic alcohols into aldehydes and ketones. Similarly, Yang and co-workers synthesized silica particles modified with octyl and triamine groups stabilizing gas bubbles in water [34]. By incorporating Pd or Au nanoparticles, the particles became active for aqueous hydrogenation and oxidation reactions in  $H_2$  and  $O_2$

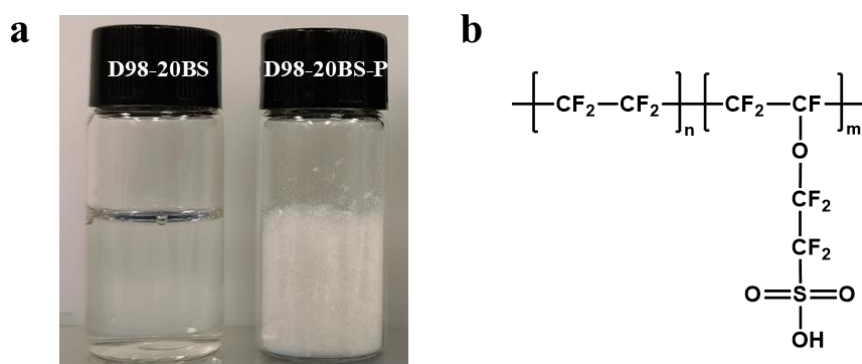
foams, respectively, under stirring at high particle concentration (7.5-12.5 wt%). The catalytic foams exhibited an enhanced activity compared to conventional multiphase reactors, which is attributed to the pronounced increase in reaction interface area.

Aquivion® PFSA is a family of perfluorosulfonic superacid resins with an acid strength comparable to that of sulphuric acid (Hammett acidity  $\sim -12$ ) [35, 36]. It is a copolymer of tetrafluoroethylene and the sulfonyl fluoride vinyl ether produced by Solvay Specialty Polymers. Aquivion® PFSA solid catalyst, formulated as coarsely grained powder (*e.g.*, PW98), has been studied for catalysis in a variety of acid-catalysed reactions [37-39]. On the other hand, Aquivion® PFSA dispersion (*e.g.*, D98) has an affinity to both water and hydrophobic substrates [40, 41]. Aquivion® PFSA has demonstrated surface activity for stabilizing emulsions, affording biphasic reactions at the oil/water and oil/oil interface [42-44]. We hypothesize that this unique property may offer the possibility of stabilizing foams both in water and organic solvents.

In this chapter, we first investigated the foaming behavior of an Aquivion® PFSA dispersion in a variety of solvents. The key parameters controlling foamability and foam stability were studied systematically. Afterwards, based on the acidic properties of Aquivion® D98-20BS-P, as well as its unique surface-active properties, we constructed a foaming system for one-pot cascade deacetalization and hydrogenation reactions by synergistically combining Aquivion® D98-20BS-P with a heterogeneous palladium catalyst.

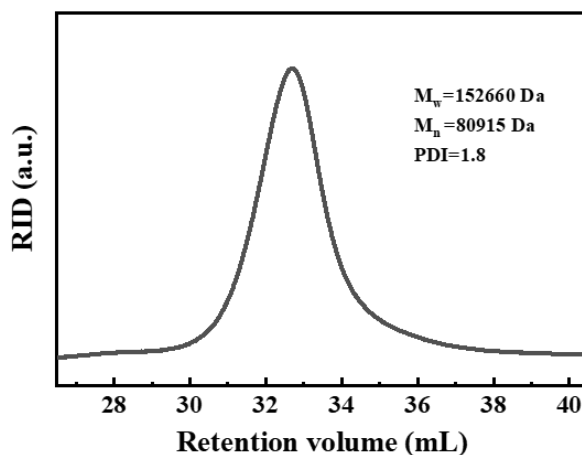
### 3.2 Characterization of Aquivion® D98-20BS-P

To obtain a surface-active material allowing the generation of stable foams, an Aquivion® D98-20BS dispersion (solid content: 19.3 wt%, acid loading:  $1.0 \text{ mmol}\cdot\text{g}^{-1}$ ) was lyophilized overnight to remove water. A photograph of the resulting product is displayed in **Figure 3.1a**.



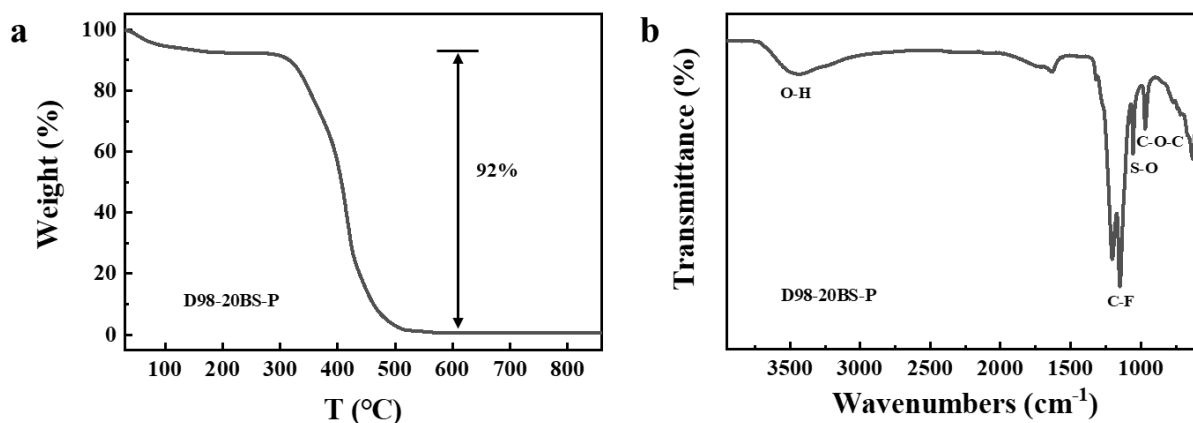
**Figure 3.1** The appearance of the D98-20BS dispersion before and after freeze-drying (a), and the structure of Aquivion® PFSA (b).

The structure of Aquivion® PFSA is shown in **Figure 3.1b**, where typically  $n$  has a value of about eight, with  $m$  has a value about two [45, 46]. The average molecular weight of D98-20BS-P was determined by gel permeation chromatography (GPC). The weight-average molecular weight ( $M_w$ ) relative to polystyrene standards was 152 kDa with a polydispersity index (PDI) of 1.8 (**Figure 3.2**).



**Figure 3.2** Gel permeation chromatography of D98-20BS-P.

The thermal properties of D98-20BS-P were measured by TG analysis, and the thermal profile matches well the experimental measurements of Aquivion® PW98 reported in previous studies [35, 43, 44]. As shown in **Figure 3.3a**, there are two primary mass loss processes. The initial weight loss below 160 °C can be attributed to the evaporation of adsorbed water. Then, a significant weight loss occurs in the range 280-550 °C that can be attributed to the decomposition of the side chain and perfluorocarbon backbone.

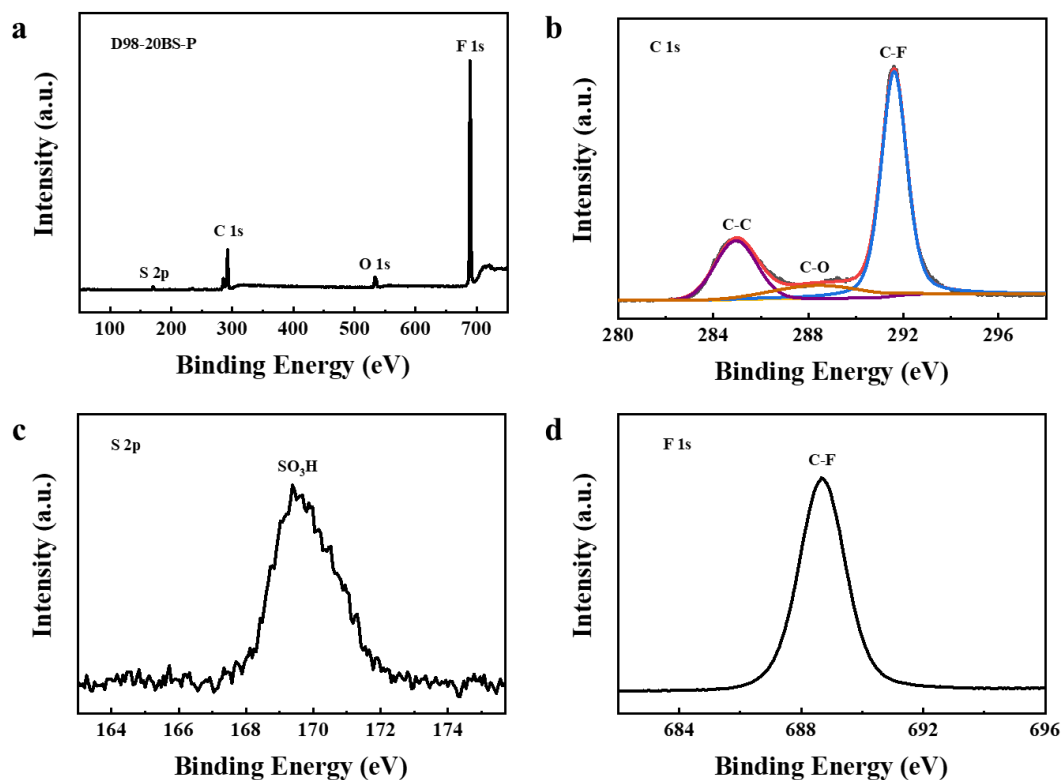


**Figure 3.3** TG profiles (a) and FT-IR spectra of D98-20BS-P (b).

The surface composition of D98-20BS-P was inspected by FT-IR spectroscopy (**Figure**

**3.3b).** The IR spectrum shows two intense peaks at  $1147\text{ cm}^{-1}$  and  $1203\text{ cm}^{-1}$ , which are ascribed to C-F stretching vibrations [35, 47]. The medium intensity peak at around  $1050\text{ cm}^{-1}$  is attributed to the asymmetric stretching in the sulfonic group [48]. Besides, a band attributed to C-O-C species is visible at  $968\text{ cm}^{-1}$ . Finally, the broad band in the region of  $3800\text{--}2800\text{ cm}^{-1}$  belongs to O-H stretching vibrations, which reflects the hydrophilic behavior of the sample.

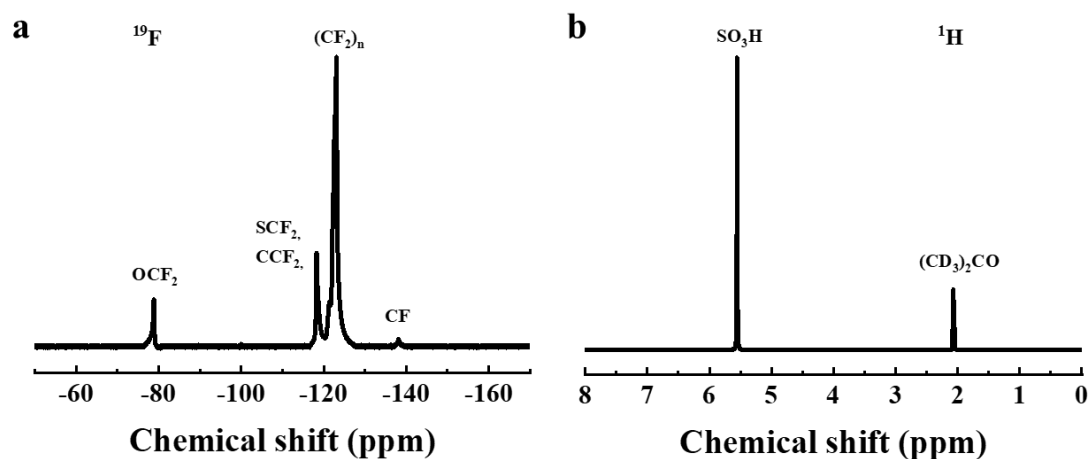
XPS measurements were carried out to gain insight into the chemical composition of Aquivion® D98-20BS-P. The bands in the wide scan of D98-20BS-P confirm the presence of C, O, S and F elements (**Figure 3.4a**). Generally, the C 1s spectrum can be deconvoluted into three different bands with binding energies of 284.9, 288.4 and 291.6 eV, corresponding to skeletal C-C bonds, C-O bonds in the side chains and in the perfluorocarbon backbone ( $\text{CF}_2\text{-CF}_2$ ), respectively [43, 49, 50]. The peak visible at around 169.3 eV can be attributed to sulfonic acid groups [50, 51]. Meanwhile, the F 1s spectrum of D98-20BS-P exhibits a single and symmetric peak at 688.6 eV that is ascribed to fluorine atoms present in the polymer backbone (**Figure 3.4d**).



**Figure 3.4** XPS patterns of D98-20BS-P: survey spectra (a), C 1s spectrum (b), S 2p spectrum (c), and F 1s spectrum (d).

The structural feature of D98-20BS-P was further investigated by liquid NMR (**Figure 3.5**). The  $^{19}\text{F}$  NMR spectra are consistent with earlier reports on Aquivion® PFSA [44, 52]. The

resonance bands at -78.8 and -138.1 ppm are signatures of OCF<sub>2</sub> groups in side chains and CF groups in the backbone of Aquivion® PFSA, respectively. A band centered at 123.1 ppm is clearly visible and can be ascribed to the CF<sub>2</sub>-CF<sub>2</sub> unit in fluoropolymers [53, 54]. In addition, the signal at -118.3 ppm corresponds to SCF<sub>2</sub> and CCF<sub>2</sub> groups. The <sup>1</sup>H NMR spectrum displays a band centered at 5.6 ppm revealing the presence of SO<sub>3</sub>H groups.

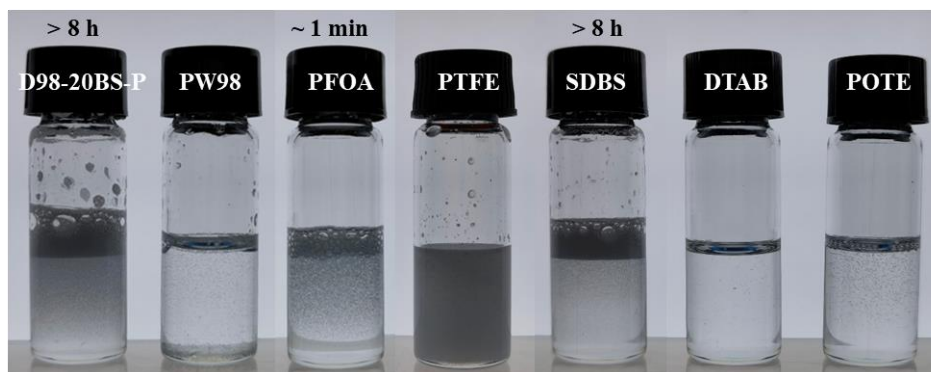


**Figure 3.5** Liquid-state <sup>19</sup>F (a) and <sup>1</sup>H (b) NMR spectra of D98-20BS-P.

### 3.3 Foaming studies of Aquivion® D98-20BS-P

Previous studies have demonstrated that polytetrafluoroethylene (PTFE) and fluorinated particles can stabilize the foams in solvents of intermediate surface tension (26-45 mN·m<sup>-1</sup>) [26-29]. For instance, the stable air-in-oil foams have been achieved based on some aromatic solvents (*e.g.*, toluene, benzene, benzyl acetate) in the presence of fluorinated particles. Nonetheless, very few studies have focused on the stabilization of foams in aromatic solvents with relatively high polarity (*e.g.*, benzyl alcohol and aniline) [32].

The foaming properties of Aquivion® D98-20BS-P was studied in benzyl alcohol by hand shaking. Afterwards, we compared the foaming performance to that of other stabilizers, including Aquivion® PW98 (in powder form), perfluorooctanoic acid (PFOA), PTFE, sodium dodecylbenzenesulfonate (SDBS), dodecyltrimethylammonium bromide (DTAB) and polyoxyethylene (10) tridecyl ether (POTE). As shown in **Figure 3.6**, only D98-20BS-P, SDBS and PFOA exhibit good foamability in the benzyl alcohol, which can be attributed to a decrease of surface tension of benzyl alcohol (**Table 3.1**). It is known that fluorinated surfactants (*e.g.*, PFOA) can lower the surface tension of liquids due to their fluorocarbon moieties (**Table 3.1, entry 3**) [25, 55]. However, in our case, the foam lifetime with PFOA is much lower (~1 min) compared to that of D98-20BS-P and SDBS (longer than 8 h).



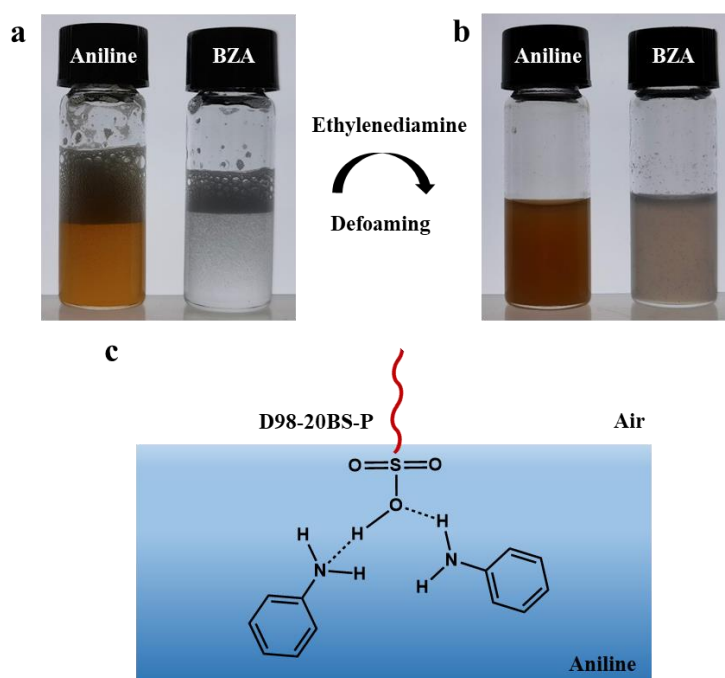
**Figure 3.6** Foamability of different stabilizers in benzyl alcohol (1%) after hand shaking.

**Table 3.1** Surface tension of benzyl alcohol after the addition of different materials.

Entry	Sample	Surface tension ( $\text{mN}\cdot\text{m}^{-1}$ )
1	Pure benzyl alcohol	38.9
2	1% D98-20BS-P in benzyl alcohol	<b>33.6</b>
3	1% PFOA in benzyl alcohol	<b>31.4</b>
4	1% SDBS in benzyl alcohol	<b>36.4</b>
5	1% PW98 in benzyl alcohol	38.3
6	1% PTFE in benzyl alcohol	38.7
7	1% DTAB in benzyl alcohol	38.7
8	1% POTE in benzyl alcohol	38.6

Unlike Aquivion® D98, Aquivion® PW98 is characterized by a high degree of polymer crystallinity, and the bad foamability is attributed to its poor dispersity in benzyl alcohol. In addition, commercial PTFE without amphiphilic properties exerts no effect on the surface tension ( $38.7 \text{ mN}\cdot\text{m}^{-1}$ ), thus no foam is produced in benzyl alcohol. The cationic and nonionic surfactants, such as DTAB and POTE, have been widely used in aqueous systems for their excellent foaming properties [56, 57]. However, none of them can reduce the surface tension and stabilize foams in benzyl alcohol.

In order to elucidate the fundamental mechanisms of foam formation, we performed a simple neutralization test by adding a small amount of organic base (**Figure 3.7**). Foams in benzyl alcohol were completely destabilized after the addition of ethylenediamine ( $10 \mu\text{L}$ ), forming a turbid suspension (**Figure 3.7b**). As a moderately strong base, ethylenediamine ( $\text{p}K_{\text{b}} = 4.7$ ) has the ability to react with the sulfonic acid groups of Aquivion® D98-20BS-P to yield insoluble salts. As a result, no foams could be obtained in this system. This indicates that the presence of sulfonic acid groups incorporated in D98-20BS-P is crucial for foam formation.



**Figure 3.7** Foams stabilized by 1% D98-20BS-P before (a) and after (b) adding ethylenediamine, and proposed interaction of D98-20BS-P with aniline at the interface (c). Thin dashed lines represent hydrogen bonds.

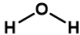
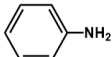
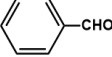
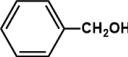
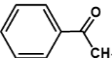
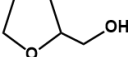
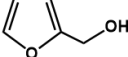
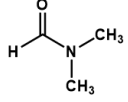
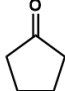
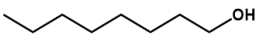

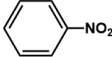
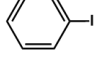
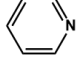
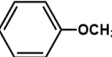
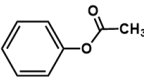
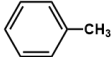
Since the basicity appears to be an important parameter governing the foaming properties, weakly basic aniline ( $\text{pK}_b = 9.3$ ) was used as solvent to investigate the foaming behavior of D98-20BS-P. Unlike benzyl alcohol, a higher foam volume was obtained in aniline (**Figure 3.7a**), which is possibly attributed to the stronger interaction between aniline and D98-20BS-P. Given the fact that no precipitate was generated in this foaming system, we assume that intermolecular hydrogen bonds could be formed between  $-\text{SO}_3\text{H}$  groups of D98-20BS-P and  $-\text{NH}_2$  groups of aniline (**Figure 3.7c**). When ethylenediamine was added into the above foaming system, the hydrogen bonds were broken and no foam could ever be obtained.

### 3.3.1 Effect of solvent type

To confirm our hypothesis, we further studied the foaming behavior of Aquivion® D98-20BS-P in a variety of solvents, ranging from non-polar hydrocarbons to polar oils and water (**Table 3.2**). Protic solvents such as water and ethanol can donate protons by hydrogen bonding [58, 59], which could facilitate foam formation (**Figure 3.8a**). Indeed, the foam volume increases dramatically by increasing the D98-20BS-P concentration from 1 wt% to 10 wt% in water. Among the different solvents, the best foaming performance is observed with aniline,

both in terms of foamability and foam stability (half-life time is longer than 12 h), keeping the concentration of D98-20BS-P (1 wt%) constant. As mentioned above, the strong interaction between aniline and D98-20BS-P is probably responsible for such excellent foaming properties. Indeed, the amino groups in the molecules can act as proton acceptors ( $N \cdots HB$ ) and donors ( $NH \cdots B$ , B stands for an acceptor) simultaneously in the H-bonded complexes [60-62].

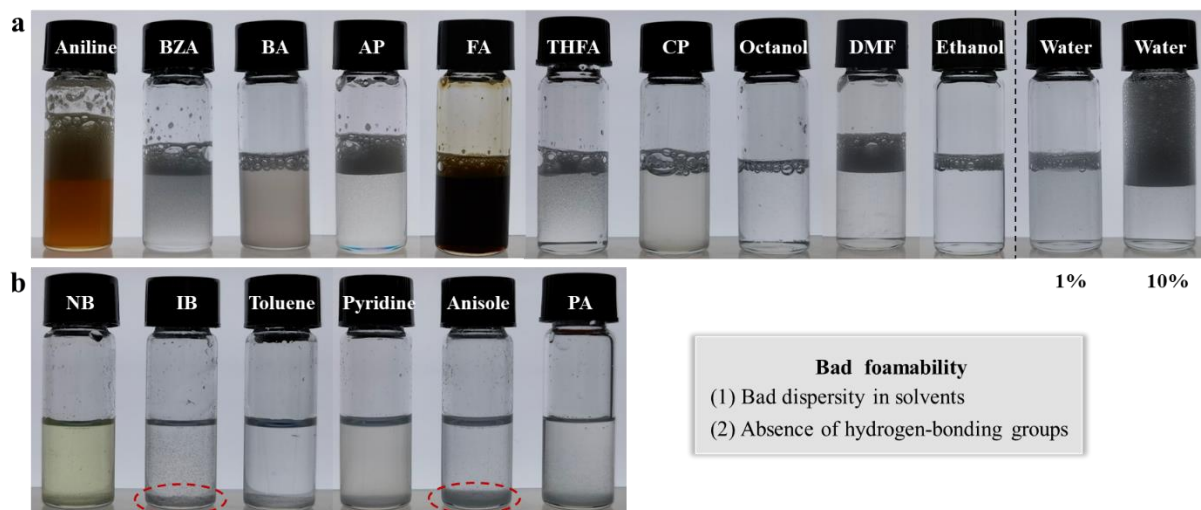
**Table 3.2** Properties and foaming behavior of solvents in the presence of 1 wt% D98-20BS-P.

Name (abbreviation)	Structure	Surface tension (mN·m <sup>-1</sup> , 20 °C)	V <sub>foam</sub> /V <sub>liquid</sub> <sup>a</sup>	Foam half-life time <sup>b</sup>
Water		72.8	0.18	20 min
Aniline		43.4	0.80	> 12 h
Benzaldehyde (BA)		40	0.18	~ 2 min
Benzyl alcohol (BZA)		39.5	0.41	6 h
Acetophenone (AP)		39.04	0.46	1 h
Tetrahydrofurfuryl alcohol (THFA)		38.3	0.27	40 min
Furfuryl alcohol (FA)		38	0.25	40 min
Dimethylformamide (DMF)		37.1	0.49	20 min
Cyclopentanone (CP)		33.1	0.29	1 h
1-Octanol		27.6	0.10	~ 1 min
Ethanol		22.3	0.18	~ 1 min
Nitrobenzene (NB)		43.9	0	0
Iodobenzene (IB)		39.7	0	0
Pyridine		38	0	0
Anisole		35	0	0
Phenyl acetate (PA)		34.9	0	0
Toluene		28.4	0	0

<sup>a</sup> V<sub>foam</sub>/V<sub>liquid</sub> (“foamability”) = foam volume/initial volume of solvent

<sup>b</sup> The foam half-life time is the time where the foam height decreased to half its original value.





**Figure 3.8** Photographs of vessels containing different solvents and D98-20BS-P (1 wt%) after hand shaking.

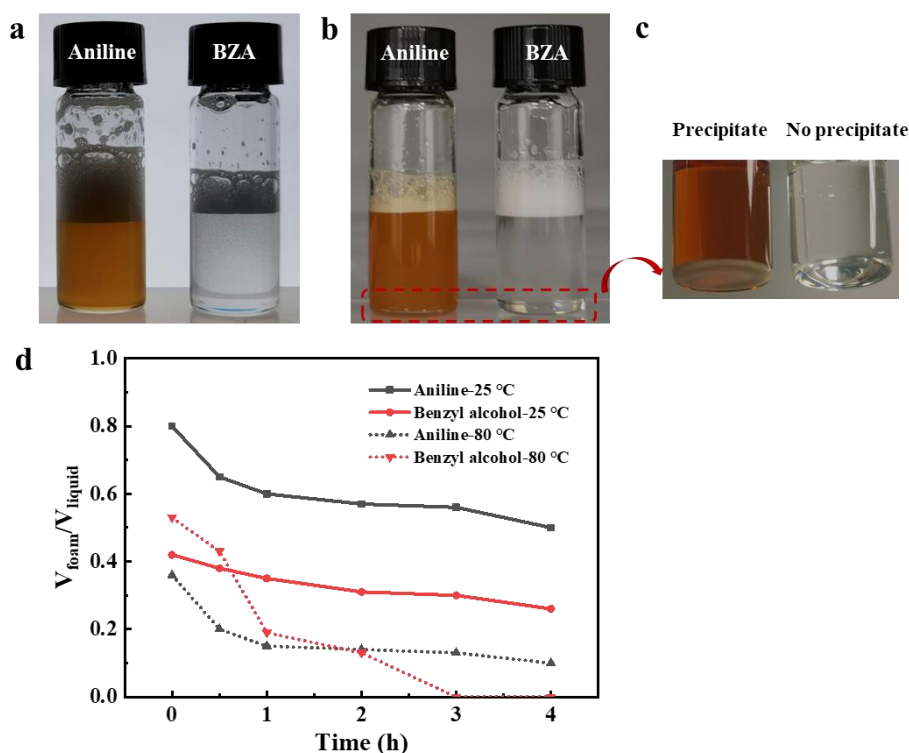
Benzyl alcohol (BZA) can behave in a similar fashion. However, the interaction of BZA molecules with D98-20BS-P is somewhat weaker than that of aniline, since  $\text{O-H}\cdots\text{O}$  hydrogen bonds are weaker than  $\text{O-H}\cdots\text{N}$  hydrogen bonds [63, 64]. The lower interaction leads to lower foamability and shorter half-life time (6 h) in benzyl alcohol. Similarly, much lower foam volume is obtained in benzaldehyde (BA), tetrahydrofurfuryl alcohol (THFA), furfuryl alcohol (FA) and 1-octanol. As expected, D98-20BS-P exhibits good foaming properties in acetophenone (AP), which has been extensively used as H-bond acceptor [65, 66].

As shown in **Figure 3.8b**, no foaming occurs in solvents with low polarity (*i.e.* pyridine, anisole, toluene), which cannot behave as hydrogen bond donors or acceptors. More importantly, the poor dispersibility in these solvents (red dashed line) is also responsible for bad foamability. Nitrobenzene is an interesting example to explore the role of hydrogen bond, as the liquid surface tension is similar to that of well-foaming aniline (43.9 and 43.4  $\text{mN}\cdot\text{m}^{-1}$ , respectively). However, it can only function as a proton acceptor. No foams were obtained in nitrobenzene, most likely due to the poor H-bonding capacity of nitro groups [67, 68]. Moreover, D98-20BS-P cannot be well dispersed in nitrobenzene, which contributes to the poor foamability.

The results above point out that hydrogen bonds have a pronounced effect on foam formation. The solvent molecules at the interface are expected to interact with the sulfonic acid head groups of D98-20BS-P by hydrogen bonding, while the oleophobic backbone prefers to stay in air. Overall, the stronger hydrogen bond between solvent and D98-20BS-P is more favourable for promoting the foaming performance.

### 3.3.2 Effect of temperature and Aquivion® D98-20BS-P concentration

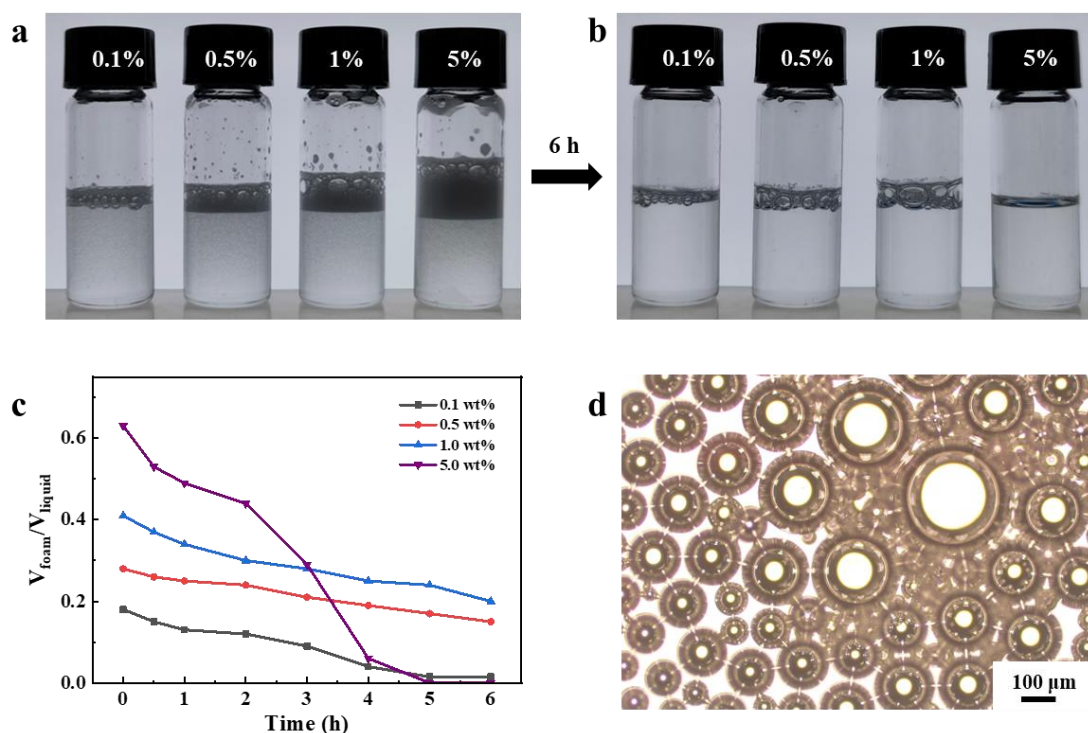
Temperature is an important parameter that can affect the foaming behaviors [69-71]. As shown in **Figure 3.9b**, an increase of temperature (from 25 to 80 °C) results in lower foamability for Aquivion® D98-20BS-P in aniline. This is possibly due to the formation of insoluble aniline/acid salts [72], which is evidenced by the precipitate at the bottom of the glass vial (**Figure 3.9c**). In the case of benzyl alcohol, the foam volume increases with the temperature, whereas the half-lifetime decreases dramatically (**Figure 3.9d**). Indeed, high temperature can lead to a reduction of the liquid surface tension, thus the adsorption of D98-20BS-P at the gas-oil interface becomes energetically unfavorable [73, 74]. Moreover, the viscosity of the liquid film can be reduced, which speeds up the kinetics of destabilization and shortens the half-lifetime [71, 75].



**Figure 3.9** Foams stabilized by 1 wt% D98-20BS-P at room temperature (a) and 80 °C (b) after hand shaking, the zoomed picture of the vial (c), and time-evolution of foam volume (d).

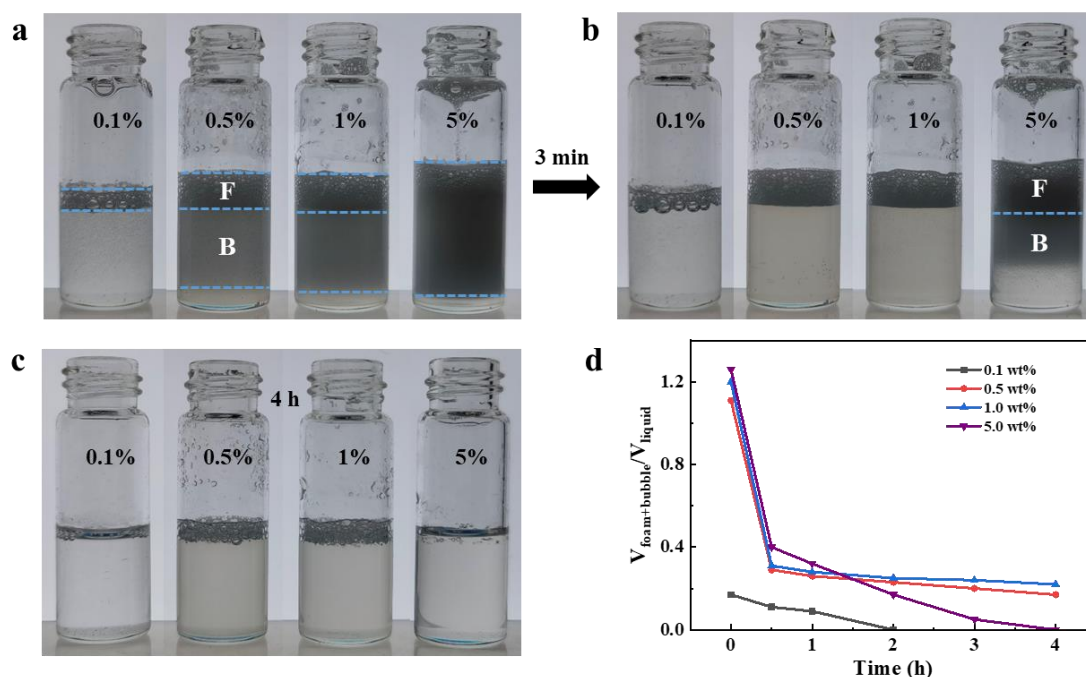
The effect of Aquivion® D98-20BS-P concentration on the foaming properties was investigated at room temperature. As plotted in **Figure 3.10**, the foamability increases progressively with D98-20BS-P concentration in benzyl alcohol, since a higher interfacial area coverage can be achieved. However, catastrophic foam collapse occurs after 4 h at the highest D98-20BS-P concentration (5 wt%). We attribute this observation to a decrease of Gibbs

elasticity of the foam film at higher D98-20BS-P concentration. A similar phenomenon has been reported for surfactant-stabilized foams [76]. The half-life time reaches a maximum (6 h) at 1 wt% of D98-20BS-P. **Figure 3.10d** displays optical microscope images of bubbles in benzyl alcohol stabilized by 1 wt% D98-20BS-P. The bubbles are polydisperse in size with diameters ranging from 40 to 310  $\mu\text{m}$ .



**Figure 3.10** Images of foams stabilized by D98-20BS-P at variable concentration taken immediately after preparation (a) and 6 h (b), time-evolution of foam evolution (c), and optical microscopy image of bubbles in benzyl alcohol stabilized by D98-20BS-P (d).

Evaluating the foaming properties by hand shaking is sometimes complex because there is limited control along the foaming process [77]. To achieve a high-energy input in a controlled way, a high-speed homogenizer (IKA Ultra-Turrax®T25 equipped with S25N-8G dispersing tool) was used to produce the foams in benzyl alcohol. After aerating at 16,000 rpm for 3 min, two layers with different foam density appear for 0.5 wt% and 1 wt% of D98-20BS-P (**Figure 3.11a**). The bottom layer with small bubbles (marked as B) vanishes within few minutes (**Figure 3.11b**), while the upper layer (marked as F) contains foams that are stable for at least 4 h after the preparation (**Figure 3.11c**). The initial foam volume fraction is as high as 94% for 5 wt% of D98-20BS-P, but a faster foam collapse rate is observed by this high-energy input approach.

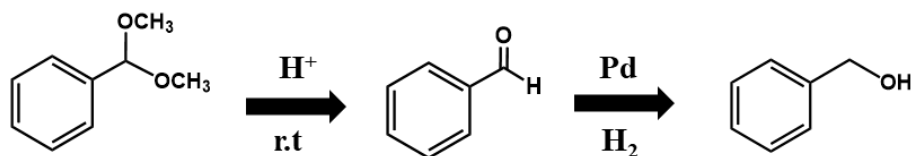


**Figure 3.11** Images of foams produced by Ultra-Turrax at variable D98-20BS-P concentration taken after preparation (a), 3 min (b) and 4 h (c) later, and time-evolution of foam volume (d).

### 3.4 Catalytic studies of Aquivion® D98-20BS-P

The catalytic performance of the solid-liquid-gas multiphase reactions is usually suppressed due to the low solubility of gases in liquids [34, 78, 79]. To address this limitation, the microbubble strategy has been developed to increase the interfacial areas in aqueous reaction system [15, 34]. Instead of conventional methods involving vigorous stirring and high pressure, high catalytic efficiency can be achieved in milder condition when applying foams. Nevertheless, only a limited number of studies investigated the catalytic enhancement effect of foams in gas-water-solid multiphase systems.

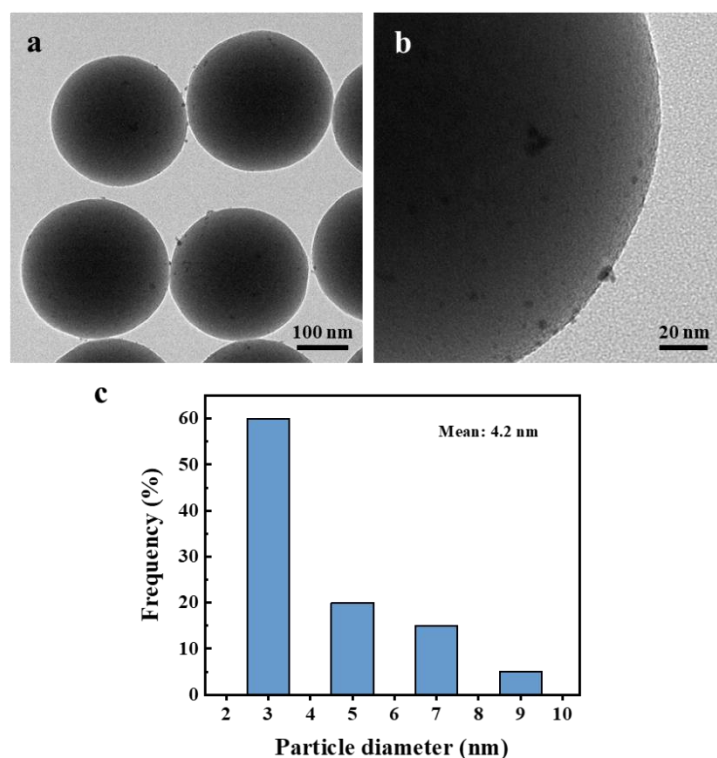
Owing to its unique structure, Aquivion® D98-20BS can behave concomitantly as foaming agent and acid catalyst. Taking advantage of these properties, we developed a facile catalyst combination strategy for one-pot cascade deacetalization and hydrogenation based on aqueous foams. This one-pot cascade reaction involves two sequential steps (**Figure 3.12**): first, benzaldehyde dimethyl acetal was hydrolyzed by D98-20BS to generate benzaldehyde; second, the homemade Pd/SiO<sub>2</sub> particles catalyzed the hydrogenation reaction of intermediate product to produce benzyl alcohol. In order to elucidate the reaction mechanism of this system, we first investigated the effect of foam and acidity on benzaldehyde hydrogenation. Afterwards, the performance of the cascade reaction starting from benzaldehyde dimethyl acetal was evaluated at the optimized reaction/foaming conditions.



**Figure 3.12** Reaction scheme for one-pot cascade reaction over Aquivion® D98 and Pd/SiO<sub>2</sub> in aqueous foam.

### 3.4.1 Characterization of the Pd/SiO<sub>2</sub> catalyst

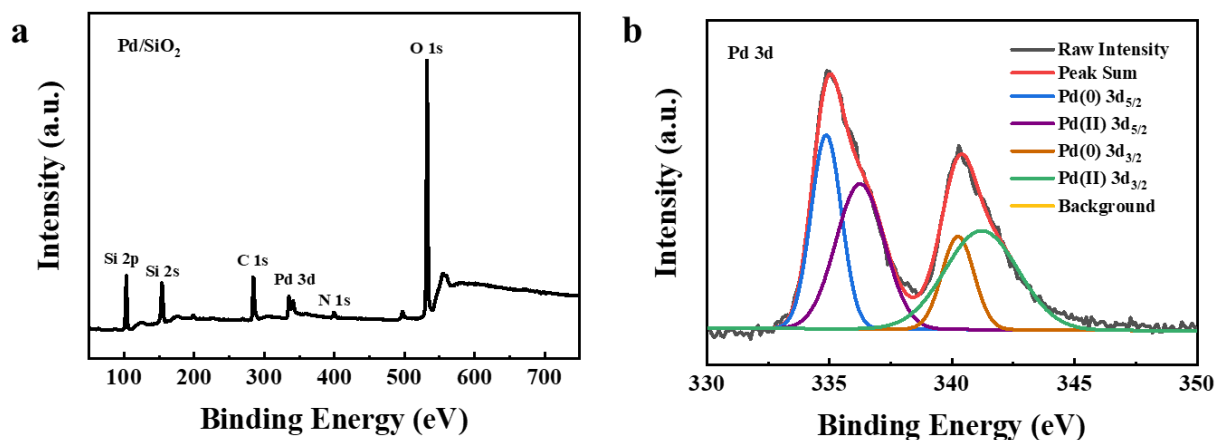
The morphology and structure of the as-prepared Pd/SiO<sub>2</sub> catalyst were elucidated by TEM (Figure 3.13). The catalyst shows uniform monodisperse spherical Pd/SiO<sub>2</sub> particles with a diameter of around 280 nm. In addition, the Pd nanoparticles with a size ranging from 2 to 10 nm (calculated from TEM micrograph) were distributed on the surface of silica particles. The Pd content of Pd/SiO<sub>2</sub> catalyst is 0.9 wt% as inferred from ICP analysis, which is consistent with the theoretical value.



**Figure 3.13** TEM images of Pd/SiO<sub>2</sub> particles (a, b), and size distribution of Pd particles (c).

XPS was used to determine the chemical oxidation state and surface composition of Pd/SiO<sub>2</sub> (Figure 3.14). The survey spectrum of Pd/SiO<sub>2</sub> reveals the presence of Si, C, N, O and Pd elements in the sample. The deconvolution of the Pd 3d XPS spectrum exhibits two distinctive bands at 334.8 and 340.2 eV, which correspond to Pd<sup>0</sup> 3d<sub>5/2</sub> and Pd<sup>0</sup> 3d<sub>3/2</sub>, respectively for

metallic Pd (0) species [80, 81]. The bands at 336.1 and 341.2 eV can be assigned to Pd (II) 3d<sub>5/2</sub> and Pd (II) 3d<sub>3/2</sub>, respectively [82].



**Figure 3.14** XPS spectra of Pd/SiO<sub>2</sub> (a), and high resolution Pd 3d XPS spectrum (b).

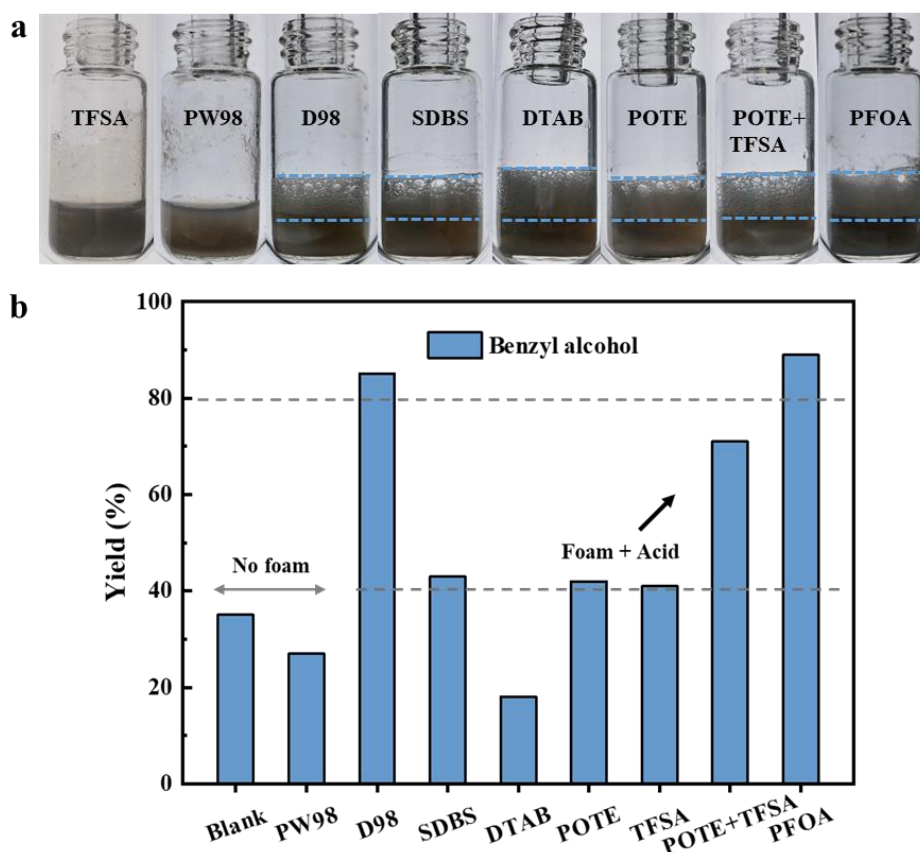
### 3.4.2 Effect of foam and acidity on benzaldehyde hydrogenation

As demonstrated in the previous foaming studies, Aquivion® D98-20BS-P exhibits good foamability in water (10 wt%) owing to its surface-active nature. Based on this result, D98-20BS was employed as foam stabilizer and acid catalyst to construct a foam reaction system. The hydrogenation of benzaldehyde over Pd/SiO<sub>2</sub> and D98-20BS-P was first performed prior to investigating the cascade reaction, and the results are summarized in **Table 3.3** and **Figure 3.15**. In the presence of D98-20BS-P (10 w%) and Pd/SiO<sub>2</sub>, a foaming system is generated (**Table 3.3**, entry 4), affording 85% within 20 min. For comparison, the hydrogenation reaction without foam was performed, which gives a maximum yield of 41% (**Table 3.3**, entries 1-3). Therefore, we speculate that the generation of foam can greatly enhance the catalytic efficiency.

**Table 3.3** Catalytic performance of different reaction systems for benzaldehyde hydrogenation.

Entry	Catalyst	Yield of benzyl alcohol (%)	Foam
1 <sup>a</sup>	Pd/SiO <sub>2</sub> (blank)	35	No
2 <sup>b</sup>	PW98 + Pd/SiO <sub>2</sub>	27	No
3 <sup>b</sup>	TFSA + Pd/SiO <sub>2</sub>	41	No
4 <sup>b</sup>	D98-20BS-P + Pd/SiO <sub>2</sub>	85	Yes
5 <sup>c</sup>	SDBS + Pd/SiO <sub>2</sub>	43	Yes
6 <sup>c</sup>	DTAB + Pd/SiO <sub>2</sub>	18	Yes
7 <sup>c</sup>	POTE + Pd/SiO <sub>2</sub>	42	Yes
8 <sup>d</sup>	TFSA + POTE + Pd/SiO <sub>2</sub>	71	Yes
9 <sup>b</sup>	PFOA + Pd/SiO <sub>2</sub>	89	Yes

Reaction conditions: [a] benzaldehyde (0.5 mmol), Pd/SiO<sub>2</sub> (10 mg), H<sub>2</sub>O (2 mL); [b] benzaldehyde (0.5 mmol), acid (210 μmol H<sup>+</sup>), Pd/SiO<sub>2</sub> (10 mg), H<sub>2</sub>O (2 mL); [c] benzaldehyde (0.5 mmol), surfactant (210 mg), Pd/SiO<sub>2</sub> (10 mg), H<sub>2</sub>O (2 mL); [d] benzaldehyde (0.5 mmol), TFSA (210 μmol H<sup>+</sup>), POTE (210 mg), Pd/SiO<sub>2</sub> (10 mg), H<sub>2</sub>O (2 mL). The reaction time is fixed at 20 min.



**Figure 3.15** Appearance of different reaction systems after reaction (a), and yield of different reaction systems (b) corresponding to **Table 3.3**.

To gain insight into the foaming properties on the catalytic performance, a variety of commercial surfactants, such as SDBS, DTAB and POTE, was introduced into the reaction system to promote foam generation (**Figure 3.15a**). However, no obvious change of yield is observed after addition of the surfactants (**Table 3.3**, entries 5-7). Meanwhile, the yield (18%) is much lower yield using a mixture of DTAB and Pd/SiO<sub>2</sub> catalyst at the same reaction conditions (**Table 3.3**, entry 6). To rationalize the difference in catalytic activity, we measured the zeta potential of Pd/SiO<sub>2</sub> particles in suspension (**Table 3.4**). The cationic surfactant is expected to be absorbed on the silica surface due to the positive charge on the polar part of DTAB molecules [83, 84]. In this case, the zeta potential is reversed and the surface charge of Pd/SiO<sub>2</sub> becomes positive after adding DTAB (**Table 3.4**, entries 1 and 6). Based on this result, we assume that the low catalytic activity is probably because DTAB molecules partially block the contact between Pd/SiO<sub>2</sub> catalyst and the reactant, thereby decreasing the activity.

Hydrogenation reactions can be affected by the acidity of the catalytic support [85, 86]. In order to explore the role of acidity on the activity, a catalytic test was performed in the presence

of trifluoromethanesulfonic acid (TFSA), a strong acid, Pd/SiO<sub>2</sub> and a non-ionic surfactant (POTE). The yield to benzyl alcohol in the foaming system (containing POTE and Pd/SiO<sub>2</sub> catalyst) is enhanced from 42% to 71% after the addition of TFSA (**Table 3.3**, entries 7 and 8). In contrast, the yield of benzyl alcohol declines when using only TFSA and Pd/SiO<sub>2</sub> (without surfactant) as catalysts (**Table 3.3**, entry 3). These results outline that both the presence of acid and good foamability play a vital role in the overall catalytic performance.

**Table 3.4** Zeta potential of the Pd/SiO<sub>2</sub> in the presence of different stabilizers in water<sup>a</sup>.

Entry	Sample	Zeta potential (mV)
1	Pd/SiO <sub>2</sub>	-42.4
2	D98-20BS-P	-33.9
3	D98-20BS-P + Pd/SiO <sub>2</sub>	-36.6
4	TFSA + Pd/SiO <sub>2</sub>	26.2
5	SDBS + Pd/SiO <sub>2</sub>	-46.7
6	DTAB + Pd/SiO <sub>2</sub>	34.4

<sup>a</sup> The amount of the catalyst and surfactant was same as that for hydrogenation reaction.

To further confirm the enhanced catalysis efficiency induced by the foams and acid, PFOA, which can simultaneously function as foaming agent and acid catalyst, was introduced to the system (**Figure 3.15b**). As expected, the hydrogenation reaction is efficiently catalysed by PFOA and Pd/SiO<sub>2</sub> with a high 89% yield (**Table 3.3**, entry 9).

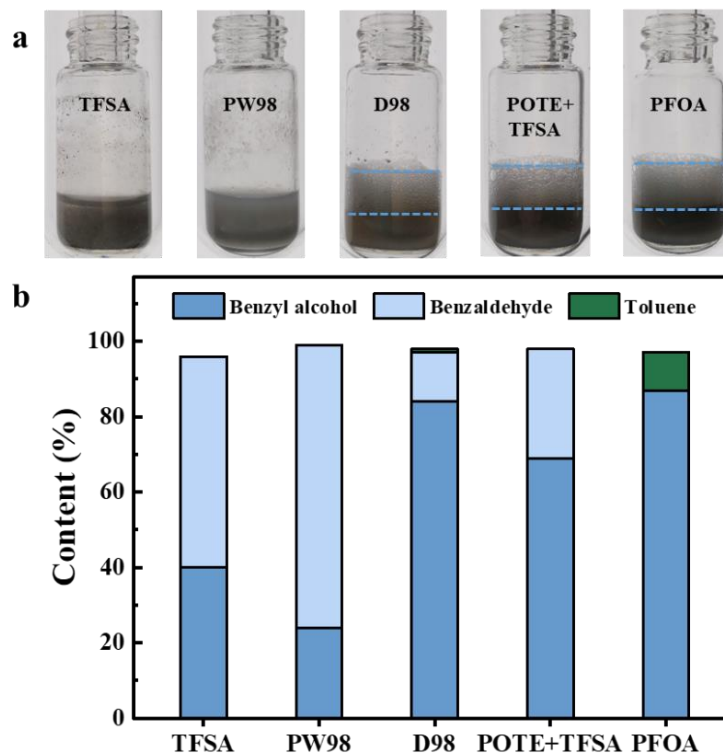
### 3.4.3 Cascade reaction: effect of stirring rate and concentration

Encouraged by these results, we investigate different foaming systems for the one-pot cascade deacetalization-hydrogenation reaction using benzaldehyde dimethyl acetal as reactant. As shown in **Figure 3.16b**, the combination of D98-20BS-P and Pd/SiO<sub>2</sub> catalyst is effective for the direct synthesis of benzyl alcohol (84% yield) *via* the one-pot cascade protocol. Interestingly, a similar yield of benzyl alcohol (85%) is achieved from the hydrogenation of benzaldehyde (**Table 3.3**, entry 4), reflecting that the second step (hydrogenation) is a rate-determining step.

When TFSA and Pd/SiO<sub>2</sub> were used as catalysts, the yield of benzyl alcohol was only 40% within 20 min. We attribute the low catalytic activity to a lack of foam formation in the cascade process. Addition of the surfactant (POTE) to the above catalytic system enables the generation of aqueous foams (**Figure 3.16a**), thereby boosting the yield of benzyl alcohol to 69%. Likewise, a high yield of benzyl alcohol (87%) is obtained by combining PFOA with Pd/SiO<sub>2</sub> as catalysts. This happens at the expense of undesired by-product (10% yield of toluene). In



contrast, only a trace amount of toluene is present in the catalytic system consisting of D98-20BS-P and Pd/SiO<sub>2</sub> catalysts.



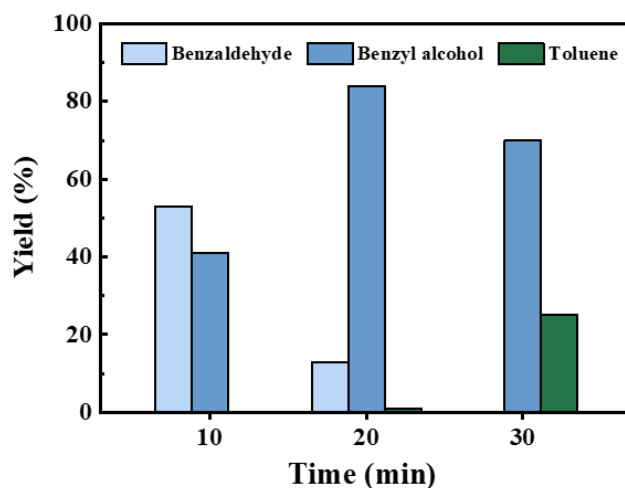
**Figure 3.16** Appearance of different reaction systems after reaction (a), and compositions after one-pot cascade reaction (b). Same reaction conditions as those used for benzaldehyde hydrogenation.

**Figure 3.17** plots the time-evolution of the products generated under foaming conditions in the presence of D98-20BS-P and Pd/SiO<sub>2</sub> catalysts. The initial yield of benzyl alcohol increases continuously with the reaction time until a maximum value of 84% after 20 min, and the maximum yield of 84% was observed at 20 min. The yield of benzyl alcohol decreases further after time in detriment of the toluene yield.

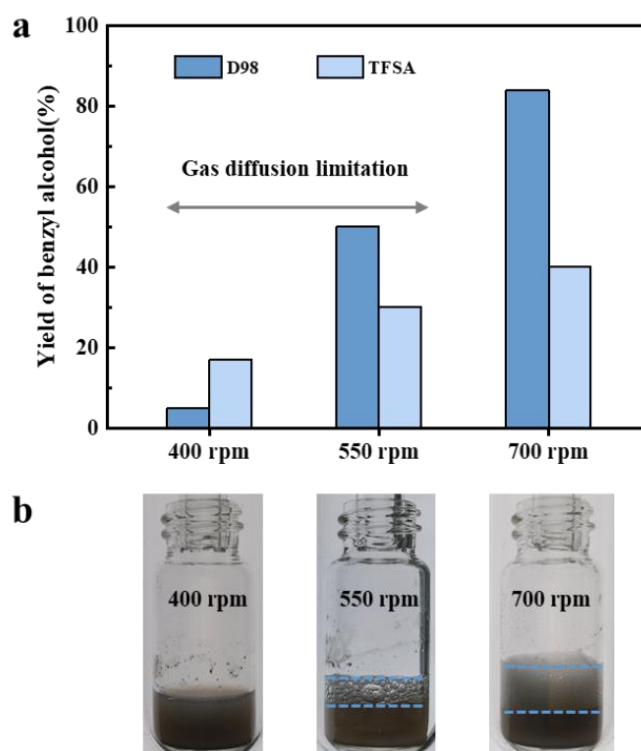
The effect of stirring rate on the catalytic properties was studied both in a foaming system (D98-20BS-P and Pd/SiO<sub>2</sub>) and in a conventional reaction system without foam (TFSA and Pd/SiO<sub>2</sub>). In the former case, the yield of benzyl alcohol increased monotonously with the stirring rate (**Figure 3.18a**), which can be credited to the increase of foam volume (**Figure 3.18b**). However, the increase of the yield for reaction system without foam is much slower, which suggests that the catalysis efficiency is affected by the mass transfer limitations.

The effect of D98-20BS-P concentration on the foaming properties and catalytic activity was explored at a stirring rate of 700 rpm. By increasing the D98-20BS-P concentration from

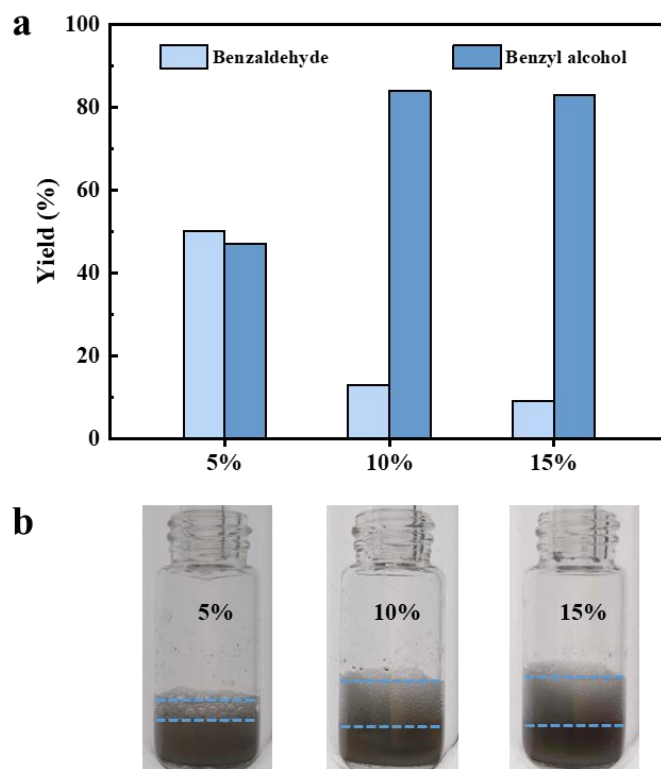
5 wt% to 10 wt%, the foam volume increases by ~50% (**Figure 3.19b**). Meanwhile, the yield of benzyl alcohol increased from 47% to 84% (**Figure 3.19a**). Further increase of the D98-20BS-P concentration (15 wt%) results in almost no change of the yield, which is consistent with foam formation. Overall, these results point out that the catalytic performance is directly related to the foam volume produced in the reaction system.



**Figure 3.17** Reaction profile of the cascade reaction in the presence of D98-20BS-P and Pd/SiO<sub>2</sub> catalysts.



**Figure 3.18** Effect of stirring rate on the benzyl alcohol yield in the one-pot cascade reaction (a), and photographs of foaming systems at different stirring rates (b).



**Figure 3.19** Benzaldehyde and benzyl alcohol yield for one-pot cascade reaction in the foaming systems as a function of the D98-28BS-P concentration (a) and corresponding images after reaction (b).

### 3.5 Conclusion

In summary, we unveiled the surface-active properties of Aquivion® D98-20BS for stabilizing stable foams in organic solvents and water. The foaming properties were studied after hand shaking and high-speed homogenization in Ultra-Turrax, and the foam volume fraction generated is 94% for 5 wt% of D98-20BS-P in benzyl alcohol. Besides, the effect of solvent properties on foam formation was systematically investigated. The presence of hydrogen bonds between D98-20BS-P and the solvent molecules was crucial for promoting the foaming performance. D98-20BS-P outperformed different stabilizers, including polytetrafluoroethylene and fluorinated particles, both in terms of foamability and foam stability in benzyl alcohol.

Taking advantage of the excellent foaming properties and acidic nature of Aquivion® D98-20-P, we constructed a foaming system for one-pot cascade deacetalization-hydrogenation reactions. The synergetic combination of D98-20BS-P and Pd/SiO<sub>2</sub> catalysts exhibited a remarkable catalytic performance, and the yield of the desired product was 2 times higher than that of conventional multiphase reaction system. Such a significant improvement is attributed

to the pronounced increase in the reaction interface area. Overall, the cooperation between acid and palladium active sites is an essential prerequisite for enhancing the catalytic activity.

This study broadens the scope of fluorinated materials as foam stabilizers. It could be helpful and inspiring to answer the open questions on stabilization mechanisms of foams. Besides, the fundamental insights from this study could pave the way for constructing novel foaming reaction systems.

### 3.6 References

1. Dedovets, D., et al., *Multiphase Microreactors Based on Liquid–Liquid and Gas–Liquid Dispersions Stabilized by Colloidal Catalytic Particles*. *Angewandte Chemie International Edition*, 2022. **61**(4): p. e202107537.
2. Jenck, J.F., *Gas-liquid-solid reactors for hydrogenation in fine chemicals synthesis*, in *Studies in Surface Science and Catalysis*. 1991, Elsevier. p. 1-19.
3. Lopes, R.J. and R.M. Quinta-Ferreira, *Evaluation of multiphase CFD models in gas–liquid packed-bed reactors for water pollution abatement*. *Chemical engineering science*, 2010. **65**(1): p. 291-297.
4. Wang, L., et al., *Impact of diffusion at the gas/liquid interface on deep hydrodesulfurization of fluid catalytic cracking naphtha*. *Chemical Engineering Journal*, 2018. **346**: p. 369-375.
5. Gemoets, H.P., et al., *Liquid phase oxidation chemistry in continuous-flow microreactors*. *Chemical Society Reviews*, 2016. **45**(1): p. 83-117.
6. Bhargava, S.K., et al., *Wet oxidation and catalytic wet oxidation*. *Industrial & engineering chemistry research*, 2006. **45**(4): p. 1221-1258.
7. Liang-Shih, F., *Gas-liquid-solid fluidization engineering*. 2013: Butterworth-Heinemann.
8. Charpentier, J.-C., *Mass-transfer rates in gas-liquid absorbers and reactors*, in *Advances in chemical engineering*. 1981, Elsevier. p. 1-133.
9. Beenackers, A. and W.P.M. Van Swaaij, *Mass transfer in gas–liquid slurry reactors*. *Chemical Engineering Science*, 1993. **48**(18): p. 3109-3139.
10. Henkel, K.D., *Reactor types and their industrial applications*. *Ullmann's Encyclopedia of Industrial Chemistry*, 2000.
11. Kobayashi, J., et al., *A microfluidic device for conducting gas-liquid-solid hydrogenation reactions*. *Science*, 2004. **304**(5675): p. 1305-1308.
12. Irfan, M., T.N. Glasnov, and C.O. Kappe, *Heterogeneous catalytic hydrogenation reactions in continuous-flow reactors*. *ChemSusChem*, 2011. **4**(3): p. 300-316.
13. Gutmann, B., D. Cantillo, and C.O. Kappe, *Continuous-flow technology—a tool for the safe manufacturing of active pharmaceutical ingredients*. *Angewandte Chemie International Edition*, 2015. **54**(23): p. 6688-6728.

14. Reif, M. and R. Dittmeyer, *Porous, catalytically active ceramic membranes for gas–liquid reactions: a comparison between catalytic diffuser and forced through flow concept*. *Catalysis today*, 2003. **82**(1-4): p. 3-14.
15. Mase, N., T. Mizumori, and Y. Tatemoto, *Aerobic copper/TEMPO-catalyzed oxidation of primary alcohols to aldehydes using a microbubble strategy to increase gas concentration in liquid phase reactions*. *Chemical Communications*, 2011. **47**(7): p. 2086-2088.
16. Zhao, H., et al., *Understanding of the foam capability of sugar-based nonionic surfactant from molecular level*. *Colloids and Surfaces A: Physicochemical and Engineering Aspects*, 2018. **551**: p. 165-173.
17. Fameau, A.-L. and A. Saint-Jalmes, *Non-aqueous foams: Current understanding on the formation and stability mechanisms*. *Advances in Colloid and Interface Science*, 2017. **247**: p. 454-464.
18. Rodrigues, J.A., et al., *Generation and manipulation of bubbles and foams stabilised by magnetic nanoparticles*. *Colloids and Surfaces A: Physicochemical and Engineering Aspects*, 2011. **384**(1-3): p. 408-416.
19. Binks, B.P. and B. Vishal, *Particle-stabilized oil foams*. *Advances in Colloid and Interface Science*, 2021: p. 102404.
20. Binks, B.P. and T.S. Horozov, *Aqueous foams stabilized solely by silica nanoparticles*. *Angewandte Chemie International Edition*, 2005. **44**(24): p. 3722-3725.
21. Braun, L., M. Kühnhammer, and R. von Klitzing, *Stability of aqueous foam films and foams containing polymers: Discrepancies between different length scales*. *Current Opinion in Colloid & Interface Science*, 2020.
22. Weißenborn, E. and B. Braunschweig, *Hydroxypropyl cellulose as a green polymer for thermo-responsive aqueous foams*. *Soft Matter*, 2019. **15**(13): p. 2876-2883.
23. Binks, B.P. and H. Shi, *Aqueous foams in the presence of surfactant crystals*. *Langmuir*, 2020. **36**(4): p. 991-1002.
24. Alargova, R.G., et al., *Foam superstabilization by polymer microrods*. *Langmuir*, 2004. **20**(24): p. 10371-10374.
25. Blázquez, C., et al., *Non-aqueous and crude oil foams*. *Oil & Gas Science and Technology–Revue d’IFP Energies nouvelles*, 2014. **69**(3): p. 467-479.
26. Binks, B.P. and A. Rocher, *Stabilisation of liquid–air surfaces by particles of low surface energy*. *Physical Chemistry Chemical Physics*, 2010. **12**(32): p. 9169-9171.
27. Binks, B.P. and A.T. Tyowua, *Influence of the degree of fluorination on the behaviour of silica particles at air–oil surfaces*. *Soft Matter*, 2013. **9**(3): p. 834-845.
28. Binks, B.P., A. Rocher, and M. Kirkland, *Oil foams stabilised solely by particles*. *Soft Matter*, 2011. **7**(5): p. 1800-1808.
29. Binks, B.P., et al., *Particles at oil–air surfaces: powdered oil, liquid oil marbles, and oil foam*. *ACS applied materials & interfaces*, 2015. **7**(26): p. 14328-14337.

30. Binks, B.P., T. Sekine, and A.T. Tyowua, *Dry oil powders and oil foams stabilised by fluorinated clay platelet particles*. *Soft Matter*, 2014. **10**(4): p. 578-589.
31. Fameau, A.-L., et al., *Foamitizer: High ethanol content foams using fatty acid crystalline particles*. *Journal of Colloid and Interface Science*, 2021. **600**: p. 882-886.
32. Bai, X., et al., *Environmentally benign multiphase solid–liquid–gas catalysis*. *Green Chemistry*, 2020. **22**(3): p. 895-902.
33. Huang, Z., et al., *Sustainable catalytic oxidation of alcohols over the interface between air and water*. *Green Chemistry*, 2015. **17**(4): p. 2325-2329.
34. Huang, J., et al., *pH-responsive gas–water–solid interface for multiphase catalysis*. *Journal of the American Chemical Society*, 2015. **137**(47): p. 15015-15025.
35. Andreoli, S., et al., *Superacid Aquivion® PFSA as an efficient catalyst for the gas phase dehydration of ethanol to ethylene in mild conditions*. *Applied Catalysis A: General*, 2020. **597**: p. 117544.
36. Liguori, F., et al., *Liquid-phase synthesis of methyl isobutyl ketone over bifunctional heterogeneous catalysts comprising cross-linked perfluorinated sulfonic acid Aquivion polymers and supported Pd nanoparticles*. *Applied Catalysis A: General*, 2021. **610**: p. 117957.
37. Karam, A., et al., *High catalytic performance of aquivion PFSA, a reusable solid perfluorosulfonic acid polymer, in the biphasic glycosylation of glucose with fatty alcohols*. *ACS Catalysis*, 2017. **7**(4): p. 2990-2997.
38. Karam, A., et al., *Conversion of cellulose into amphiphilic Alkyl glycosides catalyzed by aquivion, a perfluorosulfonic acid polymer*. *ChemSusChem*, 2017. **10**(18): p. 3604-3610.
39. Moreno-Marrodan, C., et al., *Metal Nanoparticles Supported on Perfluorinated Superacid Polymers: A Family of Bifunctional Catalysts for the Selective, One-Pot Conversion of Vegetable Substrates in Water*. *ChemCatChem*, 2017. **9**(22): p. 4256-4267.
40. Dou, Y., et al., *Etherification of 5-Hydroxymethylfurfural to Biofuel Additive Catalyzed by Aquivion® PFSA Modified Mesoporous Silica*. *European Journal of Inorganic Chemistry*, 2018. **2018**(33): p. 3706-3716.
41. Dou, Y., et al., *5-Hydroxymethylfurfural production from dehydration of fructose catalyzed by Aquivion® silica solid acid*. *Fuel*, 2018. **214**: p. 45-54.
42. Shi, H., et al., *Aquivion Perfluorosulfonic Superacid as an Efficient Pickering Interfacial Catalyst for the Hydrolysis of Triglycerides*. *ChemSusChem*, 2017. **10**(17): p. 3363-3367.
43. Fang, W., et al., *Aquivion®–carbon composites via hydrothermal carbonization: amphiphilic catalysts for solvent-free biphasic acetalization*. *Journal of Materials Chemistry A*, 2016. **4**(12): p. 4380-4385.
44. Zhang, S., et al., *Aquivion–Carbon Composites with Tunable Amphiphilicity for Pickering Interfacial Catalysis*. *ACS applied materials & interfaces*, 2018. **10**(31): p. 26795-26804.

45. Karam, A., et al., *Mechanocatalytic depolymerization of cellulose with perfluorinated sulfonic acid ionomers*. *Frontiers in chemistry*, 2018. **6**: p. 74.
46. Paris, E., et al., *Silica Nanoparticles Decorated with Polymeric Sulfonic Acids Trigger Selective Oxidation of Benzylic Methylenes to Aldehydic and Ketonic Carbonyls*. *ACS Sustainable Chemistry & Engineering*, 2019. **7**(6): p. 5886-5891.
47. Deng, Q., et al., *TGA–FTi. r. investigation of the thermal degradation of Nafion® and Nafion®/[silicon oxide]-based nanocomposites*. *Polymer*, 1998. **39**(24): p. 5961-5972.
48. Liang, Z., et al., *FT-IR study of the microstructure of Nafion® membrane*. *Journal of membrane science*, 2004. **233**(1-2): p. 39-44.
49. Martínez de Yuso, M., et al., *A study of chemical modifications of a Nafion membrane by incorporation of different room temperature ionic liquids*. *Fuel Cells*, 2012. **12**(4): p. 606-613.
50. Fang, W., et al., *Silica-immobilized Aquivion PFSA superacid: application to heterogeneous direct etherification of glycerol with n-butanol*. *Catalysis Science & Technology*, 2015. **5**(8): p. 3980-3990.
51. Chen, C., et al., *XPS investigation of Nafion® membrane degradation*. *Journal of Power Sources*, 2007. **169**(2): p. 288-295.
52. Moukheiber, E., et al., *Investigation of ionomer structure through its dependence on ion exchange capacity (IEC)*. *Journal of Membrane Science*, 2012. **389**: p. 294-304.
53. Chen, Q. and K. Schmidt-Rohr, *19F and 13C NMR signal assignment and analysis in a perfluorinated ionomer (Nafion) by two-dimensional solid-state NMR*. *Macromolecules*, 2004. **37**(16): p. 5995-6003.
54. Ghassemzadeh, L., et al., *Chemical degradation of proton conducting perfluorosulfonic acid ionomer membranes studied by solid-state nuclear magnetic resonance spectroscopy*. *Journal of Power Sources*, 2009. **186**(2): p. 334-338.
55. Yoshimura, T., A. Ohno, and K. Esumi, *Equilibrium and dynamic surface tension properties of partially fluorinated quaternary ammonium salt gemini surfactants*. *Langmuir*, 2006. **22**(10): p. 4643-4648.
56. Carey, E. and C. Stubenrauch, *Properties of aqueous foams stabilized by dodecyltrimethylammonium bromide*. *Journal of colloid and interface science*, 2009. **333**(2): p. 619-627.
57. Spagnolo, D. and K. Chuang, *Control of foaming in hydrogen sulfide/water mixtures*. *The Canadian Journal of Chemical Engineering*, 1985. **63**(4): p. 572-577.
58. Singer, S.J. and C. Knight, *Hydrogen-bond topology and proton ordering in ice and water clusters*. *Advances in chemical physics*, 2012. **147**: p. 1.
59. Gawlita, E., et al., *H-Bonding in alcohols is reflected in the Ca– H bond strength: Variation of C– D vibrational frequency and fractionation factor*. *Journal of the American Chemical Society*, 2000. **122**(47): p. 11660-11669.

60. Raveendra, M., et al., *Study on thermo physical properties of binary mixture containing aromatic alcohol with aromatic, substituted aromatic amines at different temperatures interms of FT-IR, 1H NMR spectroscopic and DFT method*. Fluid Phase Equilibria, 2018. **462**: p. 85-99.
61. Szatyłowicz, H. and T.M. Krygowski, *Varying electronegativity: Effect of the nature and strength of H-bonding in anilide/aniline/anilinium complexes on the electronegativity of NH-/NH<sub>2</sub>/NH<sub>3</sub><sup>+</sup> groups*. Journal of Molecular Structure, 2007. **844**: p. 200-207.
62. Mishra, S., J.-L. Kuo, and G.N. Patwari, *Hydrogen bond induced enhancement of Fermi resonances in N–H⋯N hydrogen bonded complexes of anilines*. Physical Chemistry Chemical Physics, 2018. **20**(33): p. 21557-21566.
63. Böhm, H.J., et al., *Oxygen and Nitrogen in Competitive Situations: Which is the Hydrogen-Bond Acceptor?* Chemistry—A European Journal, 1996. **2**(12): p. 1509-1513.
64. Emsley, J., *Very strong hydrogen bonding*. Chemical Society Reviews, 1980. **9**(1): p. 91-124.
65. Dalvit, C., C. Invernizzi, and A. Vulpetti, *Fluorine as a hydrogen-bond acceptor: Experimental evidence and computational calculations*. Chemistry—A European Journal, 2014. **20**(35): p. 11058-11068.
66. Laurence, C., et al., *An enthalpic scale of hydrogen-bond basicity. 4. Carbon  $\pi$  bases, oxygen bases, and miscellaneous second-row, third-row, and fourth-row bases and a survey of the 4-fluorophenol affinity scale*. The Journal of organic chemistry, 2010. **75**(12): p. 4105-4123.
67. Robinson, J.M., et al., *Weak interactions in crystal engineering—understanding the recognition properties of the nitro group*. New Journal of Chemistry, 2000. **24**(10): p. 799-806.
68. Kingsbury, C.A., *Why are the Nitro and Sulfone Groups Poor Hydrogen Bonders?* 2015.
69. Oetjen, K., et al., *Temperature effect on foamability, foam stability, and foam structure of milk*. Colloids and Surfaces A: Physicochemical and Engineering Aspects, 2014. **460**: p. 280-285.
70. Zakaria, Z., Z. Ariff, and C. Sipaut, *Effects of parameter changes on the structure and properties of low-density polyethylene foam*. Journal of Vinyl and Additive Technology, 2009. **15**(2): p. 120-128.
71. Li, D., et al., *CO<sub>2</sub>-sensitive foams for mobility control and channeling blocking in enhanced WAG process*. Chemical Engineering Research and Design, 2015. **102**: p. 234-243.
72. Yang, J., Y. Ding, and J. Zhang, *Uniform rice-like nanostructured polyanilines with highly crystallinity prepared in dodecylbenzene sulfonic acid micelles*. Materials Chemistry and Physics, 2008. **112**(2): p. 322-324.
73. Chen, K.-D., Y.-F. Lin, and C.-H. Tu, *Densities, viscosities, refractive indexes, and surface tensions for mixtures of ethanol, benzyl acetate, and benzyl alcohol*. Journal of Chemical & Engineering Data, 2012. **57**(4): p. 1118-1127.
74. Águila-Hernández, J., A. Trejo, and B.E. García-Flores, *Surface tension and foam behaviour of aqueous solutions of blends of three alkanolamines, as a function of temperature*. Colloids and Surfaces A: Physicochemical and Engineering Aspects, 2007. **308**(1-3): p. 33-46.



75. Valenzuela, G., et al., *Foam sclerosants are more stable at lower temperatures*. European Journal of Vascular and Endovascular Surgery, 2013. **46**(5): p. 593-599.
76. Behera, M.R., et al., *Foaming in micellar solutions: Effects of surfactant, salt, and oil concentrations*. Industrial & Engineering Chemistry Research, 2014. **53**(48): p. 18497-18507.
77. Arriaga, L.R., et al., *On the long-term stability of foams stabilised by mixtures of nano-particles and oppositely charged short chain surfactants*. Soft Matter, 2012. **8**(43): p. 11085-11097.
78. Lavelle, K. and J. McMonagle, *Mass transfer effects in the oxidation of aqueous organic compounds over a hydrophobic solid catalyst*. Chemical engineering science, 2001. **56**(17): p. 5091-5102.
79. Mavroudi, M., S. Kaldis, and G. Sakellariopoulos, *A study of mass transfer resistance in membrane gas-liquid contacting processes*. Journal of Membrane Science, 2006. **272**(1-2): p. 103-115.
80. Göksu, H., et al., *A novel hydrogenation of nitroarene compounds with multi wall carbon nanotube supported palladium/copper nanoparticles (PdCu@ MWCNT NPs) in aqueous medium*. Scientific reports, 2020. **10**(1): p. 1-8.
81. Celebi, M., et al., *Palladium nanoparticles supported on amine-functionalized SiO<sub>2</sub> for the catalytic hexavalent chromium reduction*. Applied Catalysis B: Environmental, 2016. **180**: p. 53-64.
82. Hu, C., et al., *Small-sized PdCu nanocapsules on 3D graphene for high-performance ethanol oxidation*. Nanoscale, 2014. **6**(5): p. 2768-2775.
83. Wei, X.-Q., et al., *Different cationic surfactants-modified silica nanoparticles for Pickering emulsions*. Journal of Molecular Liquids, 2019. **291**: p. 111341.
84. Lebdioua, K., et al., *Influence of different surfactants on Pickering emulsions stabilized by submicronic silica particles*. Journal of colloid and interface science, 2018. **520**: p. 127-133.
85. Lee, N. and Y.-M. Chung, *Exfoliated Pd/HNb<sub>3</sub>O<sub>8</sub> nanosheet as highly efficient bifunctional catalyst for one-pot cascade reaction*. Applied Surface Science, 2016. **370**: p. 160-168.
86. Huang, J., et al., *Tuning the support acidity of flame-made Pd/SiO<sub>2</sub>-Al<sub>2</sub>O<sub>3</sub> catalysts for chemoselective hydrogenation*. Journal of Catalysis, 2011. **281**(2): p. 352-360.

## **CHAPTER 4**

---

### **Organic Foams Stabilized by Biphenyl-bridged Particles**

---

## 4.1 Introduction

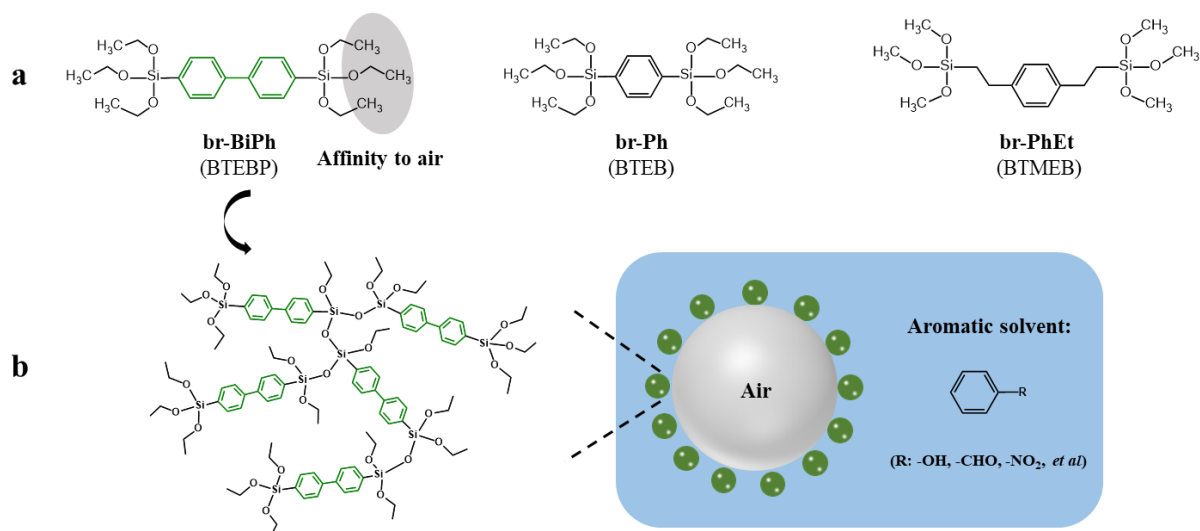
A foam is a complex system where gas bubbles are entrapped in a continuous liquid phase [1-3]. Surface-active materials such as surfactants and colloidal particles are commonly used as foaming agents and stabilizers [4-10]. By far the most frequently and deeply studied systems are aqueous foams, which are widely used in food, cosmetics, healthcare, fire extinguishing and the synthesis of porous materials [11-13]. In contrast, few studies have been reported on non-aqueous foams despite their importance in many industrial fields [14-16]. Owing to the low surface tension of organic solvents (typically ranging from 14 to 50  $\text{mN}\cdot\text{m}^{-1}$ ), the adsorption of common foam stabilizers at the gas-liquid interface is energetically unfavorable, and require stabilizers with low surface energy (*e.g.*, fluorinated surfactants), asphaltenes or fatty acid crystals [17-23]. As a result, the generation of non-aqueous foams is much more challenging compared to aqueous foams [21, 24].

Particle adsorption at the gas-liquid interface depends mainly on the particle wettability, which can be characterized by the interfacial contact angle. When the contact angle lies in the correct range (usually  $30^\circ < \theta < 90^\circ$ ) [1, 3, 25], stable foams can be produced using a variety of techniques, including shaking, stirring, bubbling, and microfluidics [26-28]. As proof of concept, Binks and coworkers investigated the foaming behavior of fluorinated particles in non-polar hydrocarbons and polar oils [8, 29-31]. The authors demonstrated that particle wettability can be easily adjusted by tuning the degree of fluorination, and in this way suitable contact angles for oil foam production could be achieved. Besides fluorinated particles, Dyab et al. successfully prepared stable foams based on glycerin and ethylene glycol in the presence of dichlorodimethylsilane-modified silica particles [32]. However, the surface tension of both polar organic solvents is relatively high ( $\gamma > 47 \text{ mN}\cdot\text{m}^{-1}$ ), limiting the scope of application. Overall, halogenated materials may become solid pollutants as they are resistant to degradation under environmental conditions. Therefore, developing novel types of non-halogenated foam stabilizers for organic solvents with tunable contact angles is highly desired.

It is known that molecular ordering of monomeric bricks of homopolymers at the air-solvent interface is conditioned by their relative interaction with the solvent and air. For instance, phenyl groups in poly(phenyl methacrylate) are preferentially solvated by chlorobenzene, while the backbone methyl and methylene groups are exposed to air [33]. Inspired by this observation, we hypothesize particles with phenyl rings and alkyl chains could assemble at the air-oil interface, thus stabilizing foams based on aromatic solvents. The polymerization of bissilylated organic precursors such as bridged bis(trialkoxysilyl)aryl monomers by the sol-gel process is a convenient route for preparing such particles [34-36]. In this approach, Si-O-Si linkages in

organosilica particles is replaced by Si-R or Si-R-Si linkages (where R represents organic groups). These hybrid materials combine the advantages of the silica skeleton (*e.g.*, high thermal and mechanical stability, and presumed chemical inertness) with the properties of the organic moiety [37-40]. Besides, the chemical and physical properties (*e.g.*, wettability, flexibility) of the materials can be readily tuned by adjusting the nature of bridging organic groups [41-43].

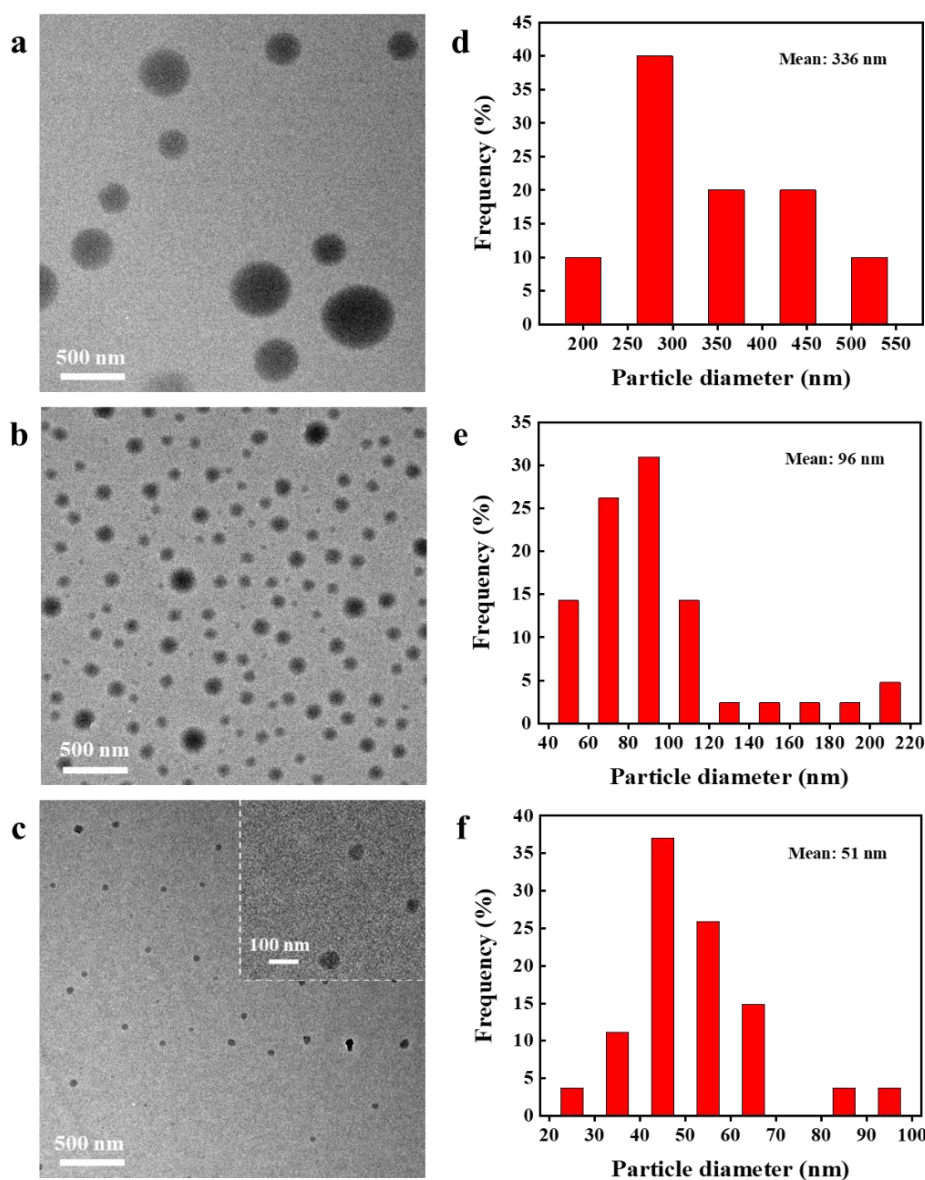
In this chapter, we synthesized a series of organosilica particles from bridged organosilanes precursors (**Figure 4.1**), which are structurally similar to aromatic solvents (*e.g.*, benzyl alcohol). By adjusting the organic architecture and surface properties of the materials, foams could be prepared in a range of aromatic solvents by hand shaking, Ultra-Turrax and microfluidics. The foam formation was correlated with the chemical structure of the different organosilica particles, and the foamability range was investigated as a function of the contact angle and surface tension of the solvents.



**Figure 4.1** Chemical structures and abbreviations of the organosilica particles and related precursors (a); and illustration of a bubble stabilized by br-BiPh particles (c).

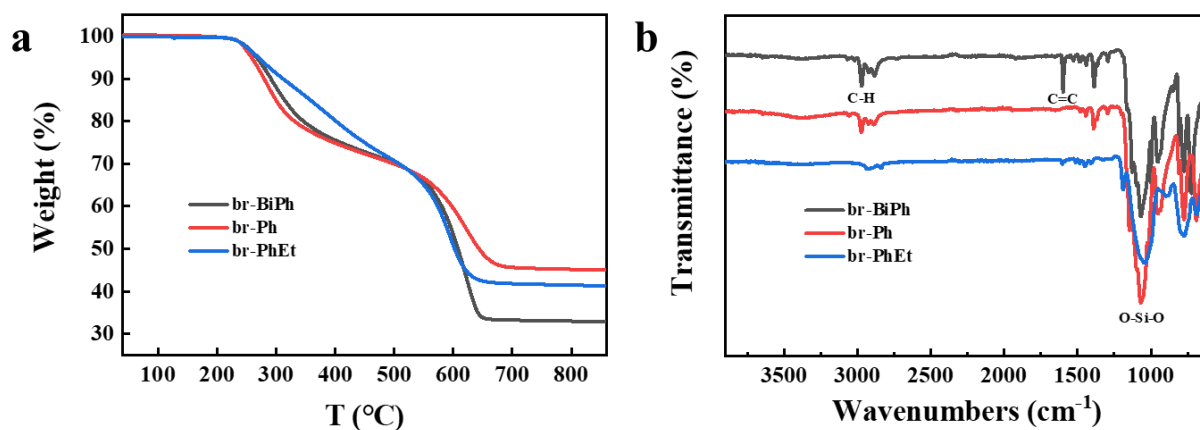
## 4.2 Characterization of bridged organosilica particles

The key to achieve good foamability is to tune the surface properties of organosilicas by variation of the organic groups incorporated into the network. We synthesized three bridged organosilica particles by sol-gel polycondensation of bissilylated precursors containing phenyl rings following a modified Stöber method [44, 45]. The structural formulas of the starting materials and resulting organosilica particles are presented in **Figure 4.1a**. The TEM images reveal regular spherical shapes for br-BiPh particles with a diameter ranging from 200 to 540 nm, while the size of br-Ph and br-PhEt particles lies in the range of 50-210 nm and 25-95 nm, respectively (**Figure 4.2**).



**Figure 4.2** TEM images of br-BiPh (a), br-Ph (b) and br-PhEt (c) and corresponding particles size distribution (d, e, f).

TG analysis of bridged organosilica particles reveals two thermal decomposition steps located in the temperature range 210-520 °C and 520-700 °C (**Figure 4.3a**). It is likely that alkyl groups undergo degradation in first range followed by decomposition of phenyl groups. The total weight loss of br-BiPh particles is around 67%. This value is higher than the expected weight loss (59.4%) on the basis of the formula  $O_{1.5}Si(C_6H_4)_2SiO_{1.5}$ , which can be explained by the presence of non-hydrolyzed ethoxy groups [46]. Both br-Ph and br-PhEt particles exhibited smaller weight losses compared to br-BiPh, which is in line with the lower organic content of the precursors.



**Figure 4.3** TG profiles and FT-IR spectra of bridged organosilica particles.

**Figure 4.3b** shows the FT-IR spectra of bridged organosilica particles. The most prominent peak at  $1068\text{ cm}^{-1}$  is ascribed to the Si-O-Si stretching band. Characteristic bands belonging to phenyl groups are visible at  $1602\text{ cm}^{-1}$  and  $1385\text{ cm}^{-1}$ . Moreover, several bands are visible in the range  $2800\text{--}3000\text{ cm}^{-1}$  that can be ascribed to C-H stretching and bending bands, confirming the presence of alkyl chains in br-BiPh particles [47].

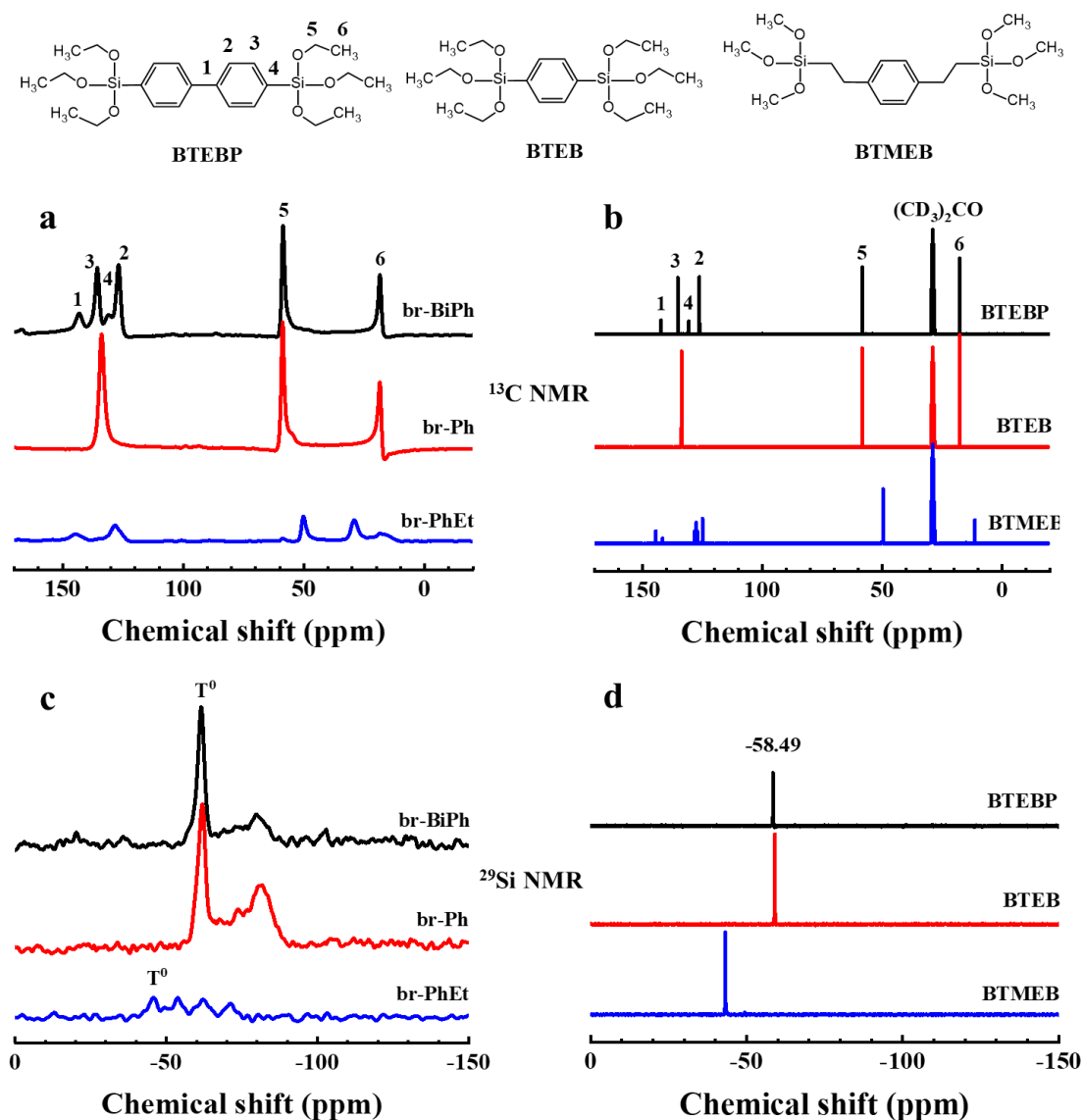
Solid-state  $^{13}\text{C}$  NMR confirms the presence of a large amount of non-hydrolyzed ethoxy groups (peak at  $\sim 58\text{ ppm}$ ) in the br-BiPh and br-Ph samples (**Figure 4.4a**), which can explain the extra mass loss in the TG profiles. The  $^{13}\text{C}$  MAS NMR spectra display four aromatic resonances including two intense signals at  $126.6\text{ ppm}$  and  $135.6\text{ ppm}$  that can be assigned to carbon atoms in positions 2 and 3 bonded to hydrogen, and substituted carbons in positions 1 and 4 of biphenyl ( $143.1$  and  $130.7\text{ ppm}$ ) [48-50].

The  $^{29}\text{Si}$  MAS NMR spectrum of br-BiPh presents two signals at  $-61.52\text{ ppm}$  and  $-79.74\text{ ppm}$  (**Figure 4.4c**). The former signal can be attributed to  $\text{T}^0$  [ $\text{CSi}(\text{OC}_2\text{H}_5)_3$ ] silicon resonances by comparison with the spectrum of the precursor. A similar assignment can be made for br-Ph particles [34, 48, 51]. The presence of dominant  $\text{T}^0$  silicon species further confirms the existence of ethoxy groups in br-BiPh and br-Ph. In contrast, a relatively weak signal corresponding to  $\text{T}^0$  silicon species centered at  $-45.86\text{ ppm}$  was observed in br-PhEt.

### 4.3 Foaming studies of bridged organosilica particles

Our previous studies have shown that sodium dodecylbenzenesulfonate (SDBS) is capable of stabilizing foams in benzyl alcohol by hand shaking (**Figure 4.5a**). However, no foam can be produced from sodium dodecyl sulfate (SDS) dispersion, since there is no change in the surface tension of benzyl alcohol ( $39.1\text{ mN}\cdot\text{m}^{-1}$ ). It is well known that the molecular structure of surfactants determines their adsorption ability at the air-oil interface, thus the foaming behaviour is strongly affected [52]. An important difference between both surfactants is that the head

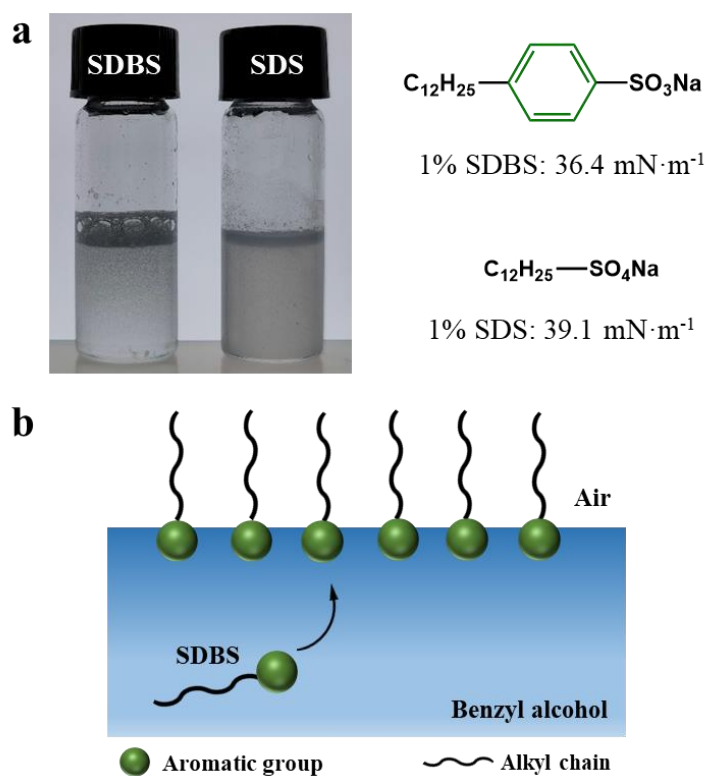
group of SDBS shows affinity to benzyl alcohol, while the head group of SDS is not compatible with the solvent. Both of them have an alkyl chain with 12 carbons, which is generally called hydrophobic tail [53-55]. By analogy with the behavior of the surfactants in aqueous foams [56], we speculate that SDBS molecules array at the air-oil interface with phenyl groups extending to benzyl alcohol and hydrophobic tails extending to the gas phase (**Figure 4.5b**). Inspired by this finding, we designed bridged organosilica particles mimicking the structural features of SDBS and hence more likely to assemble at the air-oil interface.



**Figure 4.4** Solid-state  $^{13}\text{C}$  (a) and  $^{29}\text{Si}$  (c) CP-MAS NMR spectra of bridged organosilica particles, liquid-state  $^{13}\text{C}$  (b) and  $^{29}\text{Si}$  (d) NMR spectra of related precursors.

The foamability of the as-prepared bridged organosilica particles was studied in benzyl alcohol by hand shaking. As shown in **Figure 4.6a**, stable foams can be generated from br-BiPh dispersions containing 1 wt% particles, while no foaming occurs for br-Ph and br-PhEt

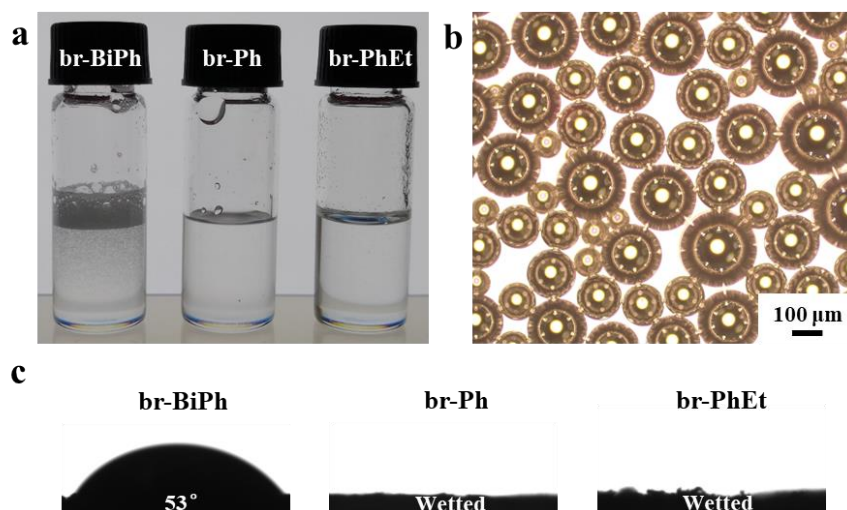
dispersions. These results suggest that the presence of biphenyl rings in br-BiPh is crucial for foamability. **Figure 4.6b** displays optical microscope images of the bubbles in benzyl alcohol stabilized by 1 wt% br-BiPh particles. The bubbles are polydisperse in size with diameters between 60 and 250  $\mu\text{m}$ .



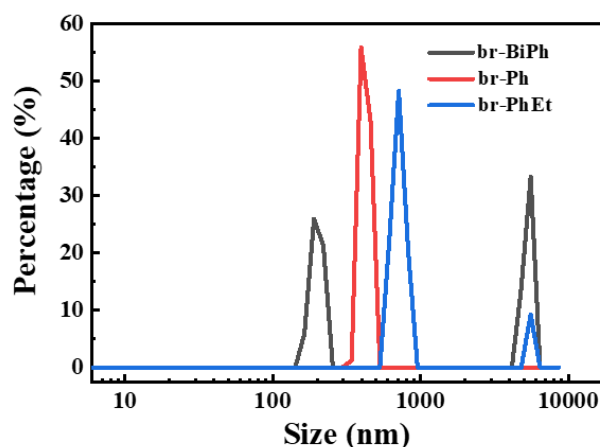
**Figure 4.5** Foamability of different anionic surfactants in benzyl alcohol (1 wt%) after hand shaking (a), and orientation behavior of SDBS molecules at the interface (b).

To rationalize the difference in the foaming properties of the different particles, we measured the contact angle of benzyl alcohol on pellets composed of compressed particles. It can be seen from **Figure 4.6c** that br-Ph and br-PhEt samples are fully wetted by benzyl alcohol, explaining the lack of foaming behavior of these particles. In contrast, br-BiPh particles exhibit a contact angles of  $53^\circ$ , which is suitable for foam generation [1, 3]. DLS analysis was used to gain insight into the particle size distribution of bridged organosilica in benzyl alcohol. As shown in **Figure 4.7**, br-BiPh particles exhibit two bands centered at 200 nm and 5  $\mu\text{m}$ , demonstrating that the particles can be well dispersed in benzyl alcohol, but tend to form larger aggregates after standing for several minutes. The size measured for br-Ph is around 400 nm, whereas that of br-PhEt is centered at 700 nm and 5.5  $\mu\text{m}$ , which is larger than that observed by TEM. This discrepancy is attributed to the strong aggregation of these particles in benzyl alcohol. The adsorption kinetics of such aggregates is expected to be slow which may further explain the lack of foamability for br-Ph and br-PhEt dispersions.



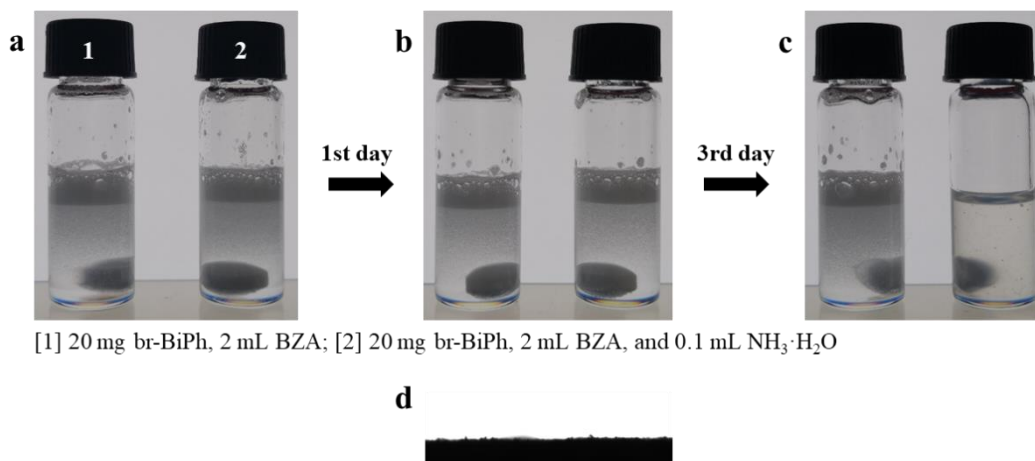


**Figure 4.6** Foams of 1 wt% bridged organosilica particles in benzyl alcohol (a), optical microscopy images of bubbles in benzyl alcohol stabilized by 1 wt% br-BiPh (b), and contact angles of bridged organosilica particles with benzyl alcohol (c).



**Figure 4.7** Particle size distribution curves of br-BiPh, br-Ph and br-PhEt in benzyl alcohol measured by DLS analysis.

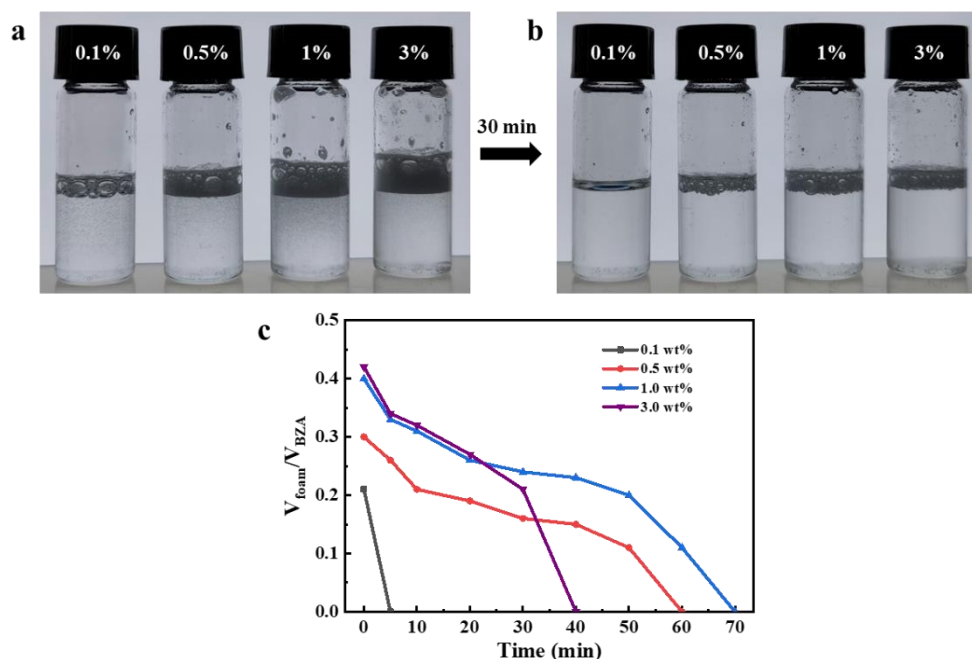
In order to understand the role of residual ethoxy groups in br-BiPh particles in the foaming properties, we performed a simple hydrolysis test under alkaline conditions (**Figure 4.8a-c**). The br-BiPh particles with ethoxy groups are fully hydrolyzed by  $\text{NH}_3 \cdot \text{H}_2\text{O}$  after continuous stirring for 3 days, and are unable to foam in benzyl alcohol as they are completely wetted by the solvent (**Figure 4.8d**), while non-hydrolyzed br-BiPh particles retain their foamability. These results suggest that the presence of ethoxy side chains in the particle structure is crucial for foam formation. Therefore, we assume that br-BiPh particles adsorbed at the air-oil interface orient their biphenyl group towards the solvent and expose their ethoxy group to air, so that the foam can be stabilized in benzyl alcohol.



**Figure 4.8** Images of foams generated by hand shaking taken after preparation (a), 1 day (b) and 3 days afterwards (c), and the contact angle of br-BiPh hydrolyzed by ammonia with benzyl alcohol (d).

The particle concentration is a well-known parameter controlling foaming. As shown in **Figure 4.9a**, the initial foam volume increases progressively with the br-BiPh concentration. A similar foam decay rate is observed for 0.5 and 1 wt% of particles (**Figure 4.9c**), and the half-life time is above 30 min. Foam collapse is faster at 0.1 wt% since a smaller interfacial area can be covered. Catastrophic foam collapse after 30 min is observed at the highest particle concentration (3 wt%), which is likely caused by particle agglomeration [57, 58].

Analyzing the properties of foams made by hand shaking is sometimes complex because there is limited control on the energy input along the foaming process. To achieve a controlled energy input, we used Ultra-Turrax<sup>®</sup>T25 equipped with a S25N-8G dispersing tool to produce foams. In these tests, a certain amount of br-BiPh was dispersed in benzyl alcohol, and the dispersion was aerated at 16,000 rpm for 3 min. At such conditions, oil foams can be generated at higher production rates compared to foams prepared by hand-shaking. The maximal foam volume fraction produced by this high-energy input method is as high as 96% for 3 wt% of particles (**Figure 4.10a**). Such excellent foamability can be explained by the reduction of the surface tension of the solvent induced by the presence of particles (**Figure 4.10d**). Indeed, the surface tension declines from 38.9 to 34.5  $\text{mN} \cdot \text{m}^{-1}$  after adding 0.1 wt% br-BiPh, with almost no further decrease at higher particle concentration. In contrast, br-Ph and br-PhEt particles exerted no effect on the surface tension of benzyl alcohol (**Table 4.1**). The lifetime of foams produced by Ultra-Turrax is surprisingly shorter than for those produced by hand shaking. This suggests lower interfacial coverage in the former case.

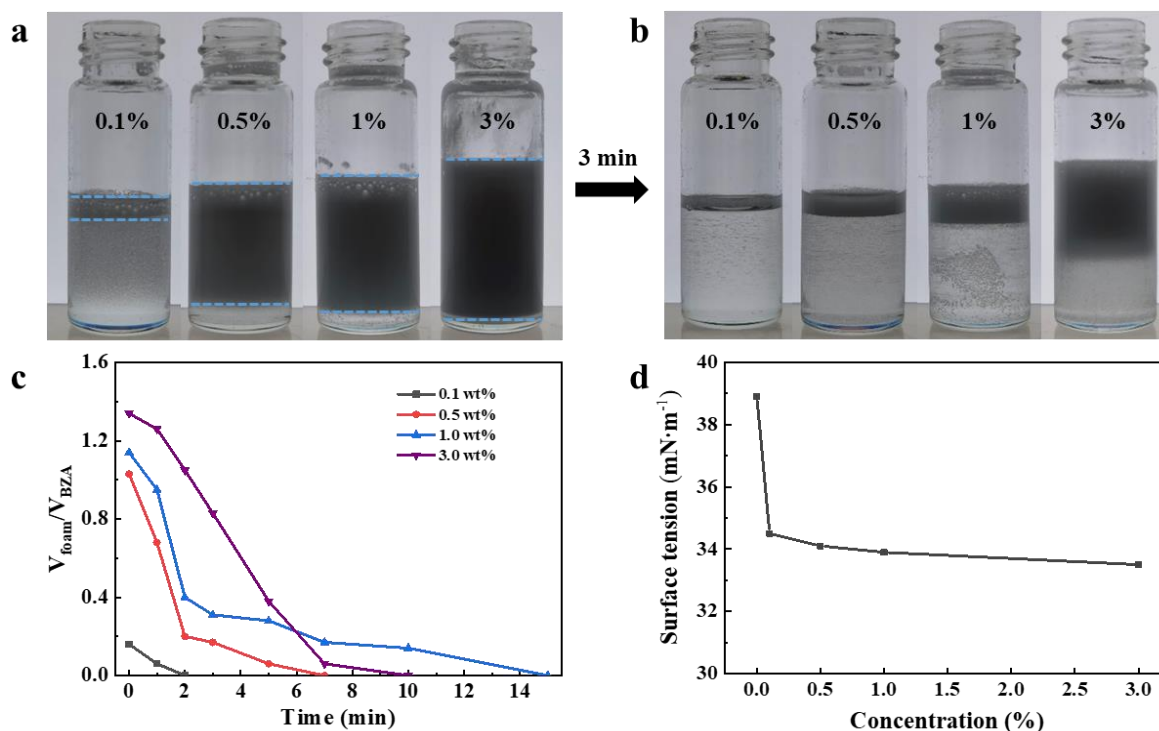


**Figure 4.9** Foams stabilized by br-BiPh with different particle fractions taken immediately after preparation (a) and 30 minutes later (b), and time-evolution of foam volume (c).

**Table 4.1** Surface tension of benzyl alcohol after addition of different stabilizers.

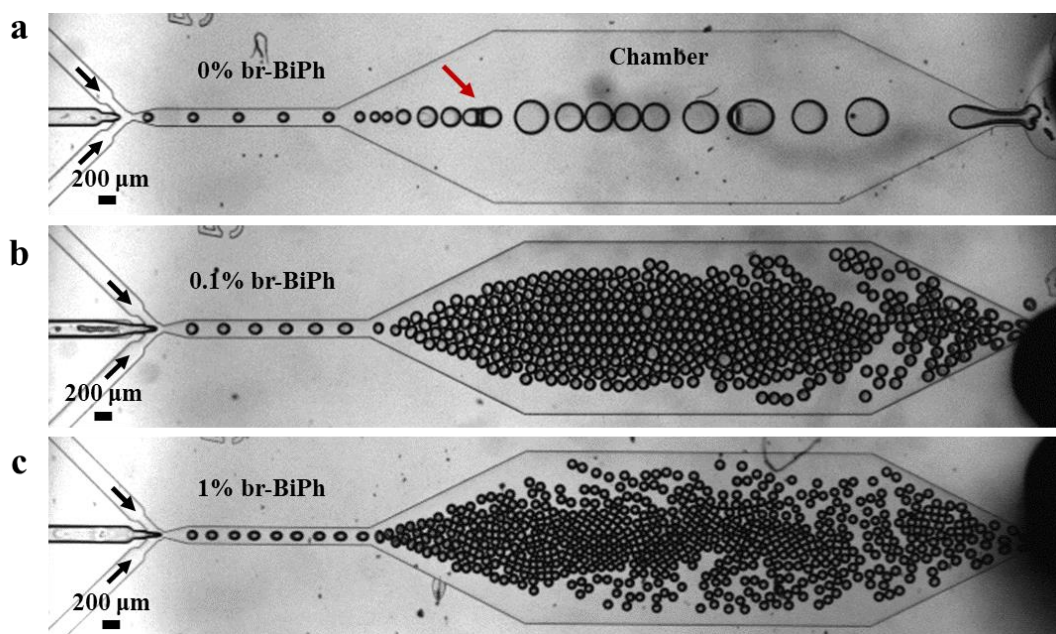
Entry	Sample	Surface tension ( $\text{mN}\cdot\text{m}^{-1}$ )
1	Pure benzyl alcohol	38.9
2	0.1% br-BiPh in benzyl alcohol	<b>34.5</b>
3	0.1% br-Ph in benzyl alcohol	38.7
4	0.1% br-PhEt in benzyl alcohol	38.8
5	0.1% PFOA in benzyl alcohol	<b>37.1</b>
6	0.1% MA in benzyl alcohol	38.7
7	0.1% PTFE in benzyl alcohol	38.8
8	0.1% $\text{SiO}_2\text{-F}_{17}$ in benzyl alcohol	39.0
9	0.1% PS in benzyl alcohol	38.5
10	0.1% POSS in benzyl alcohol	38.6

Isolated bubbles or microfoams with very well-controlled size could be generated using microfluidic device [59-61]. We therefore studied the foaming behavior of br-BiPh particles using homemade microfluidic chips. Microfluidics devices were fabricated with PDMS using a standard soft lithography procedure [62-67], as previously described in **Chapter 2**. The liquid was injected through side channels (marked by black arrow in **Figure 4.11**), while air arrived at the central channel. Both phases were injected at a desired flow rate and then passed through the flow-focusing orifice resulted in the fragmentation of the air flow and generation of monodispersed bubbles.

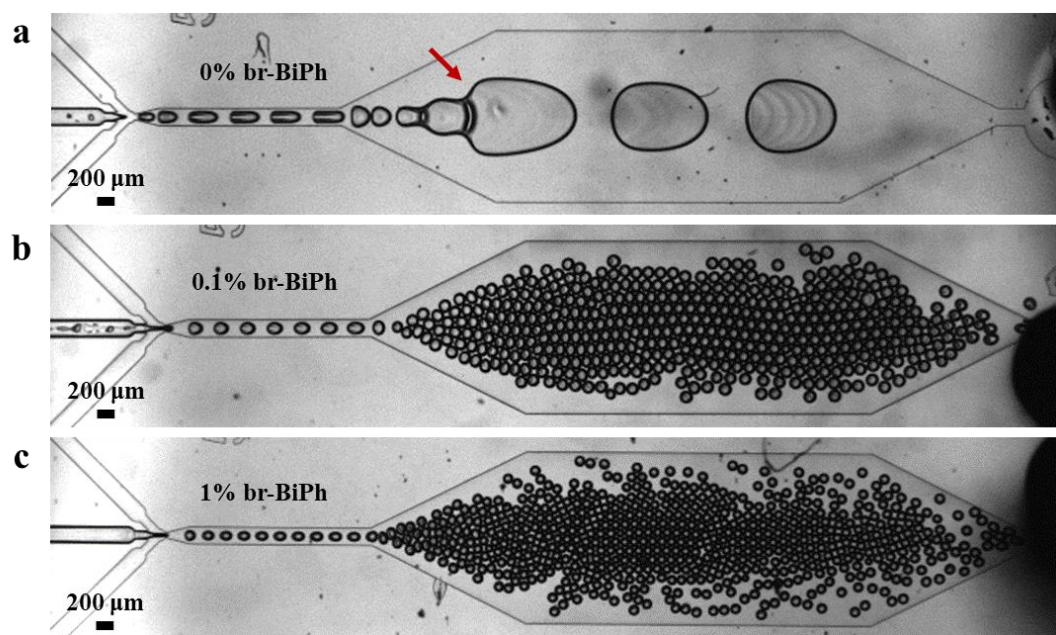


**Figure 4.10** Representative images of foams produced by Ultra-Turrax at various br-BiPh concentrations taken after preparation (a) and 3 minutes (b), foam evolution with time (c), and the surface tension of benzyl alcohol in the presence of br-BiPh (d).

**Figure 4.11** shows the generation of bubbles at  $140 \mu\text{L}\cdot\text{min}^{-1}$  and  $35 \mu\text{L}\cdot\text{min}^{-1}$  flowrate of liquid and air, respectively. In a particle-free environment (pure benzyl alcohol), bubbles tend to coalesce into bigger bubbles (red arrow in **Figure 4.11a**) when they get closer in the expansion chamber. In contrast, the bubbles with narrow polydispersity ( $80\text{-}110 \mu\text{m}$ ) are generated in the presence of 1 wt% br-BiPh particles (**Figure 4.11c**). It is worth mentioning that such monodispersed bubbles are stable against coalescence and disproportionation. The size distribution of the bubbles become broader (ranging from  $90$  to  $140 \mu\text{m}$ ) when reducing the particle concentration to 0.1 wt% (**Figure 4.11b**). Increasing the air flow rate to  $280 \mu\text{L}\cdot\text{min}^{-1}$  allows the generation of a larger amount of bubbles (**Figure 4.12**). With both concentration of br-BiPh tested, bubbles are stable to coalescence, pointing out a high stabilization efficiency of designed material even at low concentration.



**Figure 4.11** Optical microscope images showing generation of bubbles at a flow rate of liquid and air of  $140 \mu\text{L}\cdot\text{min}^{-1}$  and  $35 \mu\text{L}\cdot\text{min}^{-1}$ , respectively.



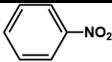
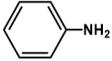
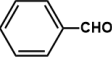
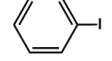
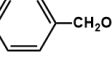
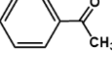
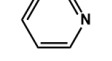
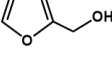
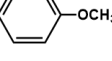
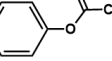
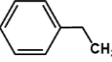
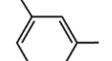
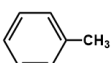
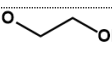
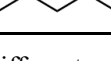
**Figure 4.12** Production of bubbles in microfluidic device at a flow rate of liquid and air of  $140 \mu\text{L}\cdot\text{min}^{-1}$  and  $280 \mu\text{L}\cdot\text{min}^{-1}$ , respectively.

#### 4.4 Effect of the solvent nature on foamability

In addition to the chemical structure and related surface properties of organosilica particles discussed above, the solvent can govern foam formation. To elucidate how the solvent affects the particle foamability, we performed hand-shaking tests using a br-BiPh dispersion (1 wt%) in fifteen organic solvents with variable surface tension and functional groups (**Table 4.2**). Foams

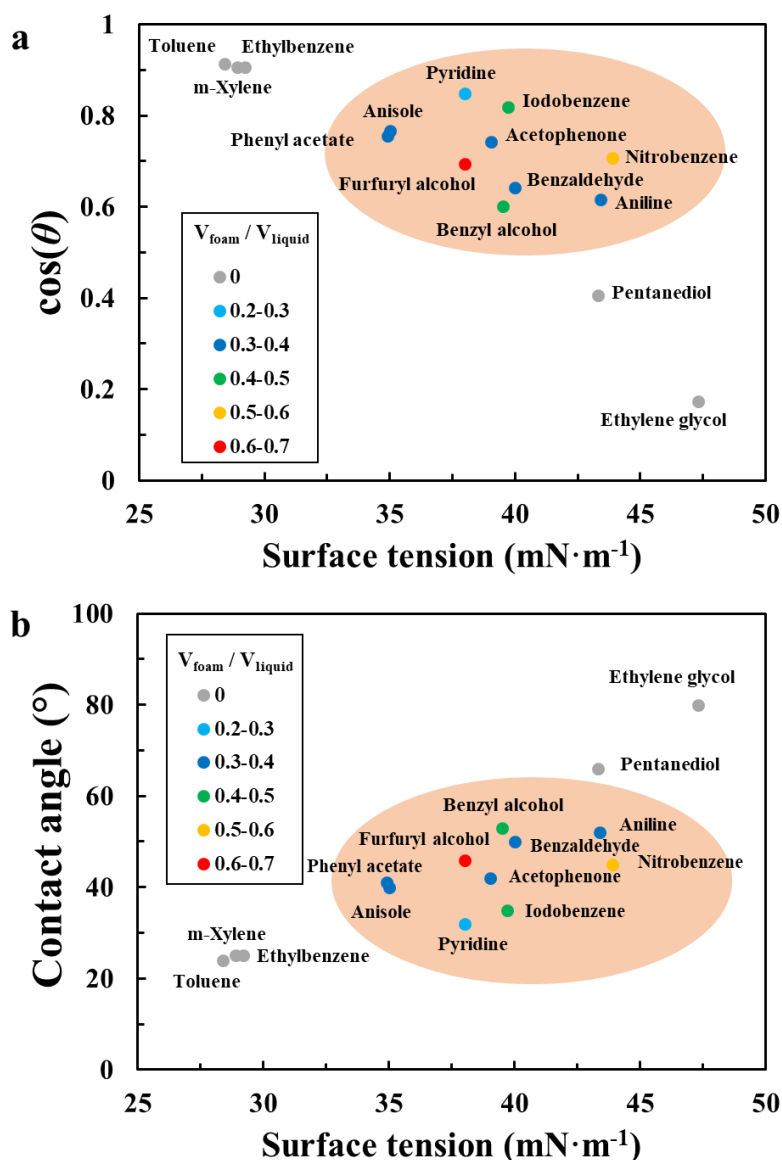
are formed from aromatic solvents with a surface tension between *ca.* 35 and 44 mN·m<sup>-1</sup> (**Figure 4.13, Figure 4.14a**). Foamability seems to correlate with the electronegativity of the groups in the solvent molecules. For instance, nitrobenzene and furfuryl alcohol show better foamability than pyridine and anisole. In terms of contact angle, foams are generated in the range between 32° and 53° (**Figure 4.15**), which is consistent with previous reports [1, 3].

**Table 4.2** Properties and foaming behaviors of the solvents in the presence of 1% br-BiPh.

Name (abbreviation)	Structure	Surface tension (mN·m <sup>-1</sup> , 20 °C)	Contact angle <sup>a</sup> (°)	V <sub>foam</sub> /V <sub>liquid</sub> <sup>b</sup>
Nitrobenzene (NB)		43.9	45	0.54
Aniline		43.4	52	0.38
Benzaldehyde (BA)		40	50	0.42
Iodobenzene (IB)		39.7	35	0.43
Benzyl alcohol (BZA)		39.5	53	0.40
Acetophenone (AP)		39.04	42	0.38
Pyridine		38	32	0.20
Furfuryl alcohol (FA)		38	46	0.60
Anisole		35	40	0.35
Phenyl acetate (PA)		34.9	41	0.33
Ethylbenzene (EB)		29.2	25	0
m-Xylene		28.9	25	0
Toluene		28.4	24	0
Ethylene glycol (EG)		47.3	80	0
1,5-Pentanediol (PD)		43.3	66	0

<sup>a</sup> Contact angles of br-BiPh with different organic solvents in Figure 4.15.

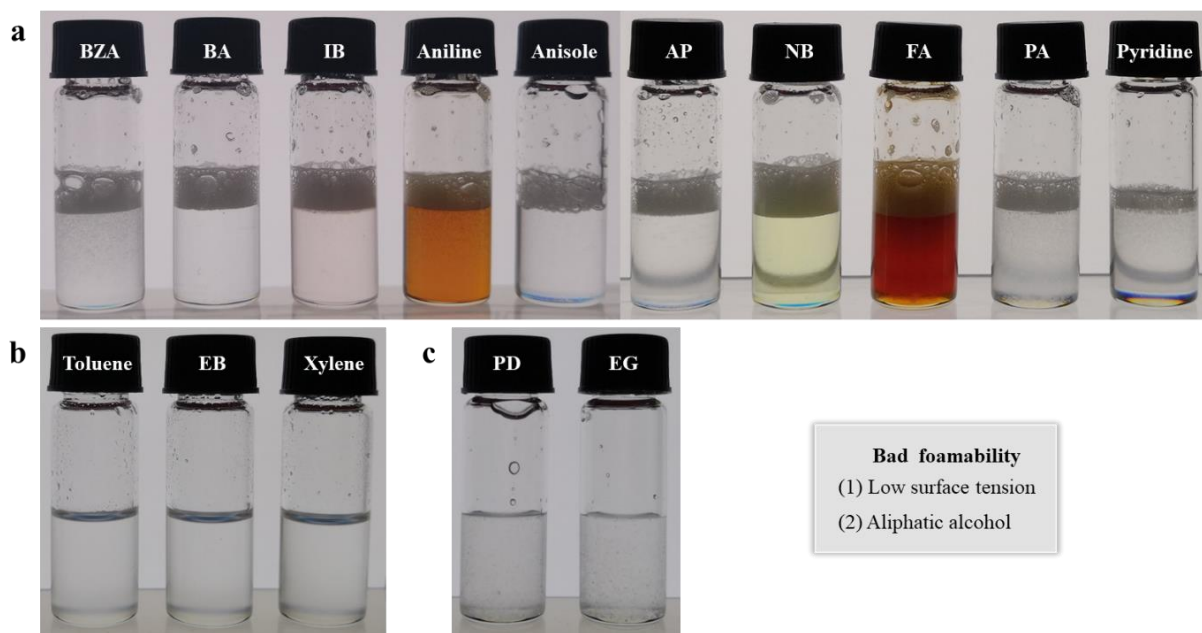
<sup>b</sup> V<sub>foam</sub>/V<sub>liquid</sub> (“foamability”) = foam volume/initial volume of the solvent.



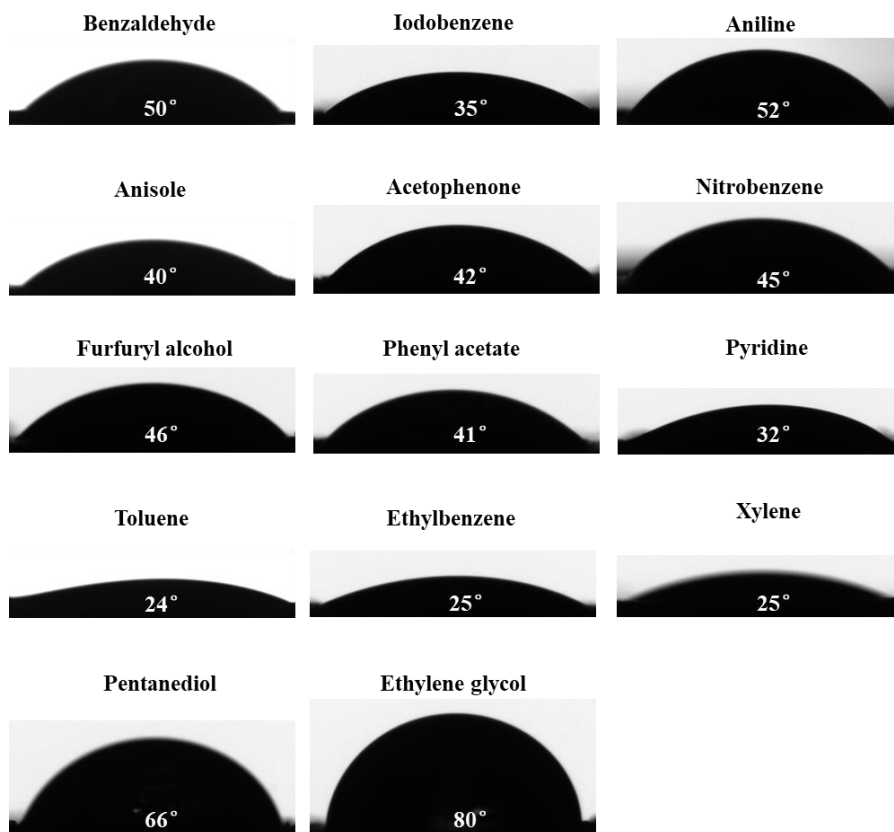
**Figure 4.13** Cosine of contact angle (a) and contact angle (b) of solvent on br-BiPh as a function of the solvent surface tension.

Apolar aromatic solvents with low surface tension ( $\gamma < 30 \text{ mN}\cdot\text{m}^{-1}$ ) such as toluene, xylene and ethylbenzene, overwet the particles (contact angle  $24\text{-}25^\circ$ ), resulting in no foam formation. No foams are either obtained for very polar aliphatic alcohols like 1,5-pentanediol and ethylene glycol (**Figure 4.14c**). The former is an interesting example as the surface tension of 1,5-pentanediol is similar to that of well-foaming nitrobenzene and aniline ( $43.3$  vs  $43.9$  and  $43.4 \text{ mN}\cdot\text{m}^{-1}$ , respectively), but the contact angle is much higher ( $66^\circ$  vs  $45^\circ$  and  $52^\circ$ , respectively). From Young's equation (eq. 1) we can derive that the solid-liquid surface tension  $\gamma_{sl}$  in this solvent is higher than in nitrobenzene and aniline as the solid-air tension  $\gamma_{sa}$ , is constant and the liquid-air tension  $\gamma_{la}$ , is nearly identical for all three solvents. Bad wetting of the particles by 1,5-

pentanediol therefore renders the thermodynamic condition of particle adsorption at the interface (eq. 2) invalid, preventing foam formation.



**Figure 4.14** Photographs of vessels containing different solvents and br-BiPh (1 wt%) after hand shaking.



**Figure 4.15** Contact angles of br-BiPh with different organic solvents.



$$\cos \theta = \frac{\gamma_{sa} - \gamma_{sl}}{\gamma_{la}} \quad (1)$$

$$\gamma_{sa} + \gamma_{sl} < \gamma_{la} \quad (2)$$

Overall, the results above point out that foamability is favored for contact angles around 45°. The presence of a polar group in the solvent molecule promotes foamability. Although the role of the surface tension seems to be less important, it should remain in the range *ca.* 35 and 44 mN·m<sup>-1</sup>.

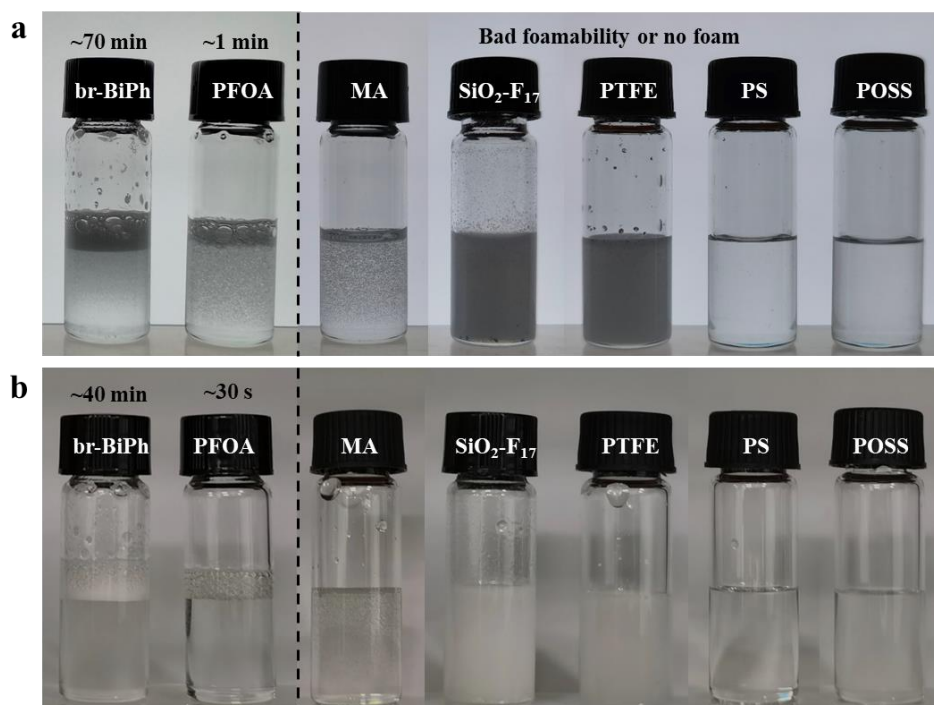
#### 4.5 Comparison of foams stabilized by different particles and surfactants

In earlier works, polytetrafluoroethylene (PTFE) and fluorinated particles were employed as foaming agents to stabilize foams in aromatic solvents (*e.g.*, toluene, benzene, benzyl acetate) [29, 30, 68]. Moreover, as demonstrated in our previous study, stable foams in benzyl alcohol can be achieved in the presence of Aquivion<sup>®</sup> D98. However, there are very few reports on foams stabilized by non-fluorinated particles in aromatic solvents with relatively high polarity (*e.g.*, benzyl alcohol and aniline). In this section, the advantages and disadvantages of various stabilizers reported in the literature are discussed (**Table 4.3**), and we compare the foaming properties of br-BiPh particles with other types of foaming agents in benzyl alcohol as a model solvent. As shown in **Figure 4.16a**, only br-BiPh particles and fluorinated surfactants (PFOA) can provide good foamability, which can be explained by a decrease of surface tension of benzyl alcohol (**Table 4.1**). However, foam stability of PFOA is much lower (~1 min) compared to that of br-BiPh particles (~70 min), and it is difficult to efficiently separate and recycle surfactants from the systems.

In addition, we studied the foaming property of the br-BiPh system at higher temperature (80 °C). It can still maintain good foamability in benzyl alcohol except that the foam lifetime was shorten (~40 min, **Figure 4.16b**), which indicates that the br-BiPh particles have a wide foaming temperature window. On the contrary, for oil foams stabilized by long chain fatty acid esters or fatty acid crystals in vegetable oils, the solid phase will melt at this temperature and become a homogeneous liquid phase and no foams remain [17, 69, 70]. As a typical example of fatty acid crystals, myristic acid (MA) can enable foam formation in high oleic sunflower oil at room temperature [70]. However, almost no foams could be obtained in benzyl alcohol at both room temperature and high temperature.

In the case of fluorinated agents, no surface tension effect is observed in the presence of PTFE and fluorinated silica particles (38.8 and 39.0 mN·m<sup>-1</sup>, respectively), thus no foam formation is observed in benzyl alcohol (**Figure 4.16a**). Besides, fluorosilica particles coated with different fluorine content are not applicable in benzyl alcohol [29]. For commercial

polymers containing benzene rings such as polystyrene (PS) and PSS-octaphenyl substituted (POSS), none of them can stabilize foams in benzyl alcohol probably due to the absence of alkyl chains. Based on these studies, it can be concluded that br-BiPh particles exhibit better foaming properties (higher foamability and stability) in benzyl alcohol compared to conventional fluorinated particles and surfactants.



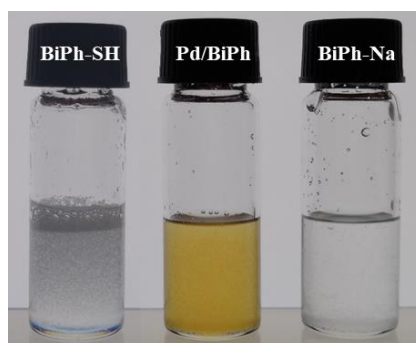
**Figure 4.16** Foamability of different agents in benzyl alcohol (1%) at room temperature (a) and 80 °C (b).

#### 4.6 Foaming studies of bridged organosilica particles after Pd loading

One of the main objectives of the present study was to extend the utility of these particles by incorporating a noble metal, rendering them catalytically active for gas involved reactions. Therefore, we prepared the thiol-modified organosilicas (BiPh-SH) by co-condensation of BTEBP with MPTMES (for synthetic method please see **section 2.5**). Afterwards, Pd species were loaded on the surface of BiPh-SH by conventional impregnation and reduction method. Unfortunately, the as-prepared samples (Pd/BiPh) were unable to foam in benzyl alcohol after the palladium loading (**Figure 4.17**). In order to elucidate the reason for such a bad foamability, the BiPh-SH materials were dispersed in the aqueous sodium borohydride (NaBH<sub>4</sub>) solution. After stirring for 2 h, the samples (denoted as BiPh-Na) were washed and collected by centrifugation. Surprisingly, no foams is generated with BiPh-Na in benzyl alcohol. We thus assume that the ethoxy groups incorporated in organosilicas fully hydrolyze during the preparation, which is possibly related to the alkaline nature of NaBH<sub>4</sub> solution [71].

**Table 4.3** Comparison of non-aqueous foams between br-BiPh particles and other foaming agents.

Entry	Additives	Non-aqueous systems	Advantages	Disadvantages	Ref.
1	br-BiPh particles	Aromatic solvents with the surface tension in the range 35 and 44 $\text{mN}\cdot\text{m}^{-1}$	Thermal stability up to 210 °C, good foamability by hand shaking and outstanding foamability with ultra-turrax	Easily hydrolyzed under acidic / alkaline conditions, low foam stability with ultra-turrax	This work
2	PTFE and oligomeric tetrafluoroethylene (OTFE)	Peanut oil, sunflower oil, rapeseed oil, eugenol, tricresyl phosphate, ahexyl cinnamaldehyde, benzyl acetate, bromonaphthalene, few bubbles in benzene	Outstanding chemical and thermal stability	Highly resistant to environmental degradation, poor dispersibility in solvent	[22, 30, 68]
3	Fluorinated particles (silica, sericite, clays and zinc oxide)	Oils with surface tensions higher than 26 $\text{mN}\cdot\text{m}^{-1}$ ( <i>e.g.</i> , sunflower oil, toluene, benzene, benzyl acetate and hexadecane)	Both liquid oil marbles and foams can be obtained by varying the degree of fluorination	Resistant to degrade under environmental conditions	[8, 29, 31]
4	Specialty surfactants ( <i>e.g.</i> , fluoroalkyl ester)	Dodecane, polyurethane	Soluble in the liquid, aggregation and sedimentation are unlikely to occur in the system	Difficult to remove or recycle from the oils	[19, 72]
5	Surfactant crystals ( <i>e.g.</i> , fatty acid ester and myristic acid crystals)	Vegetable oils ( <i>e.g.</i> , olive oil, sunflower oil, squalane and liquid paraffin)	Naturally abundant, low cost	Foams in limited oils, solubilize at elevated temperature	[17, 69, 70]
6	Asphaltenes and resins	Crude oil	Naturally occurring compounds in crude oil	Only foams in crude oil and synthetic crude oil	[20, 73]



**Figure 4.17** Foamability of br-BiPh particles after modification.

#### 4.7 Conclusion

In this study, we present one of the rare examples of non-fluorinated particles stabilizing foams of organic solvents. In order to achieve good foamability in aromatic solvents, a series of organosilicas was prepared by sol-gel synthesis using different aromatic organosilane precursors. The incorporation of organic groups in the organosilicas was confirmed by TGA, FTIR and solid-state  $^{13}\text{C}$  and  $^{29}\text{Si}$  MAS NMR. Rational designed organosilica particles outperformed polytetrafluoroethylene, myristic acid, and other fluorinated stabilizers both in terms of foamability and foam stability in benzyl alcohol. In particular, biphenyl-bridged particles could stabilize foams in a variety of organic solvents with a maximal foam volume fraction as high as 96% produced by Ultra-Turrax.

The influence of the surface properties of organosilicas on foamability was systematically investigated, and both the presence of biphenyl rings (mimicking the structure of the solvent) and ethoxy groups (well wetted by the gas phase) were essential to ensure good foaming. Moreover, the contact angle appears to be the main parameter controlling foaming. Foams were generated in the contact angle range between  $32^\circ$  and  $53^\circ$ , and the maximum foamability was achieved around  $45^\circ$ . At the same time, the surface tension of the solvent should lie in the range  $35\text{-}44\text{ mN}\cdot\text{m}^{-1}$ . However, for apolar aromatic solvents with low surface tension ( $\gamma < 30\text{ mN}\cdot\text{m}^{-1}$ ) and very polar aliphatic alcohols, the contact angle with particles was either too low or too high, preventing foam stabilization.

Overall, this study allows better understanding of Pickering foam formation in organic phases, and opens perspectives for the synthesis of new non-halogenated foaming materials. The combination of br-BiPh particles as the foaming agent with noble metal catalyst may be a plausible approach to construct the catalytic system.

## 4.8 References

1. Fameau, A.-L. and A. Saint-Jalmes, *Non-aqueous foams: Current understanding on the formation and stability mechanisms*. Advances in Colloid and Interface Science, 2017. **247**: p. 454-464.
2. Rodrigues, J.A., et al., *Generation and manipulation of bubbles and foams stabilised by magnetic nanoparticles*. Colloids and Surfaces A: Physicochemical and Engineering Aspects, 2011. **384**(1-3): p. 408-416.
3. Binks, B.P. and B. Vishal, *Particle-stabilized oil foams*. Advances in Colloid and Interface Science, 2021: p. 102404.
4. Binks, B.P. and H. Shi, *Aqueous foams in the presence of surfactant crystals*. Langmuir, 2020. **36**(4): p. 991-1002.
5. Sheng, Y., et al., *Ultra-stable aqueous foams induced by interfacial co-assembly of highly hydrophobic particles and hydrophilic polymer*. Journal of Colloid and Interface Science, 2020. **579**: p. 628-636.
6. Safouane, M., D. Langevin, and B. Binks, *Effect of particle hydrophobicity on the properties of silica particle layers at the air– water interface*. Langmuir, 2007. **23**(23): p. 11546-11553.
7. Binks, B.P. and T.S. Horozov, *Aqueous foams stabilized solely by silica nanoparticles*. Angewandte Chemie International Edition, 2005. **44**(24): p. 3722-3725.
8. Binks, B.P., T. Sekine, and A.T. Tyowua, *Dry oil powders and oil foams stabilised by fluorinated clay platelet particles*. Soft Matter, 2014. **10**(4): p. 578-589.
9. Murakami, R., et al., *Effects of contact angle and flocculation of particles of oligomer of tetrafluoroethylene on oil foaming*. Frontiers in chemistry, 2018. **6**: p. 435.
10. Huang, J., et al., *pH-responsive gas–water–solid interface for multiphase catalysis*. Journal of the American Chemical Society, 2015. **137**(47): p. 15015-15025.
11. Binks, B.P. and T.S. Horozov, *Colloidal particles at liquid interfaces*. 2006: Cambridge University Press.
12. Pugh, R.J., *Bubble and foam chemistry*. 2016: Cambridge University Press.
13. Cantat, I., et al., *Foams: structure and dynamics*. 2013: OUP Oxford.
14. Yekeen, N., et al., *A comprehensive review of experimental studies of nanoparticles-stabilized foam for enhanced oil recovery*. Journal of Petroleum Science and Engineering, 2018. **164**: p. 43-74.
15. Farajzadeh, R., et al., *Foam–oil interaction in porous media: implications for foam assisted enhanced oil recovery*. Advances in colloid and interface science, 2012. **183**: p. 1-13.
16. Heymans, R., et al., *Food-grade monoglyceride oil foams: the effect of tempering on foamability, foam stability and rheological properties*. Food & function, 2018. **9**(6): p. 3143-3154.
17. Shrestha, L.K., et al., *Foaming properties of monoglycerol fatty acid esters in nonpolar oil systems*. Langmuir, 2006. **22**(20): p. 8337-8345.

18. Robb, I.D., *Specialist surfactants*. 1996: Springer Science & Business Media.
19. Bergeron, V., J.E. Hanssen, and F. Shoghl, *Thin-film forces in hydrocarbon foam films and their application to gas-blocking foams in enhanced oil recovery*. Colloids and Surfaces A: Physicochemical and Engineering Aspects, 1997. **123**: p. 609-622.
20. Bauget, F., D. Langevin, and R. Lenormand, *Dynamic surface properties of asphaltenes and resins at the oil–air interface*. Journal of Colloid and Interface Science, 2001. **239**(2): p. 501-508.
21. Blázquez, C., et al., *Non-aqueous and crude oil foams*. Oil & Gas Science and Technology–Revue d’IFP Energies nouvelles, 2014. **69**(3): p. 467-479.
22. Murakami, R. and A. Bismarck, *Particle-Stabilized Materials: Dry Oils and (Polymerized) Non-Aqueous Foams*. Advanced Functional Materials, 2010. **20**(5): p. 732-737.
23. Wang, L., et al., *Synthesis of silicon carbide nanocrystals from waste polytetrafluoroethylene*. Dalton Transactions, 2017. **46**(9): p. 2756-2759.
24. Kauffman, G.W. and P.C. Jurs, *Prediction of surface tension, viscosity, and thermal conductivity for common organic solvents using quantitative structure– property relationships*. Journal of chemical information and computer sciences, 2001. **41**(2): p. 408-418.
25. Binks, B.P., *Particles as surfactants—similarities and differences*. Current opinion in colloid & interface science, 2002. **7**(1-2): p. 21-41.
26. Karakashev, S.I., et al., *Formation and stability of foams stabilized by fine particles with similar size, contact angle and different shapes*. Colloids and Surfaces A: Physicochemical and Engineering Aspects, 2011. **382**(1-3): p. 132-138.
27. Arriaga, L.R., et al., *On the long-term stability of foams stabilised by mixtures of nano-particles and oppositely charged short chain surfactants*. Soft Matter, 2012. **8**(43): p. 11085-11097.
28. Mase, N., T. Mizumori, and Y. Tatemoto, *Aerobic copper/TEMPO-catalyzed oxidation of primary alcohols to aldehydes using a microbubble strategy to increase gas concentration in liquid phase reactions*. Chemical Communications, 2011. **47**(7): p. 2086-2088.
29. Binks, B.P. and A.T. Tyowua, *Influence of the degree of fluorination on the behaviour of silica particles at air–oil surfaces*. Soft Matter, 2013. **9**(3): p. 834-845.
30. Binks, B.P., A. Rocher, and M. Kirkland, *Oil foams stabilised solely by particles*. Soft Matter, 2011. **7**(5): p. 1800-1808.
31. Binks, B.P., et al., *Particles at oil–air surfaces: powdered oil, liquid oil marbles, and oil foam*. ACS applied materials & interfaces, 2015. **7**(26): p. 14328-14337.
32. Dyab, A.K. and H.N. Al-Haque, *Particle-stabilised non-aqueous systems*. RSC Advances, 2013. **3**(32): p. 13101-13105.
33. Myers, J.N., et al., *Influence of casting solvent on phenyl ordering at the surface of spin cast polymer thin films*. Journal of colloid and interface science, 2014. **423**: p. 60-66.

34. Shea, K., D.A. Loy, and O. Webster, *Arylsilsesquioxane gels and related materials. New hybrids of organic and inorganic networks*. Journal of the American Chemical Society, 1992. **114**(17): p. 6700-6710.
35. Ciriminna, R., et al., *The sol–gel route to advanced silica-based materials and recent applications*. Chemical reviews, 2013. **113**(8): p. 6592-6620.
36. Hoffmann, F., et al., *Silica-based mesoporous organic–inorganic hybrid materials*. Angewandte Chemie International Edition, 2006. **45**(20): p. 3216-3251.
37. Mizoshita, N., T. Tani, and S. Inagaki, *Syntheses, properties and applications of periodic mesoporous organosilicas prepared from bridged organosilane precursors*. Chemical Society Reviews, 2011. **40**(2): p. 789-800.
38. Dral, A.P., C. Lievens, and J.E. ten Elshof, *Influence of monomer connectivity, network flexibility, and hydrophobicity on the hydrothermal stability of organosilicas*. Langmuir, 2017. **33**(22): p. 5527-5536.
39. Ferré, M., et al., *Recyclable organocatalysts based on hybrid silicas*. Green chemistry, 2016. **18**(4): p. 881-922.
40. Zamboulis, A., et al., *Hybrid materials: versatile matrices for supporting homogeneous catalysts*. Journal of Materials Chemistry, 2010. **20**(42): p. 9322-9338.
41. Croissant, J.G., et al., *Organosilica hybrid nanomaterials with a high organic content: syntheses and applications of silsesquioxanes*. Nanoscale, 2016. **8**(48): p. 19945-19972.
42. Diaz, U., D. Brunel, and A. Corma, *Catalysis using multifunctional organosiliceous hybrid materials*. Chemical Society Reviews, 2013. **42**(9): p. 4083-4097.
43. Croissant, J.G., et al., *Syntheses and applications of periodic mesoporous organosilica nanoparticles*. Nanoscale, 2015. **7**(48): p. 20318-20334.
44. Zou, H., et al., *An organosilane-directed growth-induced etching strategy for preparing hollow/yolk–shell mesoporous organosilica nanospheres with perpendicular mesochannels and amphiphilic frameworks*. Journal of Materials Chemistry A, 2014. **2**(31): p. 12403-12412.
45. Stöber, W., A. Fink, and E. Bohn, *Controlled growth of monodisperse silica spheres in the micron size range*. Journal of colloid and interface science, 1968. **26**(1): p. 62-69.
46. Yang, Y. and A. Sayari, *Molecularly ordered biphenyl-bridged mesoporous organosilica prepared under acidic conditions*. Chemistry of materials, 2007. **19**(17): p. 4117-4119.
47. Du, H., et al., *A facile synthesis of highly water-soluble, core–shell organo-silica nanoparticles with controllable size via sol–gel process*. Journal of colloid and interface science, 2009. **340**(2): p. 202-208.
48. Kapoor, M.P., Q. Yang, and S. Inagaki, *Self-assembly of biphenylene-bridged hybrid mesoporous solid with molecular-scale periodicity in the pore walls*. Journal of the American Chemical Society, 2002. **124**(51): p. 15176-15177.

49. Park, M., et al., *Hydrophobic mesoporous materials for immobilization of enzymes*. *Microporous and Mesoporous Materials*, 2009. **124**(1-3): p. 76-83.
50. Theivendran, S., et al., *Synthesis of biphenyl bridged dendritic mesoporous organosilica with extremely high adsorption of pyrene*. *Journal of Materials Chemistry A*, 2019. **7**(19): p. 12029-12037.
51. Yang, Y. and A. Sayari, *Mesoporous Organosilicates from Multiple Precursors: Co-Condensation or Phase Segregation/Separation?* *Chemistry of Materials*, 2008. **20**(9): p. 2980-2984.
52. You, Y., et al., *Effect of alkyl tail length of quaternary ammonium gemini surfactants on foaming properties*. *Colloids and Surfaces A: Physicochemical and Engineering Aspects*, 2011. **384**(1-3): p. 164-171.
53. Clint, J.H., *Surfactant aggregation*. 2012: Springer Science & Business Media.
54. Zhang, J., et al., *Self-assembly of organic– inorganic hybrid amphiphilic surfactants with large polyoxometalates as polar head groups*. *Journal of the American Chemical Society*, 2008. **130**(44): p. 14408-14409.
55. Holmberg, K., *Natural surfactants*. *Current Opinion in Colloid & Interface Science*, 2001. **6**(2): p. 148-159.
56. Zhao, H., et al., *Understanding of the foam capability of sugar-based nonionic surfactant from molecular level*. *Colloids and Surfaces A: Physicochemical and Engineering Aspects*, 2018. **551**: p. 165-173.
57. Yekeen, N., et al., *Bulk and bubble-scale experimental studies of influence of nanoparticles on foam stability*. *Chinese Journal of Chemical Engineering*, 2017. **25**(3): p. 347-357.
58. Holthoff, H., et al., *Coagulation rate measurements of colloidal particles by simultaneous static and dynamic light scattering*. *Langmuir*, 1996. **12**(23): p. 5541-5549.
59. Hashimoto, M., P. Garstecki, and G.M. Whitesides, *Synthesis of composite emulsions and complex foams with the use of microfluidic flow-focusing devices*. *small*, 2007. **3**(10): p. 1792-1802.
60. Park, J.I., et al., *A microfluidic approach to chemically driven assembly of colloidal particles at gas–liquid interfaces*. *Angewandte Chemie*, 2009. **121**(29): p. 5404-5408.
61. Huerre, A., V. Miralles, and M.-C. Jullien, *Bubbles and foams in microfluidics*. *Soft matter*, 2014. **10**(36): p. 6888-6902.
62. Qin, D., Y. Xia, and G.M. Whitesides, *Soft lithography for micro-and nanoscale patterning*. *Nature protocols*, 2010. **5**(3): p. 491.
63. Xia, Y. and G.M. Whitesides, *Soft Lithography*. *Angew. Chem. Int. Ed*, 1998. **37**: p. 550-575.
64. San-Miguel, A. and H. Lu, *Microfluidics as a tool for C. elegans research*. *WormBook: The Online Review of C. elegans Biology [Internet]*, 2018.
65. Prado, E., et al., *SERS spectra of oligonucleotides as fingerprints to detect label-free RNA in microfluidic devices*. *The Journal of Physical Chemistry C*, 2014. **118**(25): p. 13965-13971.



66. Beneyton, T., et al., *CotA laccase: high-throughput manipulation and analysis of recombinant enzyme libraries expressed in E. coli using droplet-based microfluidics*. *Analyst*, 2014. **139**(13): p. 3314-3323.
67. Ma, K., et al., *Wettability control and patterning of PDMS using UV–ozone and water immersion*. *Journal of colloid and interface science*, 2011. **363**(1): p. 371-378.
68. Binks, B.P. and A. Rocher, *Stabilisation of liquid–air surfaces by particles of low surface energy*. *Physical Chemistry Chemical Physics*, 2010. **12**(32): p. 9169-9171.
69. Shrestha, L.K., et al., *Stabilization of nonaqueous foam with lamellar liquid crystal particles in diglycerol monolaurate/olive oil system*. *Journal of colloid and interface science*, 2008. **328**(1): p. 172-179.
70. Binks, B.P., E.J. Garvey, and J. Vieira, *Whipped oil stabilised by surfactant crystals*. *Chemical science*, 2016. **7**(4): p. 2621-2632.
71. Banfi, L., E. Narisano, and R. Riva, *Sodium Borohydride*, in *Encyclopedia of Reagents for Organic Synthesis*.
72. W.R. Rossen, R. Prud'homme, S. Khan, *Foams: theory, measurements and applications, Foams in enhanced oil recovery*, 1996, 413-464.
73. Zaki, N.N., M.K. Poindexter, and P.K. Kilpatrick, *Factors contributing to petroleum foaming. 2. Synthetic crude oil systems*. *Energy & fuels*, 2002. **16**(3): p. 711-717.

## **CHAPTER 5**

---

### **Organic Foams Stabilized by Fluorinated Organosilica Particles**

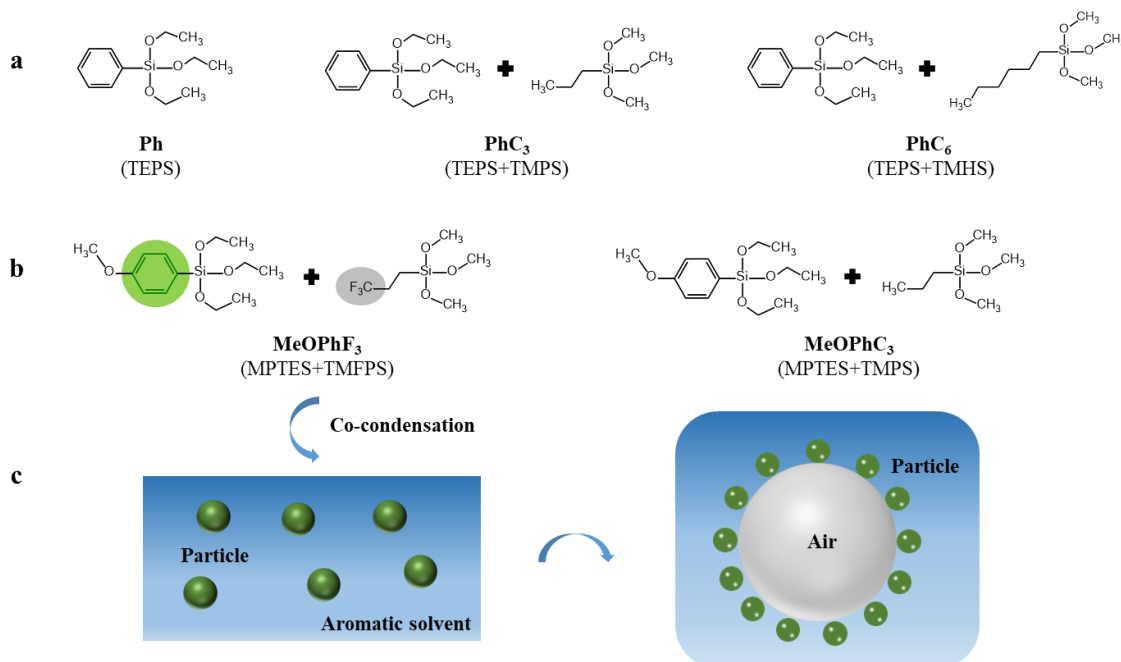
---

## 5.1 Introduction

In the previous chapter, we designed the surface-active particles by mimicking the structure of the aromatic solvent and the gas. The resulting biphenyl-bridged particles (br-BiPh) could stabilize foams in a variety of organic solvents. It was demonstrated that both the presence of phenyl rings and ethoxy groups (short alkyl chains) is crucial for foam formation. However, after treatment with acid or base, the br-BiPh particles were unable to stabilize non-aqueous foams due to fast hydrolysis of ethoxy groups. Therefore, it would be highly desirable to develop a novel foam stabilizer with higher chemical resistance.

Triethoxyphenylsilane (TEPS) is a relatively inexpensive precursor and thus an attractive candidate for preparing organosilicas with pendant phenyl moieties [1-3]. Multifunctional organosilica particles can be prepared by co-condensation of different silane precursors (*e.g.*, a mixture of TEPS and TEOS) to achieve the desired surface properties [4-6].

In this chapter, a library of organosilica particles was prepared by a one-pot co-condensation route (**Figure 5.1**). Our aim was to obtain stable organosilica particles with good foaming properties in aromatic solvents. The surface properties of organosilica particles were finely tuned by adjusting the chemical composition, and fluorinated organosilica particles showed optimal performance for foam stabilization. Comprehensive characterization of the resulting organosilica particles was performed, and the parameters affecting the foaming behavior were studied in detail.



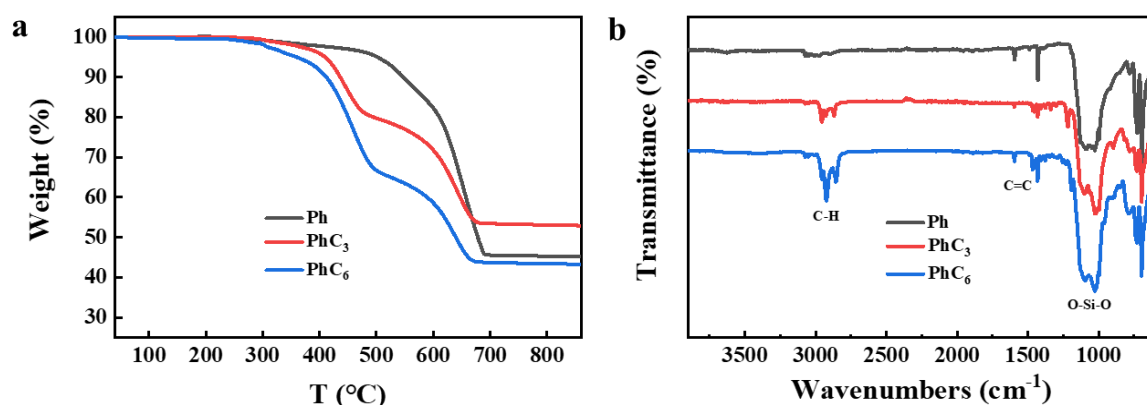
**Figure 5.1** Chemical structures and abbreviations of the organosilicas and related precursors (a, b), and illustration of the formation of the bubble (c).

## 5.2 Organic foams stabilized by alkyl-modified organosilicas

To further explore the role of alkyl chains in the foaming performance, we prepared a series of organosilicas containing phenyl groups and alkyl chains with variable length using alkyltrimethoxysilanes and phenyltriethoxysilane as co-precursors (**Figure 5.1a**). The foaming behavior of the as-prepared organosilicas was studied in benzyl alcohol by hand shaking and high-speed homogenization in Ultra-Turrax.

### 5.2.1 Characterization of alkyl-modified organosilicas

TG analysis reveals good thermal stability for all particles (**Figure 5.2a**). A two-step degradation process is observed in PhC<sub>3</sub> and PhC<sub>6</sub>. The first-stage mass loss is mainly attributed to the degradation of alkyl chains, while the second mass loss is attributed to the decomposition of phenyl groups. The total weight loss of PhC<sub>3</sub> is lower than that of unmodified organosilicas (Ph), which indicates the successful incorporation of propyl chains into the framework.

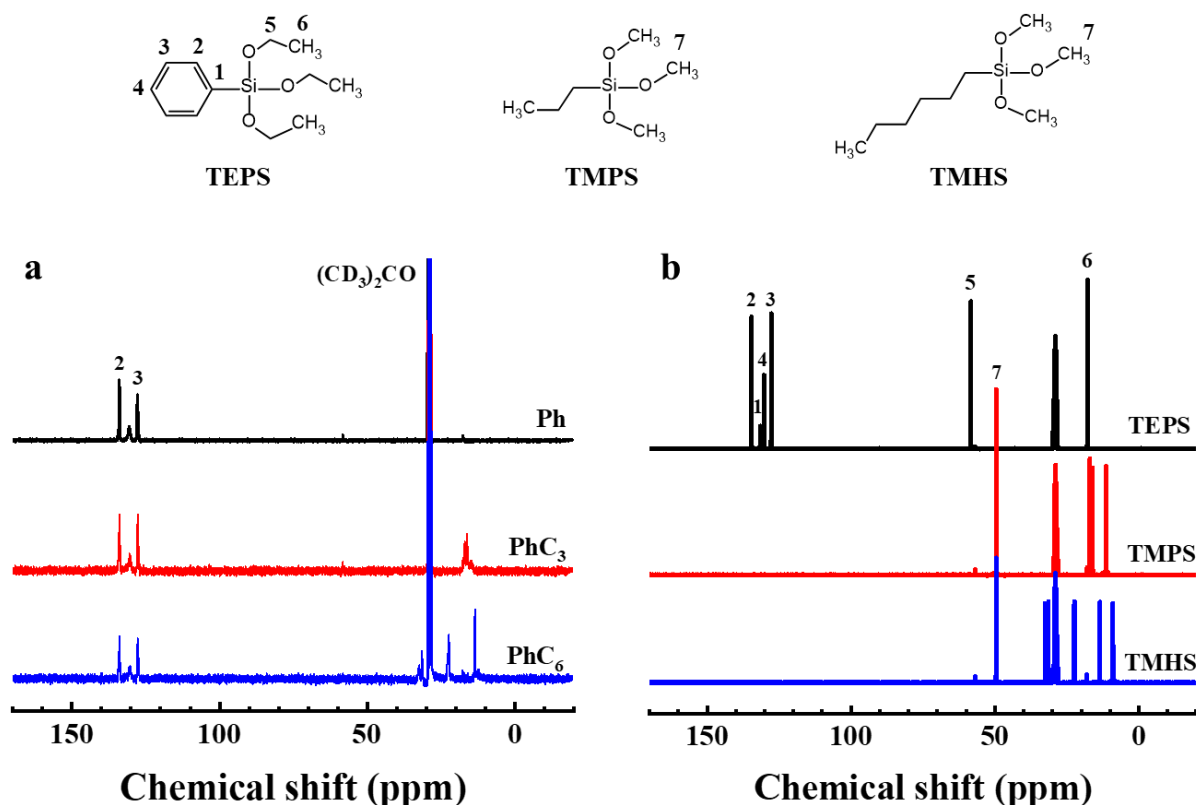


**Figure 5.2** TG profiles (a) and FT-IR spectra (b) of alkyl-modified organosilicas.

The surface composition of the alkyl-modified organosilicas particles was further analyzed by FT-IR spectroscopy (**Figure 5.2b**). All the samples exhibit an intense band at 1028 cm<sup>-1</sup>, which can be assigned to asymmetric stretching and bending vibrations of Si-O-Si bonds [7]. Besides, a characteristic band at 1429 cm<sup>-1</sup> is attributed to C=C stretching vibrations of aromatic rings in alkyl-modified organosilicas [8]. Compared with the pristine organosilicas (Ph), a slight change appears at 2928 cm<sup>-1</sup> after functionalization with alkyl chains, which can be ascribed to C-H stretching and bending vibrations [9].

The <sup>13</sup>C NMR spectra confirm the presence of alkyl groups and phenyl moiety in PhC<sub>3</sub> and PhC<sub>6</sub> organosilicas (**Figure 5.3**). The bands at 13, ~16 and 22 ppm can be attributed to carbon moieties of alkyltrimethoxysilanes. Noteworthy, these peaks are not observed in the unmodified organosilicas (Ph), confirming the absence of alkyl chains. Moreover, the signals observed at

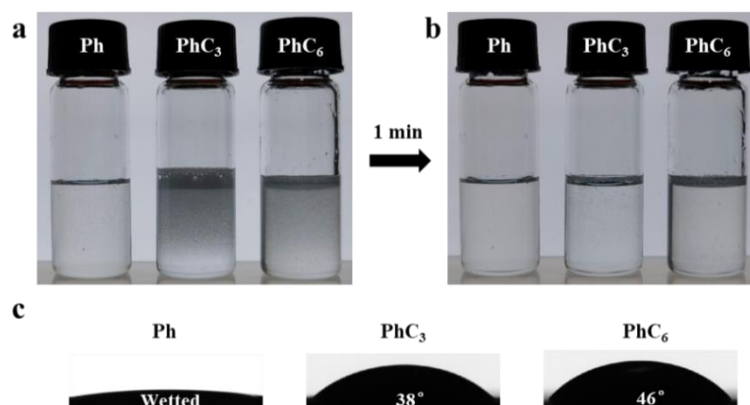
127 and 134 ppm are attributed to phenyl groups in alkyl-modified organosilicas [10].



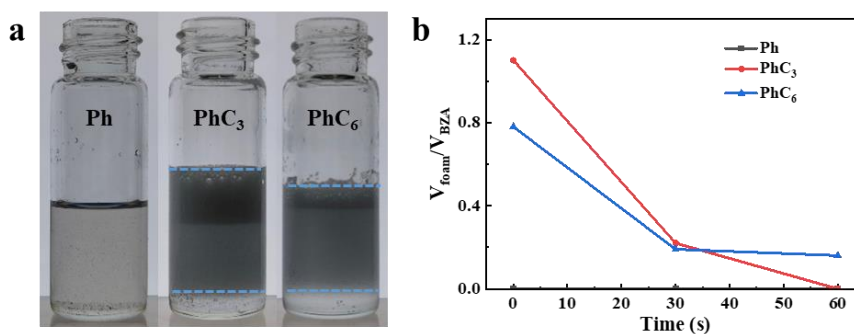
**Figure 5.3** Liquid-state  $^{13}\text{C}$  NMR spectra of alkyl-modified organosilicas (a) and corresponding precursors (b).

### 5.2.2 Foaming studies of alkyl-modified organosilicas

The foamability of the as-prepared organosilicas was investigated in benzyl alcohol both by hand shaking and homogenization in Ultra-Turrax. The Ph sample with no alkyl chains is completely wetted by the solvent and cannot foam (**Figure 5.4**). Foams can be stabilized by  $\text{PhC}_3$  organosilicas, but they collapse just after 1 min. A similar phenomenon is observed for foams produced by Ultra-Turrax (**Figure 5.5**). Interestingly,  $\text{PhC}_6$  organosilicas (with six carbons side chains) display lower foamability, even though the contact angle of this material is closer to that measured for well-foaming br-BiPh particles ( $46^\circ$  and  $53^\circ$ , respectively). While, at first sight, this result might appear somewhat contradictory, the lower foamability can be explained by the poor dispersibility of  $\text{PhC}_6$  samples in benzyl alcohol. Moreover, the simultaneous increase of particle-gas and particle-liquid surface tensions with the chain length makes particle adsorption at the gas-oil interface energetically unfavorable. The relationship between the carbon chain length and foamability is in good agreement with a previous study [11]. Accordingly, a chain length of 2-3 carbons appears to be optimal for foam formation.



**Figure 5.4** Foamability of 1 wt% alkyl-modified organosilicas in benzyl alcohol after preparation (a) and 1 min (b), and contact angles of alkyl-modified organosilicas with benzyl alcohol (c).



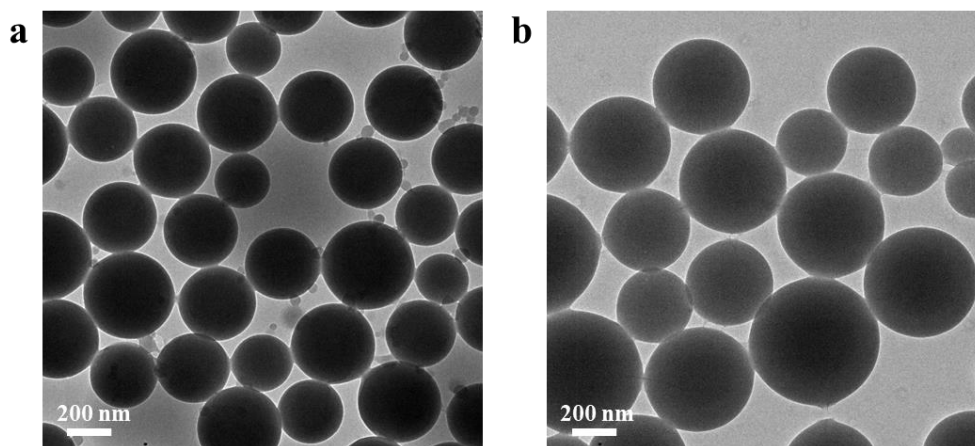
**Figure 5.5** Images of vessels with 1 wt% alkyl-modified organosilicas in benzyl alcohol produced by Ultra-Turrax taken after preparation (a) and time-evolution of foam volume (b).

### 5.3 Organic foams stabilized by fluorinated organosilica particles

As mentioned in Chapter 3, fluorocarbon moieties can lower the surface tension of solvents, thus stable foams can be obtained from fluorinated particles in a wide range of organic solvents [12-14]. In order to improve the foam stability in aromatic solvents, the organosilica particles were functionalized with fluoroalkylsilane (**Figure 5.1b**). Afterwards, the palladium supported on fluorinated particles (Pd/PhF<sub>3</sub>) were prepared by impregnation-reduction method [15-17].

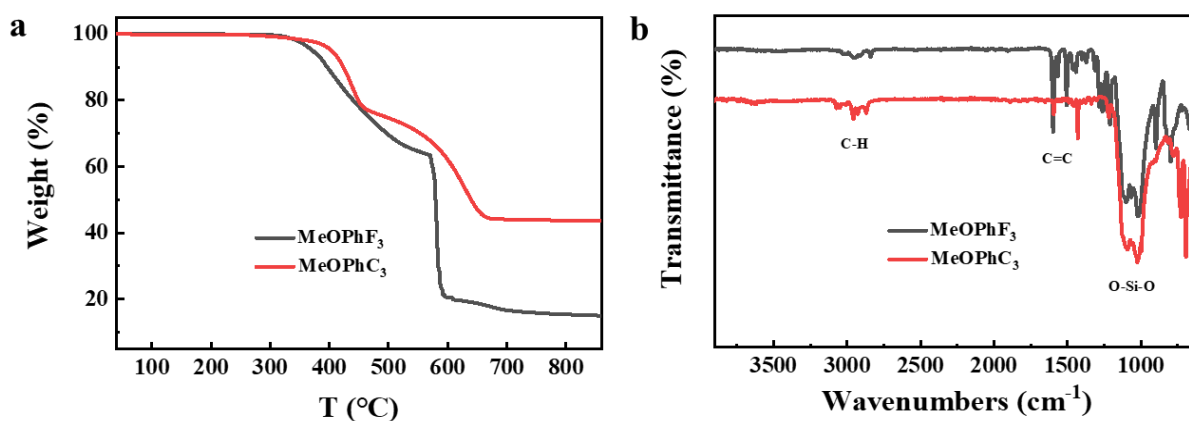
#### 5.3.1 Characterization of fluorinated organosilica particles

The morphology of as-prepared fluorinated organosilica particles was characterized by TEM. MeOPhF<sub>3</sub> organosilicas with fluorinated side chains consist mainly of 230-450 nm spherical particles accompanied by irregular much smaller particles (~50 nm) (**Figure 5.6a**). MeOPhC<sub>3</sub> particles with alkyl side chain show globular shapes with diameters in the range of 170-580 nm (**Figure 5.6b**).



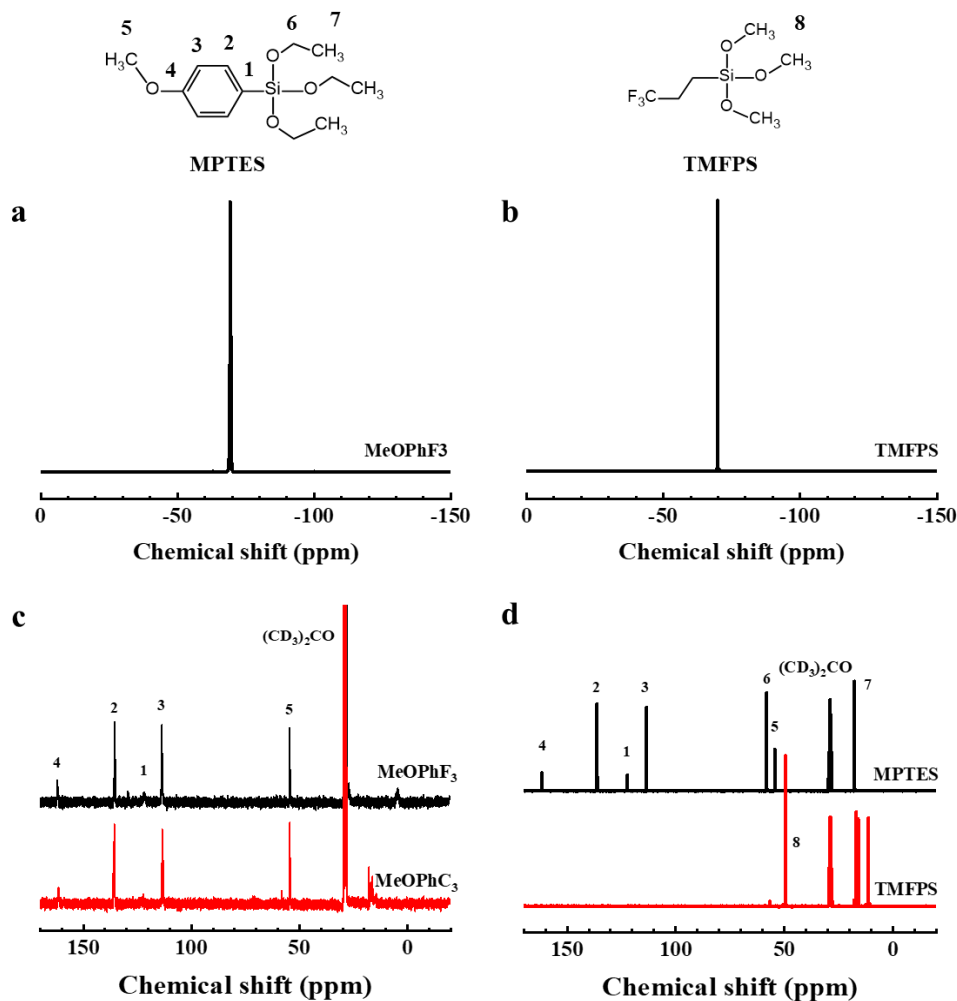
**Figure 5.6** TEM images of MeOPhF<sub>3</sub> (a) and MeOPhC<sub>3</sub> (b).

TG analysis was used to explore the thermal stability of fluorinated organosilica particles. Two thermal decomposition steps are observed that are located in the temperature range 300-570 °C and 570-740 °C (**Figure 5.7a**). The apparent difference in molecular weight between TMFPS and TMPS (218 vs 164) is responsible for the higher weight loss in fluorinated organosilica particles (84 wt%). The C-F and Si-O-Si species in MeOPhF<sub>3</sub> particles are not easy to be determined by FT-IR spectroscopy due to overlapping of the characteristic absorption bands at close wavenumbers (**Figure 5.7b**).



**Figure 5.7** TG profiles of organosilica particles under air atmosphere (a), and FT-IR spectra of organosilica particles (b).

The <sup>19</sup>F and <sup>13</sup>C NMR spectra demonstrate the existence of phenyl groups and fluorinated alkyl chains in MeOPhF<sub>3</sub> particles. A sharp resonance band is observed at -69 ppm that can be ascribed to CF<sub>3</sub> groups (**Figure 5.8a**). The spectra exhibit four bands at 113, 122, 135 and 162 ppm that can be attributed to phenyl groups incorporated in the particles (**Figure 5.8c, d**).



**Figure 5.8**  $^{19}\text{F}$  (a) and  $^{13}\text{C}$  (c) NMR spectra of organosilica particles and corresponding precursors (b, d).

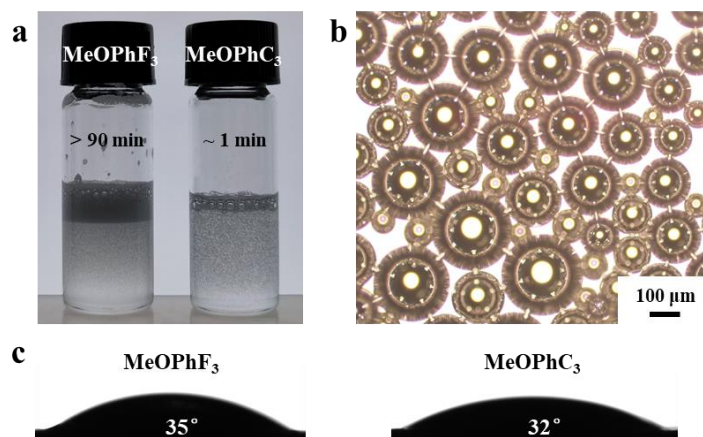
### 5.3.2 Foaming studies of fluorinated organosilica particles

The foaming properties of fluorinated organosilica particles were first studied in benzyl alcohol by hand shaking. As shown in **Figure 5.9a**, stable foams are generated from  $\text{MeOPhF}_3$  dispersions, while the foam stability of  $\text{MeOPhC}_3$  is much lower ( $\sim 1$  min). Surprisingly, the contact angle of  $\text{MeOPhC}_3$  particles with benzyl alcohol is closer to that of well-foaming  $\text{MeOPhF}_3$  particles ( $32^\circ$  and  $35^\circ$ , respectively). However, a lower surface tension is observed in the presence of  $\text{MeOPhF}_3$  particles compared to that obtained with  $\text{MeOPhC}_3$  particles (**Table 5.1**). These results point out that fluorinated alkyl chains in  $\text{MeOPhF}_3$  exert a pronounced effect on the foam stability.

The foaming properties (foamability and foam stability) in organic solvents depend on the particle concentration [18, 19]. Foam formation is favored by increasing the  $\text{MeOPhF}_3$  concentration, since a larger interfacial area can be covered. In the meantime, an increase in the



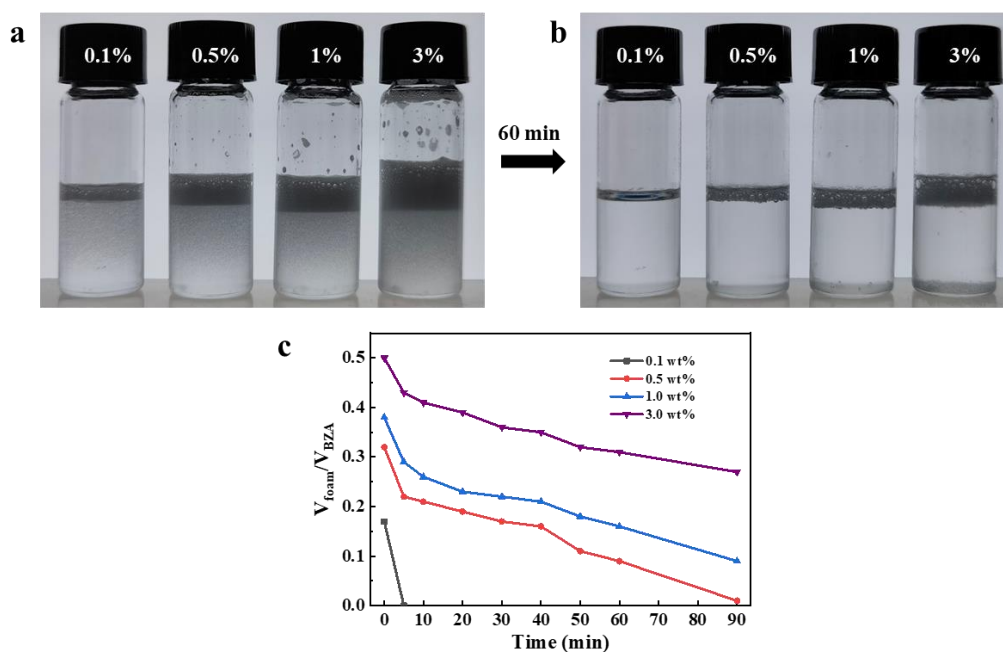
particle concentration from 0.1 to 3 wt% leads to a higher foam half-life time (**Figure 5.10c**). More importantly, the foam stability of MeOPhF<sub>3</sub> particles is comparable to that of biphenyl-bridged particles.



**Figure 5.9** Foams of 1 wt% MeOPhF<sub>3</sub> and MeOPhC<sub>3</sub> particles in benzyl alcohol (a), optical microscopy images of bubbles in benzyl alcohol stabilized by 1 wt% MeOPhF<sub>3</sub> (b), and contact angles of organosilica particles with benzyl alcohol (c).

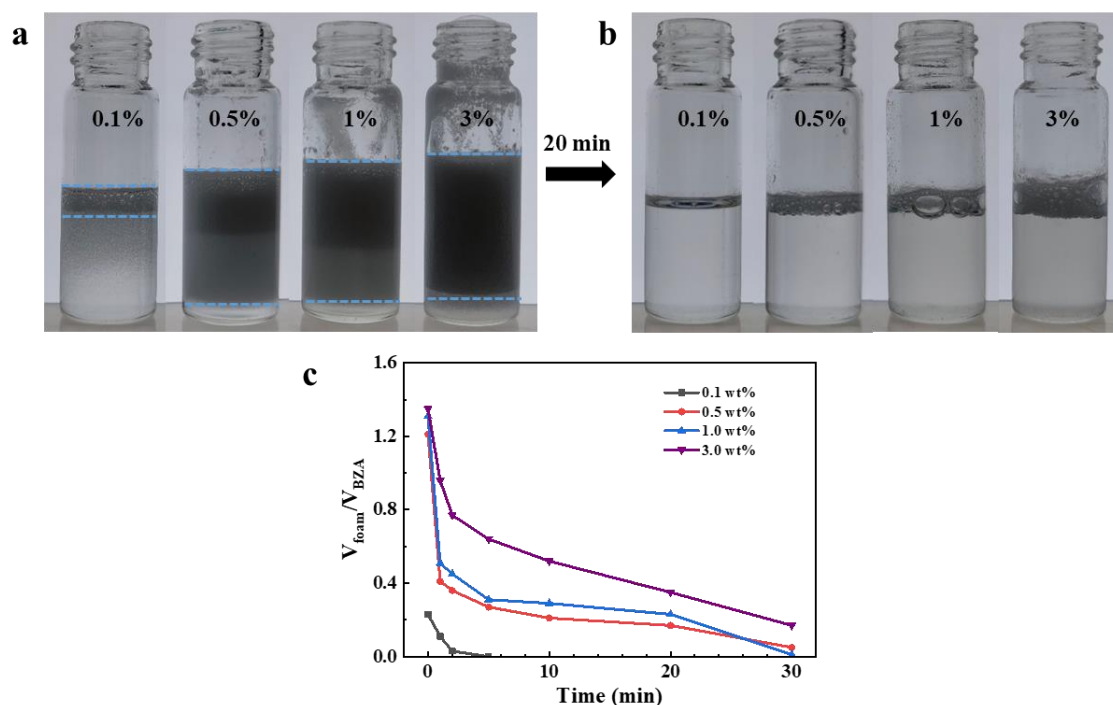
**Table 5.1** Surface tension of benzyl alcohol after the addition of organosilica particles.

Entry	Sample	Surface tension (mN·m <sup>-1</sup> )
1	0.1% MeOPhF <sub>3</sub> in benzyl alcohol	31.8
2	0.1% MeOPhC <sub>3</sub> in benzyl alcohol	37.4



**Figure 5.10** Images of foams stabilized by MeOPhF<sub>3</sub> at variable particle concentration taken after preparation (a) and 60 min (b), and time-evolution of the foam volume (c)

Likewise, we used a high-speed homogenizer (IKA Ultra-Turrax<sup>®</sup>T25 equipped with S25N-8G dispersing tool) to achieve a controlled energy input during the foaming process. After aerating at 16,000 rpm for 3 min, a larger volume of non-aqueous foams is generated compared to foams produced by a low energy method such as hand shaking (**Figure 5.11a**). Besides, higher foam height and half-life time are observed at higher concentration (**Figure 5.11c**). As a conclusion, foam stability increases dramatically by addition of fluorinated organosilica particles.



**Figure 5.11** Images of foams produced by Ultra-Turrax at various MeOPhF<sub>3</sub> concentrations taken after preparation (a) and 20 min (b), and time-evolution of foam volume (c)

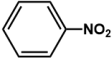
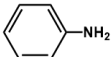
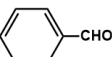
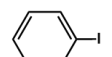
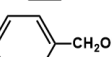
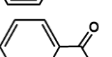
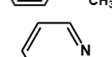
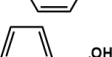
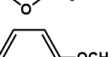
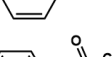
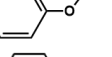
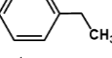
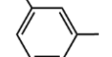
To elucidate the effect of solvents on the foaming behavior, we performed hand-shaking tests using MeOPhF<sub>3</sub> particles in a range of aromatic solvents (**Table 5.2**). Non-aqueous foams are generated from aromatic solvents with a surface tension between *ca.* 28 and 44 mN·m<sup>-1</sup> (**Figure 5.12**). It is worth mentioning that MeOPhF<sub>3</sub> particles can foam in apolar aromatic solvents (*e.g.*, toluene, xylene, ethylbenzene), although the half-life time of foam is very short (1 min).

### 5.3.3 Foaming studies of fluorinated organosilica particles after Pd loading

Palladium-based catalysts have been studied in a wide range of oxidation and hydrogenation reactions [20-24]. However, the catalytic efficiency can be significantly suppressed due to the extremely low solubility of gases in liquids [11, 25]. Therefore, it is quite desirable to develop

surface-active particles that can behave concomitantly as foaming agent and catalyst. By taking advantage of thiol group modification, palladium particles can be loaded on the surface of fluorinated organosilica particles. More information on the preparation of these bifunctional materials have been provided in **section 2.7**. The Pd content of resulting Pd/PhF<sub>3</sub> samples was 0.6 wt% as measured by ICP-OES.

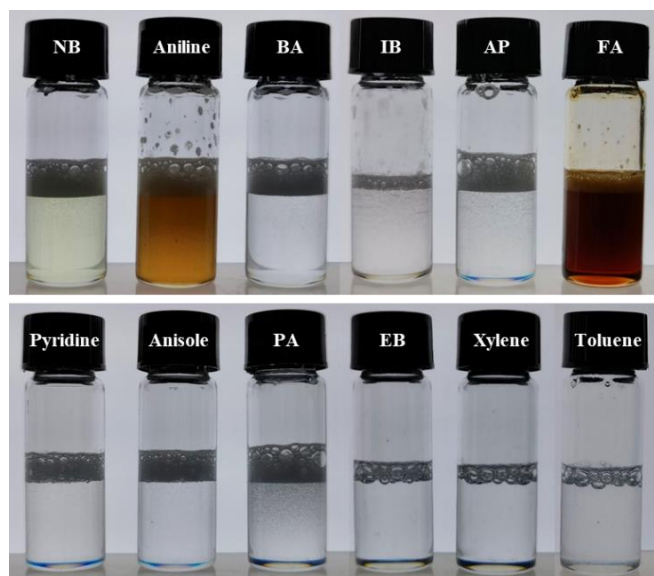
**Table 5.2** Properties and foaming behavior of the solvents in the presence of 1 wt% MeOPhF<sub>3</sub>.

Name (abbreviation)	Structure	Surface tension (mN·m <sup>-1</sup> , 20 °C)	V <sub>foam</sub> /V <sub>liquid</sub> <sup>a</sup>	Half-life time <sup>b</sup>
Nitrobenzene (NB)		43.9	0.42	1 min
Aniline		43.4	0.41	70 min
Benzaldehyde (BA)		40	0.39	2 min
Iodobenzene (IB)		39.7	0.14	1 min
Benzyl alcohol (BZA)		39.5	0.38	50 min
Acetophenone (AP)		39.04	0.43	2 min
Pyridine		38	0.31	1 min
Furfuryl alcohol (FA)		38	0.21	20 min
Anisole		35	0.34	1 min
Phenyl acetate (PA)		34.9	0.41	3 min
Ethylbenzene (EB)		29.2	0.20	1 min
m-Xylene		28.9	0.15	1 min
Toluene		28.4	0.16	1 min

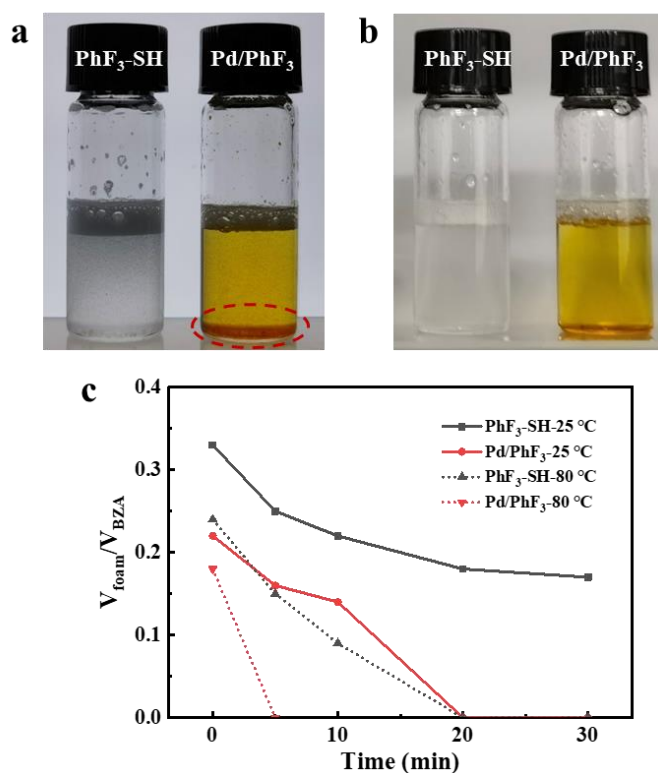
<sup>a</sup> V<sub>foam</sub>/V<sub>liquid</sub> (“foamability”) = foam volume/initial volume of solvent.

<sup>b</sup> The foam half-life time is the time where the foam height decreased to half its original value.

The foaming properties of Pd/PhF<sub>3</sub> were studied in benzyl alcohol by hand shaking. The foamability and foam stability decrease significantly after palladium loading both at room temperature and high temperature (**Figure 5.13**). This is mainly related to the high surface tension of Pd species [26], which makes particle adsorption at the air-oil interface energetically unfavorable. Moreover, it is difficult to disperse Pd/PhF<sub>3</sub> in benzyl alcohol (red dashed line). For these reasons, Pd/PhF<sub>3</sub> may be inefficient in promoting gas-liquid-solid reactions.



**Figure 5.12** Foams stabilized by 1 wt% MeOPhF<sub>3</sub> in aromatic solvents after hand shaking.



**Figure 5.13** Foams stabilized by 1 wt% PhF<sub>3</sub>-SH and Pd/PhF<sub>3</sub> at room temperature (a) and 80 °C (b) after hand shaking, and time-evolution of foam volume (c).

## 5.4 Conclusions

In order to achieve good foamability and chemical resistance, we prepared a series of organosilica particles by one-pot co-condensation method. The organic architecture affected the

foaming properties of alkyl-modified organosilicas. The presence of short alkyl chains was essential to ensure good foaming properties. Alkyl side chains incorporated in the organosilicas should be about 2-3 carbon long to promote foam formation, whereas the absence of side chains led to the particles overwettted by the solvent.

To obtain surface-active particles with catalytic centers, short fluorinated chains and aromatic groups were introduced onto organosilica particles. The incorporation of fluorinated alkyl chains with phenyl groups enhanced the foaming properties in benzyl alcohol. The foaming performance of fluorinated organosilica particles was comparable to that of biphenyl-bridged particles. However, the foam volume and life time of fluorinated organosilica particles were significantly shortened after the palladium loading. Further studies are needed to optimize the synthesis protocols and design surface-active catalyst for gas-liquid-solid reactions.

## 5.5 References

1. Weinberger, M., et al., *Submicron-sized silicon oxycarbide spheres as anodes for alkali ion batteries*. Journal of Materials Chemistry A, 2015. **3**(47): p. 23707-23715.
2. Hashimoto, R. and M. Ogawa, *Facile syntheses of nanoporous organosilica spherical particles*. Journal of Porous Materials, 2018. **25**(2): p. 425-431.
3. Wei, L., T. Tang, and B. Huang, *Novel acidic porous clay heterostructure with highly ordered organic-inorganic hybrid structure: one-pot synthesis of mesoporous organosilica in the galleries of clay*. Microporous and mesoporous materials, 2004. **67**(2-3): p. 175-179.
4. Olkhovyk, O., S. Pikus, and M. Jaroniec, *Bifunctional periodic mesoporous organosilica with large heterocyclic bridging groups and mercaptopropyl ligands*. Journal of Materials Chemistry, 2005. **15**(15): p. 1517-1519.
5. Gao, P., et al., *Enhanced adsorption of steroid estrogens by one-pot synthesized phenyl-modified mesoporous silica: Dependence on phenyl-organosilane precursors and pH condition*. Chemosphere, 2019. **234**: p. 438-449.
6. Osta, O., et al., *Direct synthesis of mesoporous organosilica and proof-of-concept applications in lysozyme adsorption and supported catalysis*. ACS omega, 2020. **5**(30): p. 18842-18848.
7. Dral, A.P., C. Lievens, and J.E. ten Elshof, *Influence of monomer connectivity, network flexibility, and hydrophobicity on the hydrothermal stability of organosilicas*. Langmuir, 2017. **33**(22): p. 5527-5536.
8. Fan, J., et al., *Phenyl-functionalized mesoporous silica materials for the rapid and efficient removal of phthalate esters*. Journal of colloid and interface science, 2017. **487**: p. 354-359.
9. Du, H., et al., *A facile synthesis of highly water-soluble, core-shell organo-silica nanoparticles with controllable size via sol-gel process*. Journal of colloid and interface science, 2009. **340**(2): p. 202-208.

10. Dai, J., et al., *Synthesis of zeolite nanocrystals with intercrystal mesopores using an organosilane as the structure directing agent*. RSC advances, 2016. **6**(111): p. 109897-109901.
11. Bai, X., et al., *Environmentally benign multiphase solid–liquid–gas catalysis*. Green Chemistry, 2020. **22**(3): p. 895-902.
12. Blázquez, C., et al., *Non-aqueous and crude oil foams*. Oil & Gas Science and Technology–Revue d’IFP Energies nouvelles, 2014. **69**(3): p. 467-479.
13. Binks, B.P., et al., *Particles at oil–air surfaces: powdered oil, liquid oil marbles, and oil foam*. ACS applied materials & interfaces, 2015. **7**(26): p. 14328-14337.
14. Binks, B.P., A. Rocher, and M. Kirkland, *Oil foams stabilised solely by particles*. Soft Matter, 2011. **7**(5): p. 1800-1808.
15. Bulut, A., et al., *Pd-MnOx nanoparticles dispersed on amine-grafted silica: highly efficient nanocatalyst for hydrogen production from additive-free dehydrogenation of formic acid under mild conditions*. Applied Catalysis B: Environmental, 2015. **164**: p. 324-333.
16. Yuan, M., et al., *Ultra-fine Pd nanoparticles confined in a porous organic polymer: A leaching- and-aggregation-resistant catalyst for the efficient reduction of nitroarenes by NaBH<sub>4</sub>*. Journal of colloid and interface science, 2019. **538**: p. 720-730.
17. Celebi, M., et al., *Palladium nanoparticles supported on amine-functionalized SiO<sub>2</sub> for the catalytic hexavalent chromium reduction*. Applied Catalysis B: Environmental, 2016. **180**: p. 53-64.
18. Fameau, A.-L. and A. Saint-Jalmes, *Non-aqueous foams: Current understanding on the formation and stability mechanisms*. Advances in Colloid and Interface Science, 2017. **247**: p. 454-464.
19. Binks, B.P., E.J. Garvey, and J. Vieira, *Whipped oil stabilised by surfactant crystals*. Chemical science, 2016. **7**(4): p. 2621-2632.
20. Durand, J., E. Teuma, and M. Gómez, *An overview of palladium nanocatalysts: surface and molecular reactivity*. European Journal of Inorganic Chemistry, 2008. **2008**(23): p. 3577-3586.
21. Liao, F., T.W.B. Lo, and S.C.E. Tsang, *Recent Developments in Palladium-Based Bimetallic Catalysts*. ChemCatChem, 2015. **7**(14): p. 1998-2014.
22. Shao, M., *Palladium-based electrocatalysts for hydrogen oxidation and oxygen reduction reactions*. Journal of Power Sources, 2011. **196**(5): p. 2433-2444.
23. Modak, A., et al., *A new periodic mesoporous organosilica containing diimine-phloroglucinol, Pd (II)-grafting and its excellent catalytic activity and trans-selectivity in C–C coupling reactions*. Journal of Materials Chemistry, 2010. **20**(37): p. 8099-8106.
24. Modak, A., J. Mondal, and A. Bhaumik, *Pd-grafted periodic mesoporous organosilica: an efficient heterogeneous catalyst for Hiyama and Sonogashira couplings, and cyanation reactions*. Green chemistry, 2012. **14**(10): p. 2840-2855.
25. Huang, J., et al., *pH-responsive gas–water–solid interface for multiphase catalysis*. Journal of the American Chemical Society, 2015. **137**(47): p. 15015-15025.

26. Ramezani-Dakhel, H., et al., *Stability, surface features, and atom leaching of palladium nanoparticles: toward prediction of catalytic functionality*. *Physical Chemistry Chemical Physics*, 2013. **15**(15): p. 5488-5492.

---

## **Conclusion and Perspectives**

---



## General conclusion

This thesis focused on the design of novel surface-active particles for foam stabilization and their applications in catalysis. Rationally designed particles with intermediate wettability could assemble at the air-liquid interface, thus stabilizing aqueous and non-aqueous foams. The foaming behavior of the resulting particles was systematically studied using different energy input methods.

First, we unveiled the surface-active properties of Aquivion<sup>®</sup> D98-20BS-P for producing stable foams in a variety of organic solvents and water. The foaming properties were studied after hand shaking and high-speed homogenization in Ultra-Turrax. The foam volume fraction generated by Ultra-Turrax was as high as 94% for 5 wt% of D98-20BS-P in benzyl alcohol. Unlike polytetrafluoroethylene and conventional fluorinated particles, D98-20BS-P exhibited excellent foamability and foam stability. Besides, the effect of the solvent properties on foam formation was systematically investigated. The presence of hydrogen bonds between sulfonic acid groups of D98-20BS-P and solvent molecules played a key role in enhancing the foaming properties.

By taking advantage of the excellent foaming properties and strong acidity of Aquivion<sup>®</sup> D98-20BS-P, we built a cascade catalytic system for deacetalization and hydrogenation. The combination of Aquivion<sup>®</sup> D98-20BS-P and homemade Pd/SiO<sub>2</sub> catalysts exhibited remarkable catalytic performance, and the yield of benzyl alcohol was two times higher than that achieved using conventional non-foam multiphase system. This was attributed to a pronounced increase of the reaction interface area. Moreover, cooperation between acid and palladium active sites was found to be an essential prerequisite for improving the catalytic activity in the foam system.

Next, we developed non-halogenated surface-active particles stabilizing foams in organic solvents. Biphenyl-bridged particles could adsorb at the air-oil interface, facilitating the generation of high-volume foams in benzyl alcohol. The particle structure was directly related to the foamability, and both the presence of biphenyl rings (mimicking the structure of the aromatic solvent) and ethoxy groups (well wetted by the gas phase) were essential to ensure good foaming. The contact angle was found to be a key parameter controlling foam formation. Foams were generated in the contact angle range between 32° and 53°. At the same time, the surface tension of the solvent should lie in the range 35-44 mN·m<sup>-1</sup>.

Finally, in order to achieve good foamability and chemical resistance, a series of organosilica particles was synthesized by the co-condensation method. Incorporation of fluorinated alkyl chains with phenyl groups was beneficial to improve the foam stability in

benzyl alcohol. However, the foam life time of fluorinated particles was significantly shortened after the palladium loading.

## Perspectives

Research activities in the field of foams have been blossoming throughout the past decade. Their physicochemical properties are highly dependent on the type of stabilizers and continuous liquid phase. Innovative developments have been reported for multiphase reactions based on microbubble systems promoting the G-L-S contact in water. The extension of this concept to other catalytic systems will certainly lead to emergence of new applications for oxidation and hydrogenation reactions.

Aquivion<sup>®</sup> PFSA combined with Pd-based catalyst (microbubble strategy) was found to efficiently convert benzaldehyde dimethyl acetal into benzyl alcohol in aqueous foams. As a perspective, this catalytic system could be reshaped using non-aqueous foams. For instance, acid-catalyzed C-C coupling reactions encompassing aniline could be combined with a further hydrogenation step using an aniline foam in hydrogen.

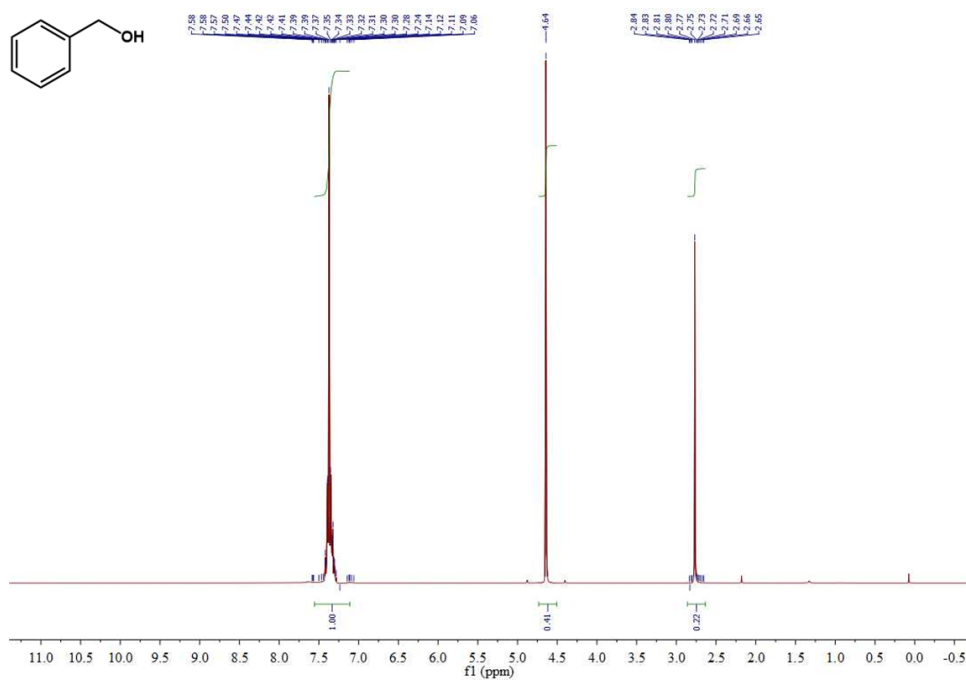
Although stable non-aqueous foams can be obtained from biphenyl-bridged particles in aromatic solvents, there are still some limitations associated with these materials. Since ethoxy groups in the particles are labile in the presence of acid or base, biphenyl-bridged particles are far from perfect to satisfy practical applications. However, these materials allow the preparation of controlled foams in a wider range of organic solvents, which may lead to the emergence of new applications of foams. Besides, the *rationale* used to prepare biphenyl-bridged (*i.e.* with groups showing affinity both to the solvent and gas) reveals as promising for further design of surface-active particles.

At the present stage, a key challenge is to develop surface-active bifunctional particles with catalytic sites due to the high surface tension of transition metals. More efforts should be dedicated to design efficient catalyst for G-L-S reactions. Despite the drawbacks of fluorinated organosilica particles after palladium loading, the findings in this study may provide guidance to prepare successful catalytic particles for engineering G-L-S microreactors, stimulating new research directions in this field.

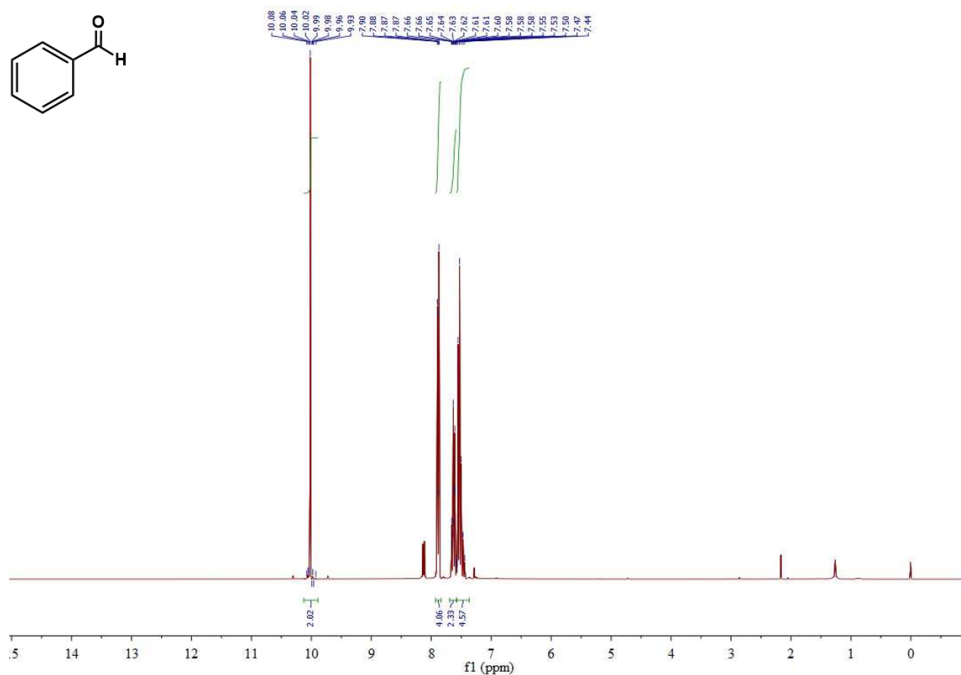
## Annex

### <sup>1</sup>H NMR spectra data of the products in chapter 3

Benzyl alcohol, <sup>1</sup>H NMR (300 MHz, CDCl<sub>3</sub>): δ 7.56-7.11 (m, 5H), 4.64 (s, 2H), 2.86-2.63 (m, 1H).



Benzaldehyde, <sup>1</sup>H NMR (300 MHz, CDCl<sub>3</sub>): δ 10.13-9.89 (m, 1H), 7.88 (dd, J = 5.2, 3.2 Hz, 2H), 7.69-7.58 (m, 1H), 7.57-7.37 (m, 2H).



## Publications

1. **Andong Feng**, Dmytro Dedovets, Yunjiao Gu, Shi Zhang, Jin Sha, Xia Han, and Marc Pera-Titus\*, Organic Foams Stabilized by Biphenyl-bridged Organosilica Particles, *Journal of Colloid and Interface Science*, 2022, 617, 171-181.
2. **Andong Feng**, Dmytro Dedovets, Shi Zhang, Jin Sha, Renate Schwiedernoch, Jie Gao, Yunjiao Gu, and Marc Pera-Titus\*, Foams Stabilized by Aquivion® PFSA: Application to Interfacial Catalysis for Cascade Reactions, *Advanced Materials Interfaces*, submitted.
3. Shi Zhang, Dmytro Dedovets, **Andong Feng**, Kang Wang, and Marc Pera-Titus\*, *Journal of the American Chemical Society*, 2022, 144, 4, 1729-1738.